DOE/PC/88911--T8

DE92 017807

THERMALLY INDUCED STRUCTURAL CHANGES IN COAL COMBUSTION

FINAL REPORT, JANUARY 1992

R. C. Flagan and G. R. Gavalas

Work Performed Under Grant No. DE-FG22-88PC88911

For
U.S. Department of Energy
Pittsburgh Energy Technology Center
Pittsburgh, PA 15236

By
California Institute of Technology
Pasadena, CA 91125

TABLE OF CONTENTS

SUMMARY

The effects of the temperature-time history during coal devolitization and oxidation on the physical properties and the reactivity of resulting char were studied experimentally for temperatures and residence times typical of pulverized combustion. Experiments were also carried out at somewhat lower temperatures and correspondingly longer residence times.

An electrically heated laminar flow reactor was used to generate char and measure the rates of oxidation at gas temperatures about 1600K. Partially oxidized chars were extracted and characterized by gas adsorption and mercury porosimetry, optical and scanning electron microscopy, and oxidation in a thermogravimetric analysis system (TGA). A different series of experiments was conducted using a quadrople electrodynamic balance. Single particles were suspended electrodynamically and heated by an infrared laser in an inert or oxygen-containing atmosphere. During the laser heating, measurements were taken of particle mass, size/shape, and temperature.

A question pervading interpretation of drop tube oxidation experiments, or single particle oxidation experiments using the electrodynamic balance is the effect of particle shape. For convenience, previous modeling studies and data analyses have postulated spherical particles. In this part of the project we set out to examine the error made by assuming spherical particles and to find out how well a nonspherical particle may be approximated by a spherical particle of suitable effective radius.

The results of the two series of experiments and of the theoretical study will now be briefly outlined and described in more detail in Chapters 1-4 below.

Flow Reactor Experiments

Chars were generated from a hvA bituminous coal in a laminar flow tube reactor in an atmosphere of N_2 or 1-5% O_2 in N_2 and at 1600K temperature. The chars were characterized by elemental analysis for carbon and hydrogen contents, N_2 adsorption for BET surface area and pore size distribution, and by oxidation in a thermogravimetric analyzer at a temperature of 773K. When heated in neutral or oxidizing atmosphere, the great majority of the hvA bituminous coal (PSOC 1451) particles undergo a series of structural changes. Hollow spheres are formed, followed by particle fragmentation. In 1 or 5% oxygen, oxidation proceeds both externally and internally at approximately constant diameter until the onset of fragmentation. For all of the chars, the surface area and the pore

volume in the size range 15 to 120 Å increased dramatically within the first 100 ms from the values of the original coal. The ratio of carbon to hydrogen increases with residence time. Carbon conversion at 1600K also increased with increasing oxygen pressure, while the low temperature (~500°C) char reactivity measured in the TGA experiments decreased. Significant structural reorganization occurred either simultaneously with devolatilization or after devolatilization depending on the oxygen concentration. The presence of oxygen appeared to accelerate the structural changes and decrease the reactivity of the char. The experimental results indicate a strong relation between char properties and experimental conditions. This relation could have important implications on the modeling of coal combustion and on combustion design and operation.

Electrodynamic Balance Experiments

An electrodynamic balance was constructed having hemispherical endcap electrodes and a right cylinder ring. The electrode cell was housed in an evacuable stainless steel chamber of 250 cm^3 volume. The atmosphere in the chamber was controlled by the flow of gases of the desired composition. A 20-watt CO_2 laser was used to heat the particle. Before, during, and after heating the particle was observed with a microscope and a video camera. The temperature of the particle was measured with a two-color IR pyrometer.

One series of experiments concentrated on the ignition behavior of Pittsburgh No. 8 coal char particles of 150-300 μm diameter and synthetic char particles (Spherocarb) of 140-240 μm diameter. In a typical experiment, a charged char particles was suspended in the electrodynamic balance and heated by a 500 ms pulse of radiation from a CO_2 laser. The oxygen concentration in the ambient gas, initially only nitrogen, was slowly increased as successive laser pulses were given, until the particle ignited. Once ignition occurred, the particle lost charge and dropped from the center of the balance.

The temperature traces of particles that ignited clearly show an induction time, or ignition time lag, as predicted by the solution of the time dependent equation for a heated particle. The effect of increasing the oxygen concentration is also seen in the increasing equilibrium temperature at sub-ignition conditions, though it was not quantifiable in this study. A simple isothermal sphere model was used with parameters obtained from the literature which adequately predicted the experimentally obtained time-temperature histories of igniting Spherocarb particles. A reasonable fit to the bituminous char data was achieved using rate parameters determined in an earlier drop tube study. These experiments provide the first examples in which the oxidation of char during ignition is rigorously modeled and

compared with existing literature data. The electrodynamic balance can be used in ignition experiments to measure the apparent char oxidation rate parameters, and probe particle-to-particle variations in the apparent kinetics.

The second series of experiments using the electrodynamic balance focused on the densification and other structural changes of char during heating and oxidation.

A typical experiment started by trapping a single particle in the electrodynamic balance. The size of the particle was measured in the horizontal and vertical directions using the eyepiece micrometer. Photographs were taken through the viewing microscope. The CO_2 laser was allowed to stabilize with an external shutter closed. Particle heating was then initiated by opening the shutter. The pyrometer signal was monitored on the oscilloscope and recorded by the data acquisition system. The particle position was balanced manually. The heating pulse was ended by closing the external shutter. Photographs were again taken to record any changes in particle size and shape.

Coal chars (Pittsburgh No. 8) generated at 1600K and 1200K were heated in nitrogen and in air. Heating the 1600K char in N_2 at about 1000K did not induce any change in size or shape—the char was not densified. Likewise the "greener" char generated at 1200K underwent no change in size or shape following heating at 1000K. When the 1600K char was heated in air to as much as 56% conversion, no change in size or shape was observed but the particle became lacy and translucent, indicating full oxygen penetration into the macropores, and no densification. The 1200K char, on the other hand, underwent significant shrinkage upon oxidation in air under the same conditions. The shrinkage was largely due to densification by thermal rearrangement of this "greener" char. Inasmuch as no shrinkage took place upon heating in nitrogen, the observed densification was not purely thermal but could only take place in the presence of oxygen. The synthetic char (Spherocarb) exhibited behavior similar to that of the 1200K coal char. Heating in nitrogen engendered no shrinkage, but heating in oxygen resulted in significant shrinkage despite the fact that reaction proceeded in regime I (low Thiele modulus).

The experiments on shrinkage have important implications for modeling of char combustion. The particle size change is not merely a result of the balance between reaction and pore diffusion. The Thiele modulus may not be sufficient for predicting whether the particle burns at constant size, constant density or at an intermediate mode. Densification must also be considered, at least for "green" chars those that had not been previously exposed to very high temperatures.

Analysis of Combustion of Nonspherical Particles

The analysis of nonspherical particle combustion was made for the regime of shrinking core reaction. The first problem addressed was the calculation of the pseudosteady temperature and oxidation rate for a particle of given shape. This problem involves the solution of the external diffusion and heat conduction equations with the reaction entering as a boundary condition over the particle surface. Using the boundary integral method, the problem was reformulated as a system of two coupled integral equations which were solved numerically yielding the following results. For particles of equal volume, the pseudosteady temperature is nearly independent of shape, but the combustion rate increases with increasing aspect ratio. The local combustion rate varies moderately over the particle surface increasing with the distance from the particle center. The total combustion rate depends on the particle surface area alone, i.e., particles of equal surface area but different volumes and shapes have the same rate. This dependence on the surface area is less than linear, becoming linear only in the limit of low Damköhler numbers. The complete transient problem addressing the evolution of particle shape and particle temperature during burnout, was similarly formulated by the boundary integral method and solved numerically. Over a broad range of parameters, the pseudosteady particle temperature and rate of oxidation are very nearly equal to those of spherical particles of equal volume and surface area respectively. The transient solutions obtained for parameters typical of pulverized combustion show that during burnout the particle becomes increasingly nonspherical. As expected, nonspherical particles burn faster than spherical particles of the same initial volume, but the difference in burnout times is less than 20% for initial aspect ratios between one and three.

CHAPTER 1

INTRODUCTION

1. INTRODUCTION

Coal combustion is a major source of energy for electric power generation in the United States. Currently 50% of electric power is generated from coal, 19% from nuclear fission, and the remainder from hydroelectric, oil- and gas-fired, and miscellaneous solar and wind power stations. Solar power generation is very expensive and is currently economical only in small scale specialized applications. Although technical progress is made continuously gradually reducing the cost, solar power is not expected to become a major factor in the next two decades. Wind power is becoming competitive but is limited to certain favorable geographic regions. Among the fossil fuels coal is by far the most abundant in the U.S. and will remain the major source of electrical power generation in the foreseeable future. The share of nuclear power generation is also expected to remain significant and possibly grow over the next few decades.

Although practiced for more than seventy years, pulverized coal combustion—the workhorse of the industry—is presently undergoing active development. The main issues as well known are the control of sulfur dioxide, nitrogen oxides and particulates. Several competing technologies have been developed but the cost of control remains high, hence the continuing research and development effort. As far as sulfur oxide removal is concerned, postcombustion wet or dry processes and precombustion beneficiation are mature technology which, however, will continue undergoing incremental improvement. Nitrogen oxide control is less settled with combustion modification and postcombustion catalytic reduction, both undergoing development and limited commercialization. Modification by staged air addition, or special burner designs intervenes in the basic chemistry of combustion and hence can affect both NO_x generation and the composition and size distribution of flyash. These pollution control issues cannot override the requirement of complete combustion within the residence times afforded by the boiler.

The design of coal-fired boilers has been, in the past, guided by experience and relatively simple empirical procedures. The demands of tighter pollution control and higher combustion efficiency, provide now the incentive for using detailed and fundamentally based mathematical models to assist the design of new or retrofit installations. A detailed mathematical model of a coal-fired boiler is inevitably very complex, for it must incorporate turbulent fluid dynamics and heat transfer with the homogeneous and heterogeneous combustion chemistry. Two-dimensional and three-dimensional models have been developed tracking the fluid and particle phases and a simple treatment of the combustion

chemistry. It is impractical to attempt a complete description of all these phenomena. Idealization and empiricism are still essential.

This research project has been addressed to certain problems in heterogeneous char oxidation. Although only one component of the combustion process, heterogeneous oxidation takes up the bulk of the residence time in the boiler and is responsible for the generation of most of the flyash pollutions. Seemingly a simple process in reality is a microcosm of physical and chemical phenomena and has been a long standing subject of experimental and theoretical research.

It is traditional to differentiate between the physical properties and chemical structure as controlling in distinct ways the course of heterogeneous oxidation. However at the level of the finest pores, below 10 Å diameter, the physical and chemical properties blend and cannot be clearly differentiated. It remains useful, nevertheless, to retain this distinction and we shall do so in this discussion. In both experimental characterization and modeling work, the physical properties of interest are size/shape surface area, and pore size distribution, the latter often summarized into an effective pore diffusion coefficient. During burnout, the pores are enlarged with the surface area, pore size distribution and effective diffusivity changing accordingly. Recent modeling work has attempted to characterize these changes with idealized geometrical models but major difficulties remain. For example, the statistical averaging implicit in all pore models becomes highly questionable when the penetration depth of oxygen is comparable with the size of the larger voids in the char, as is often the case in pulverized combustion.

The chemical property needed to describe char oxidation is the intrinsic reaction rate, i.e., the rate per unit pore surface area. There is no unambiguous choice of surface area for this purpose. Both the N_2 BET surface area and the Dubinin-Polanyi CO_2 surface area have been used, and one may be better than the other for a given experimental situation. Whichever of the two areas is used, however, the idea is that the local reaction rate r can be expressed as the product of the local intrinsic rate r_i and the local pore surface area per unit volume, S(X):

$$r\,(p,T) = r_i\,(p,T)\,S(X)$$

where p is the local pressure of oxygen, T is the local temperature, and where X is the local conversion. In this simple decomposition, which has been the basis of all detailed modeling work todate the intrinsic rate incorporates all chemical factors and would vary

from char to char, but is assumed independent of conversion. The surface area on the other hand, varies with conversion tracking the changing pore geometry.

This project was addressed to the efforts of the thermal history of char on its subsequent reactivity towards oxidation. Thermal history here means the temperature-time history during both devolatilization and oxidation. Posed in terms of the reaction rate expression above, the issues under consideration are:

i) the effect of temperature time history of devolatilization on the intrinsic rate and the porous structure at the onset of oxidation

ii) whether the intrinsic rate (at fixed T,c) remains constant or varies during oxidation.

1.2 Organization of Report

Chapter 2 of this report describes the experiments on coal devolatilization, char characterization, and measurement of char reactivity at high temperatures (~1600K) and lower temperatures (~800K). These experiments focus on the effects of the thermal history on the physical properties and reactivity of the char.

Chapter 3 describes the experiments on the oxidation of single char particles in the electrodynamic balance. The major result of this chapter is that certain chars suffer thermal densification or shrinkage upon heating in the presence of oxygen, quite apart from the shrinkage due to burnout. Chapter 3 also describes some interesting ignition measurements carried out with the electrodynamic balance.

Chapter 4 is based on a paper recently accepted by COMBUSTION SCIENCE AND TECHNOLOGY. It describes our theoretical work on the combustion of nonspherical particles. This work is not directly related with the effects of thermally induced changes, but is of more general interest in the modeling of particle combustion.

CHAPTER 2

THE EFFECT OF TEMPERATURE-TIME HISTORY ON CHAR STRUCTURE AND REACTIVITY

INTRODUCTION

Devolatilization and char oxidation are the two major steps involved in coal combustion. The first step is rapid and the second is slow. In pulverized coal combustion devolatilization takes 10-100 ms. Char burnout requires as much as 1 second, making it the rate limiting step for the overall process. However, devolatilization determines the initial physical and chemical properties of the char, e.g., particle density, surface area, porosity, as well as molecular structure. These properties, in turn, govern the char combustion kinetics.

Wells and Smoot (1991) used canonical correlation analysis to determine the relationship between the reactivity and the chemical and physical properties. For different coals, rank had a significant correlation with reactivity. The same result was found for chars extracted by pyridine. For pyrolyzed chars, the relative importance of effective factors was found to be catalysis by metal ions > porosity > total hydrogen. The cation activity was found to be in the order of Na > Mg > Ca >> K.

Anson et al. (1971) described in great detail the structural change of a low rank and a medium rank bituminous coal burning in air. On being exposed to high intensities of radiation, coal particles typically soften. The rapid generation of volatiles causes particle swelling and production of large holes on the particle external surfaces. With the completion of devolatilization, the swelling ceases, and after a short time interval (about 40 ms for 250 μm diameter particles) the particles undergo a marked contraction forming rigid skeletons. After contraction, the initial burning of the residue took place at approximately constant diameter. Reactions occurred around the pore mouths until the char particles fragmented. Samples of lithotypes of both low and medium rank coals were heat-treated in the furnace at a temperature of 1073K for 150 ms. The measurements of the surface areas of these samples by xenon adsorption confirmed the trend toward increasing surface with decreasing rank. The surface area for 53-63 μm Ackton Hall coal (CRC 502) burning in air at about 75 ms was about twice that of the original coal. As the residence time increased to 85 ms, the surface area increased from 111 to 125 m^2/g on dry ash free basis. The surface area started to drop near the completion of devolatilization. It was 88.5 m^2/g at approximately 130 ms, while the devolatilization ended at about 150 ms. Under the same conditions, the measured surface area of Rawdon coal (CRC 902) was almost constant at residence time of 85 ms, then decreased progressively with time. The surface area dropped rapidly around the time of the completion of devolatilization from 121 m^2/g at 130 ms to 55 m^2/g at 180 ms. The variation of surface area of semi-anthracite coal particles during

combustion was measured by Smith and Tyler (1972) at temperatures of 1400K to 2200K and oxygen fractions about 0.1 and 0.2 atm. The surface areas first increased then steadily decreased with burnout. The peak appeared between about 15 to 35% burnout, corresponding to the coal particle sizes 78 to 6 μm. The surface areas also decreased with increasing gas temperatures. The particle size and density both decreased with burnout, indicating that oxygen partially penetrated into the pore structure.

Particle size, density, porosity, pore size, and surface area have been found to have important influence on the combustion behavior of particles. When combustion is limited to a shallow zone below the outer surface, particles burn with constant density but with a steady reduction of size. When oxygen penetrates completely within a porous particle, combustion occurs at constant size but with decreasing density. Thin-walled cenospheres were concluded to burn with reducing density but at constant size whether oxygen penetrated the pore or not (Smith, 1982).

Anson, et al. (1971) reported that the composition of coal influenced the morphology of hollow spheres formed during devolatilization. Particles of vitrain and clarain, composed mainly of vitrinite, produced spheres with thinner walls compared to those obtained from durain particles. Moreover for vitrain and clarain particles there was a natural progression toward more extensive internal structures with decreasing rank.

The structural transformations that occur when carbons are heated to high temperatures have been studied extensively, but measurements of structural changes occurring on the short time scale of pulverized coal combustion are extremely limited. Smith and Tyler (1972) collected partially burned chars of a semianthracite from a laminar flow furnace and examined them by optical microscopy, porosimetry and X-ray diffraction. The micropore surface area was found to decrease with burnout. A sharpening of a graphite band in the X-ray pattern indicated that some structural ordering took place. Such ordering was also observed after partial combustion of glassy carbons (Levendis and Flagan, 1987). Oxygen was observed to catalyze the structural transformation (Levendis et al., 1989). Haussmann and Kruger (1988) measured the change in the hydrogen and nitrogen to carbon ratios with carbon conversion at 1750K and 7.6% O_2, and at 1300K and pure argon for 55 μm Montana Rosebud subbituminous coal. In the oxidizing atmosphere, both H/C and N/C ratios decreased until around 50% carbon conversion, then varied very slowly. The chars exposed to pure argon underwent a decrease of the H/C ratio, but almost no change in the N/C ratio with carbon conversion. The change of H/C ratio indicates reorganization of the carbon matrix, but the chemical structures evolved have not been

studied in any detail. The decrease in the reactivity of the carbonaceous material that is expected to accompany these changes could have important implications to combustor design and operation. In the present work, we examine the structural changes occurring at combustion temperatures and times typical of pulverized combustion and probe the effect of the changes on the rate of char oxidation.

EXPERIMENTAL METHODS

Char Formation

Chars were made from a high-volatile A bituminous coal (PSOC 1451), the properties of which are given in Table 1. The coal was pulverized in a mechanized mortar and pestle in air. It was then size classified by sieving on a mechanical shaker. The 45-53 μm coal size fraction was dried by heating in nitrogen at 100°C for one hour and then cooled to room temperature before char production. The experimental system has been described in detail elsewhere (Sahu, 1988) and is only briefly described here. Combustion experiments were conducted in a laminar flow tube furnace (Applied Test System, Series 3310) consisting of an alumina tube of 5 cm internal diameter and 71 cm length heated by Kanthal Super 33 elements. The gas temperatures were measured with a suction pyrometer. The isothermal zone of the reactor was about 30 cm long. The wall temperature was maintained at 1748K to 1773K, depending on the residence time, to produce a gas temperature of 1600K at the center of the isothermal zone in all experiments. The temperature at the ends of the isothermal zone dropped about 10%. Coal particles were injected into the alumina tube through a water-cooled injector at a rate of 3 gm hr^{-1}. Experiments were performed in pure nitrogen or in mixtures of 1 or 5% oxygen in nitrogen. The coal chars were collected on 0.4 μm nuclepore filters with a water-cooled, gas dilution quench probe. The residence times of the coal particles inside the furnace were varied by adjusting the gas flow rate and the position of the sampling probe. Both size classified, dried coal and the chars produced in the drop-tube furnace were stored under nitrogen atmosphere.

Char Characterization

Elemental Analysis

The mass fractions of carbon, hydrogen, and nitrogen in various char samples were determined by a Model 240 Elemental Analyzer. These analyses were based on detecting

and measuring the combustion products of carbon dioxide, water, and nitrogen in pure oxygen at a temperature of 860°C.

Surface Area

The surface areas of the chars were obtained by a modified volumetric adsorption technique described by Northrop et al. (1987). The gas adsorption isotherms were measured by continuous addition of adsorbate gas (N_2 at 77K) to the sample (see Appendix A). The apparatus was calibrated with γ-alumina. The relative measurement uncertainty is about ±15% for a surface area of 1 $m^2\,gm^{-1}$ and decreases with increasing sample surface area. The repeatability of the measurements was tested with duplicates using (1) the same sample; (2) or different samples of the same material. Each pair of measurements agreed to within 20% (Table 2).

Pore Volume Distribution

The BET model is usually applied to a relative pressure range $0.04 < P/P^\circ < 0.30$, where P° is the vapor pressure of adsorbate. At higher relative pressure, capillary condensation occurs in porous solids due to the surface tension induced pressure difference across the curved meniscus of the condensed vapor. The size of the capillary can be calculated by the Kelvin equation,

$$\ln \frac{P}{P^\circ} = \frac{2\gamma v \cos\theta}{LRT} \qquad (1)$$

where γ is the surface tension, v is the molar volume, θ is the contact angle, L is the radius of a cylindrical pore. For a slit pore, L is half the distance between the walls. R is the gas constant and T is the absolute temperature.

Using the capillary condensation model including multilayer adsorption in cylindrical pores, Wheeler (1946) deduced that the specific pore volume $V(r)$ was related to the volume of nitrogen desorbed over a small segment on the desorption branch of the isotherm $v(r)$ by

$$v(r) = \left(\frac{r - t(r)}{r}\right)^2 V(r) + \frac{dt}{dr} \int_{r_0}^{r} \frac{2r' - t(r')}{r'^2} V(r')dr' \qquad (2)$$

where r is the radius of the pore, t is the thickness of the adsorbed layer of gas. The first term on the right accounts for liquid evaporated from the pores, and the second term represents the amount of gas desorbed from free surfaces. However, Wheeler was not able to solve Eq. 2 for the unknown $V(r)$ at that time. Cranston and Inkley (1957) later developed a method to calculate $V(r)$. The volume of pores having radii, r, in the range $r_1 \le r \le r_2$ is estimated to be

$$V_{12} = R_{12}\left(v_{12} - k_{12} \sum_{r_2 + \frac{\Delta r}{2}}^{r_{max}} \frac{r - t_{12}}{2r^2} V_r \Delta_r\right) \qquad (3)$$

where

$$R_{12} = \left(\frac{1}{r_2 - r_1} \int_{r_2}^{r_1} \frac{r - t_1}{r} dr\right)^{-1}$$

$k_{12} = 4(t_2 - t_1)$, and $t_{12} = (t_2 + t_1)/2$. $V_r\Delta_r$ is the volume of pores having radii between r and $r+\Delta_r$, where Δ_r is very small compared with r. The quantity v_{12} is the total volume of nitrogen adsorbed during the adsorption step from pressure P_1 to pressure P_2, where P_1 corresponds to the critical radius r_1 and P_2 to radius r_2. The quantities t_1 and t_2 are the adsorbed layer thicknesses at the pressures P_1 and P_2, respectively. The t values were given by Lippens et al. (1964). We used Eq. 3 to estimate pore volume distributions from our adsorption measurements.

Char Reactivity

High Temperature Conversion

To calculate the conversion of the chars generated under different atmospheres and residence times, the ash content of the samples was used as a tracer by assuming that the mass of the ash remains constant. Measured amounts of air-dried chars were burned in air at a temperature of 800°C for more than 5 hours. The ash content was then determined gravimetrically from mass measurements made before and after complete combustion. From the known ash content, the char conversion can be derived as follows:

$$M_{coal} = M_{ash} + M_c \tag{4}$$

$$M_{char} = M'_{ash} + M'_c \tag{5}$$

where M_c is the mass of combustible material. The relative ash contents of the coal and char samples, $R_{ash} = \frac{M_{ash}}{M_{coal}}$, and $R'_{ash} = \frac{M'_{ash}}{M_{char}}$, are determined experimentally. The measurement error is about ± 5%. The mass of char produced from a given mass of coal is,

$$M_{char} = M_{coal} \frac{R_{ash}}{R'_{ash}} \tag{6}$$

Combining Eqs. 4 to 6, the conversion of combustible material, η, becomes

$$\eta = \frac{M_{coal} - M_{char}}{M_c} = \frac{R'_{ash} - R_{ash}}{R'_{ash}(1 - R_{ash})} \tag{7}$$

Low Temperature Conversion

Chars were oxidized under a flow of 5% O_2 in N_2 at 773K in a Dupont model 951 Thermogravimetric Analyzer (TGA). The typical sample size was about 5 mg. The sample was first heated in nitrogen at a rate of 30 K min^{-1} to the desired temperature. Oxygen was then immediately introduced. The measurements were conducted under isothermal conditions. The gas flow rate was 150 cm^3 min^{-1} for all runs. This flow rate was selected to avoid entrainment of the low density materials while eliminating diffusion resistance. The sample mass was continuously recorded using a data acquisition system. To correct for different ash contents of the various chars, the mass of ash was deducted from the total mass. Although the reaction was allowed to proceed for 2 hours, some unreacted combustible material remained. The temperature of the TGA was increased to 1073K after about 90% conversion to burn out completely the residual carbon then reduced back to 773K when the ash mass was recorded. To discriminate between the TGA measurements and those obtained in drop-tube reactor experiments at high temperature, the TGA conversion is labeled χ, and defined separately as

$$\chi = \frac{M_{initial} - M_{measured}}{M_{initial} - M_{ash}} \qquad (8)$$

where $M_{initial}$ is the sample mass at the moment oxygen was admitted.

Results and Discussion

Properties of chars produced under different conditions are listed in Table 3. The char morphology was examined by scanning electron microscopy. As Fig. 1 shows, the original coal particles were angular with a maximum aspect ratio about 5. Upon exposure to 1600K in nitrogen for 100 ms (Fig. 2), the particles started to change shape to spherical. At the same time the evolution of volatiles and trapped gases opened the pores on the particle surface (Fig. 2). These pores had a very broad size range from less than 1 μm to larger than 20 μm. Numerous ash particles appeared on the surface of char particles. When the residence time was increased to 200 ms, the particles became quite spherical (Fig. 3), and "Blow holes" (following the terminology of Anson et al., 1971) appeared on the particle surface. As the residence time was further increased to 300 ms, the coal particles became cenospheres (Fig. 4). In 1% oxygen, the "blow-holes" appeared only for the 100 ms sample (Fig. 5). At 200 ms, the particles had lost a large fraction of their mass but kept their integrity by cross partitions (Fig. 6). Fragmentation occurred after 300 ms of combustion (Fig. 7). Raising the oxygen concentration increased the combustion rate. In 5% oxygen, the morphology of char particles collected at 100 ms was similar to that of the particles generated at 200 ms in 1% oxygen (Fig. 8). At 200 ms residence time, the large loss of mass caused some particles to lose their integrity (Fig. 9). The fragmentation was significant after 300 ms residence time (Fig. 10). Comparing the original coal and the chars produced in nitrogen and oxygen, the char particles are more spherical as a result of the softening and swelling of the coal particles upon injection in the furnace. Although the original coal was sieved into a narrow size cut, the irregular particle shape prevents a direct evaluation of the degree of swelling. This irregular shape as well as the variation of the chemical composition among individual coal particles resulted in char particles possessing varied visible structures. The char particles seemed to burn at constant size until they fragmented. Comparison of the chars generated in nitrogen and oxygen showed some differences. Firstly, a great number of pores of less than 5 μm diameter appear on the surface of char particles produced at 100 ms in nitrogen. After devolatilization, cracks were formed at the thinner walls of the hollow particles (Figs. 3 and 4). Some particles were

then broken into small fragments. In an oxidizing atmosphere, oxygen penetrated into the interior of the particles through the opened pores and mass removal by oxidation was observed around the pore mouths. Fragmentation took place only when almost all carbon was consumed (Figs. 6-8). Secondly, quite large ash particles appeared on the surface of nitrogen chars. The ash particles for oxygen chars were relatively small and adhered on the carbon skeleton. They grew gradually by coalescence as reactions proceeded.

Figs. 1 to 10 show the formation and growth of macropores. Information about the micropores ($15 \leq r \leq 120$ Å) and the total surface area was obtained by N_2 adsorption. For all of the chars, the surface area and the volume of micropores increased dramatically within the first 100 ms over the values for the original coal, indicating new pore formation and the pore growth (Figs. 11 to 15). The trends at later times, however, differed. The surface areas and pore volumes of nitrogen chars increased with time. The peak observed at about 20 Å in the pore volume distribution of N2 char, and the change of C/H ratio (Table 3) suggested that there were still some small molecules released when the residence time was increased to 200 ms. In oxygen atmospheres, both surface area and volume of micropores first increased and then decreased after 100 ms. The decrease of micropores could be caused either by pore closure or pore growth to larger sizes. It should be noted that although the oxygen concentration in these experiments was only 1 to 5%, the bulk gas concentration did not change appreciably along the reactor because of the small coal feed rate.

Little information is available about the change of char surface area with the pyrolysis time of coal. Anson et al. (1971) and Smith and Tyler (1972) reported direct observation of surface area changes during coal combustion. The surface area for 53-63 μm Ackton Hall coal (CRC 502) particles burning in air at about 75 ms was about twice that of the original coal (Anson et al., 1971). As the residence time increased to 85 ms, the surface area increased continuously, from 111 to 125 $m^2 g^{-1}$ on dry ash free basis. The surface area started to drop near the completion of devolatilization. It was 88.5 $m^2 g^{-1}$ at approximately 130 ms, while the devolatilization ended at about 150 ms. Smith and Tyler (1972) measured the variation of surface area of semi-anthracite coal particles during combustion at temperatures of 1400K to 2200K and oxygen pressures about 0.1 and 0.2 atm. The surface areas first increased then steadily dropped with increasing burnout. The peak appeared between about 15 to 35% burnout, corresponding to the coal particle sizes 78 to 22 μm. The surface areas also decreased with increasing gas temperatures. The particle size and density were found both to reduce with burnout, indicating that the oxygen partially penetrated into the pore structure. The surface area of char generated in nitrogen

for two seconds was also reported to decrease when burning in air (Sahu, 1988). Smith and Tyler (1972) collected partially burned chars and examined them by optical microscopy, porosimetry and X-ray diffraction. They reported that macropores (> 0.02 μm) increased with burnout, but micropores (< 0.02 μm) decreased. A sharpening of a graphite band in the X-ray pattern indicated that some structural ordering took place. The decrease in surface area was believed to be related to the closure of micropores associated with thermally induced alterations in solid structure.

The ash content and the carbon conversion (η as defined in Eq. 7) in chars produced under different conditions are plotted in the Figs. 16 and 17. In our drop-tube reactor experiments, the bulk of devolatilization of coal particles in nitrogen was completed within 100 ms as shown by the approximately equal ash contents of N1 and N2 chars, although there were some changes of C, H, and N contents measured by elemental analysis. The volatile yield was 10% higher than the value given by the ASTM proximate volatile analysis (Table 1) due to high temperature and the rapid mass and heat transfer. The weight loss, or conversion, increased with oxygen concentration. For the chars generated in oxygen, conversion also increased with residence time. The conversion calculated with initial carbon the carbon remaining after pyrolysis in N_2 for 100 ms, and excluding ash is given by

$$\eta' = \frac{\eta - \eta_{N1}}{(1 - \eta_{N1})} \tag{9}$$

are listed in Table 3. Even within 100 ms, there was 26% fixed carbon burned in 1% O_2 and 18% more in 5% O_2. By 300 ms, more than one third of the fixed carbon was lost in 1% O_2, and over 80% fixed carbon was consumed in 5% O_2. Jost et al. (1984) studied the devolatilization of pulverized coal in a flow tube reactor at gas temperatures between 1300K and 2000K and oxygen concentrations between 7% and 16%. They reported that the devolatilization rates increased with increasing oxygen concentration for a given gas temperature. They suggested that energy from the oxidizing volatiles was fed back to the coal particles, increasing their temperature and thereby the volatile release rate and yield. An increase of the particle temperature due to the oxidation of volatiles was also reported by Seeker et al. (1981). Devolatilization rates and yields increase with particle temperature have also been observed in experiments by Kimber and Gray (1967) and Kobayashi et al. (1977).

The char conversions, χ as defined in Eq. 8, are measured with the TGA and plotted in Figs. 18 to 20. The apparent reaction rates in Figs. 18 to 20 were obtained by differentiating the conversion curves. The char reactivities were obviously affected by the charring history. In all cases the char reactivity decreased with the content of oxygen. As shown in Figs. 18 to 20, the apparent rates increase sharply during the first 5 to 10% carbon conversion and then decrease. This phenomenon could result from the gradual chemisorption of oxygen. The sample was initially heated in nitrogen to reach the desired temperature. Oxygen was then immediately introduced. The gas composition over the sample, however, changes gradually from pure nitrogen to a final mixture of 5% oxygen in nitrogen. Jenkins et al. (1973) suggested that oxygen complex formation at the surface and char activation may also be important at this early stage of conversion. After the apparent rates reached the maximum, they decreased with time. The difference in apparent rate among the various chars decreased with conversion. After 60 to 70% carbon conversion, all the chars oxidized with quite similar rates. At the low temperature of the TGA experiments, the reaction is under kinetic control as it can be shown by an estimate of the Thiele modulus for the reaction. To achieve 70% conversion needs 40 to 60 minutes. During this long period, the more reactive fraction of the combustible material would have burned, leaving behind the more inert fraction. Significant reorganization of char structure could also have been completed. Therefore, the difference in chemical and physical properties of the various chars, which affect the reaction rate, could have been largely eliminated resulting in more uniform oxidation rates.

Conclusions

Structural changes of char and their effect on char reactivity have been examined under pulverized coal combustion conditions. When heated in neutral or oxidizing atmosphere, the great majority of the hvA bituminous coal (PSOC 1451) particles undergo a series of structural changes. Hollow sphere are formed, followed by particle fragmentation. In 1 or 5% oxygen, oxidation proceeds both externally and internally at approximately constant diameter until the onset of fragmentation. For all of the chars, the surface area and the pore volume in the size range 15 to 120 Å increased dramatically within the first 100 ms compared with the original coal. The ratio of carbon to hydrogen increases with residence time. Carbon conversion at 1600K also increases with increasing oxygen pressure. But the char reactivity measured at the low temperature TGA experiments was decreased. Significant structural reorganization occurred either simultaneously with devolatilization or continuously after devolatilization depending on the oxygen

concentration. Oxygen appeared to accelerate the structural changes and to change the reactivity of the char.

ACKNOWLEDGEMENTS

This work was supported by the U.S. Department of Energy, University Coal Research Program under grant number DE-FG22-88PC88911.

REFERENCES

Anson, D., Moles, F. D., and Street, P. J. (1971), *Comb. & Flame*, 16, 265.

Cranston, R. W., and Inkley, F. A. (1957), *Adv. In Cat.*, 9, 143.

Haussmann, G. J., and Kruger, C. H. (1988), *22nd Symp. (Int.) on Comb.*, The Combustion Institute, Pittsburgh, PA, 223.

Jenkins, R. G., Nandi, S. P. and Walker Jr., P. L. (1973), *Fuel*, 52, 288.

Jost, M., Leslie, I., and Kruger, C. (1984), *20th Symp. (Int.) on Comb.*, The Combustion Institute, Pittsburgh, PA, 1531.

Kimber, G. M., and Gray, M. D. (1967), *Comb. & Flame*, 11, 360.

Kobayashi, H., Howard, J. B., and Sarofim, A. F. (1977), *16th Symp. (Int.) on Combustion*, The Combustion Institute, Pittsburgh, PA, 411.

Levendis, Y. A., and Flagan, R. C. (1987), *Comb. Sci. & Tech.*, 53, 117.

Levendis, Y. A., Flagan, R. C., and Gavalas, G. R. (1989), *Comb. & Flame*, 76, 221.

Lippens, B. C., Linsen, B. G., and de Boer, J. H. (1964), *J. cat.*, 3, 32.

Northrop, P. S. (1988), *A Fundamental Study of Char Combustion: Chunges in Particle Morphology during Oxidation*, Ph. D. Thesis, California Institute of Technology.

Northrop, P. S., Gavalas, G. R., and Flagan, R. C. (1987), *Langmuir*, 3, 300.

Sahu, R. (1988), *On the Combustion of Bituminous Coal Chars*, Ph. D. Thesis, California Institute of Technology.

Seeker, W. R., Samuelsen, G. S., et al. (1981), *18th Symp. (Int.) on Comb.*, The Combustion Institute, Pittsburgh, PA, 1213.

Smith, I. W. (1982), *19th Symp. (Int.) on Comb.*, The Combustion Institute, Pittsburgh, PA, 1045.

Smith, I. W. and Tyler, R. J. (1972), *Fuel*, 51, 312.

Wells, W. F. and Smoot, L. D. (1991), *Fuel*, 70, 454.

Wheeler, A. (1946), *Catalyst Symposium, Gibson Island AAAS Conference*.

Table 1 Properties of Raw Coal

PSOC #	1451
Rank	HVAB
Location	Pennsylvania
Seam	Pittsburgh
Proximate Analysis (%)	
moisture	2.54
ash	13.32
volatiles	33.56
fixed carbon	50.58
Ultimate Analysis (%)	
ash	13.32
carbon	70.05
hydrogen	4.55
nitrogen	1.33
sulfur	1.33
chlorine	0.07
oxygen*	6.81
FSI	7.5

*moisture excluded

Table 2 Repeatability of the Surface Area Measurements

a. The measurements with the same sample:

Sample	Sample Size (gm)	Surface area (m^2)	Specific Surface Area (m^2/gm)	$\frac{\Delta S}{Si}$
1% O_2	0.0596	0.412	8.28	0.259
200 ms		0.511	10.43	0.205
5% O_2	0.1066	0.378	3.54	0.198
200 ms		0.453	4.25	0.166
5% O_2	0.0908	0.410	4.51	0.176
300 ms		0.482	5.31	0.149
γ-Al_2O_3	0.0136	2.12	155.1	0.118
		2.37	173.9	0.105

b. The measurements with the same material:

Sample	Sample Size (gm)	Surface area (m^2)	Specific Surface Area (m^2/gm)	$\frac{\Delta S_{max}}{Si}$
N_2*	0.2181	2.77	15.7	0.013
200 ms	0.2145	2.68	15.5	0.013
1% O_2	0.1164	0.811	8.36	0.248
200 ms	0.0596	0.511	10.43	0.198
	0.1405	24.0	170.8	0.092
γ-Al_2O_3	0.0497	8.39	168.8	0.093
	0.0136	2.12	155.1	0.101

*The char was 53-90 μm, and generated from 38-74 μm coal.

Table 3 Characterization of PSOC 1451 1600K Chars

char	time (ms)	name	R'_{ash} (%)	conversion (%)		S ($m^2\ gm^{-1}$)		mean mass fraction (%)			C/H
				η^1	η'^2	total	d.a.f.[3]	C	H	N	
N_2	100	N1	18.0 (21.6)[4]	46.6	-	4.15 (3.04)[4]	4.58 (3.27)[4]	68.02	0.86	1.14	79.09
	200	N2	17.7 (22.63)[4]	45.5	-	14.2 (12.7)[4]	16.8 (15.7)[4]	83.49	0.98	1.08	85.19
	300	N3	-	-	-	-	-	82.97	0.81	0.845	102.4
1% O_2	100	O11	22.9 (21.7)[5]	60.5	26.0	10.2 (9.33)[5]	12.6 (11.3)[5]	73.96	0.80	1.32	93.03
	200	O12	22.5 (27.5)[4]	59.6	24.3	6.97 (5.01)[4]	8.36 (6.08)[4]	74.51	0.69	1.30	108.0
	300	O13	25.5	65.7	35.8	-	-	74.99	0.65	1.20	115.4
5% O_2	100	O51	28.3	70.3	44.4	17.2	23.1	64.63	0.88	1.21	73.17
	200	O52	37.2	80.2	62.9	3.54	4.34	60.04	0.73	1.12	82.81
	300	O53	58.4	91.6	84.3	4.51	7.77	48.16	0.64	0.835	75.83

*1. R_{ash} = 10.5 (%); 2. η'_{N1} = 46.6 (%); 3. S_{ash} = 2.19 ($m^2\ gm^{-1}$)

4. The char was 53-90 μm, and generated from 38-74 μm coal; the coal feed rate is 5 gm $hour^{-1}$.

5. The char was generated from 53-61 μm.

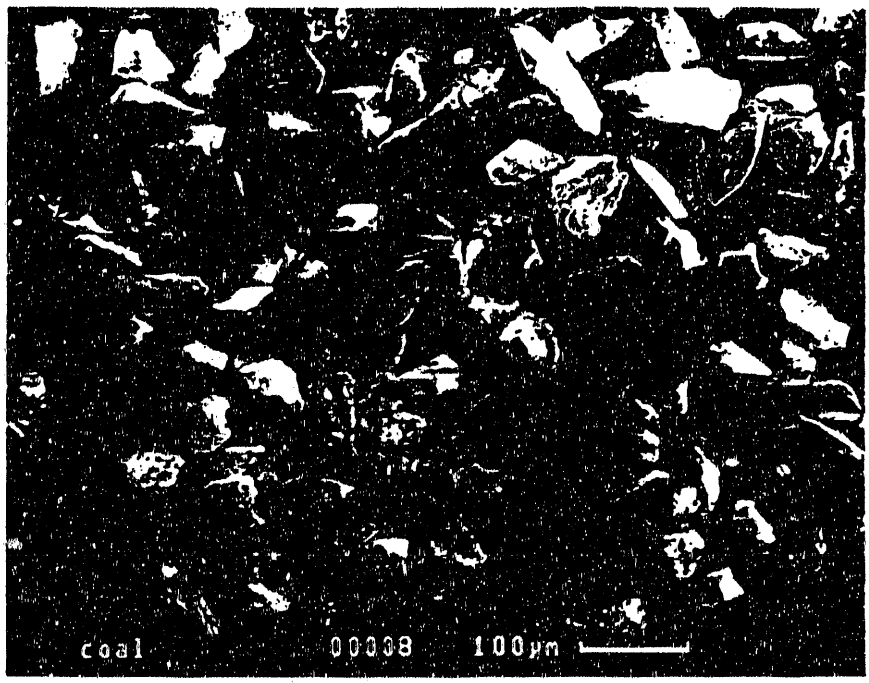

Fig. 1 Unreacted PSOC 1451 coal particles

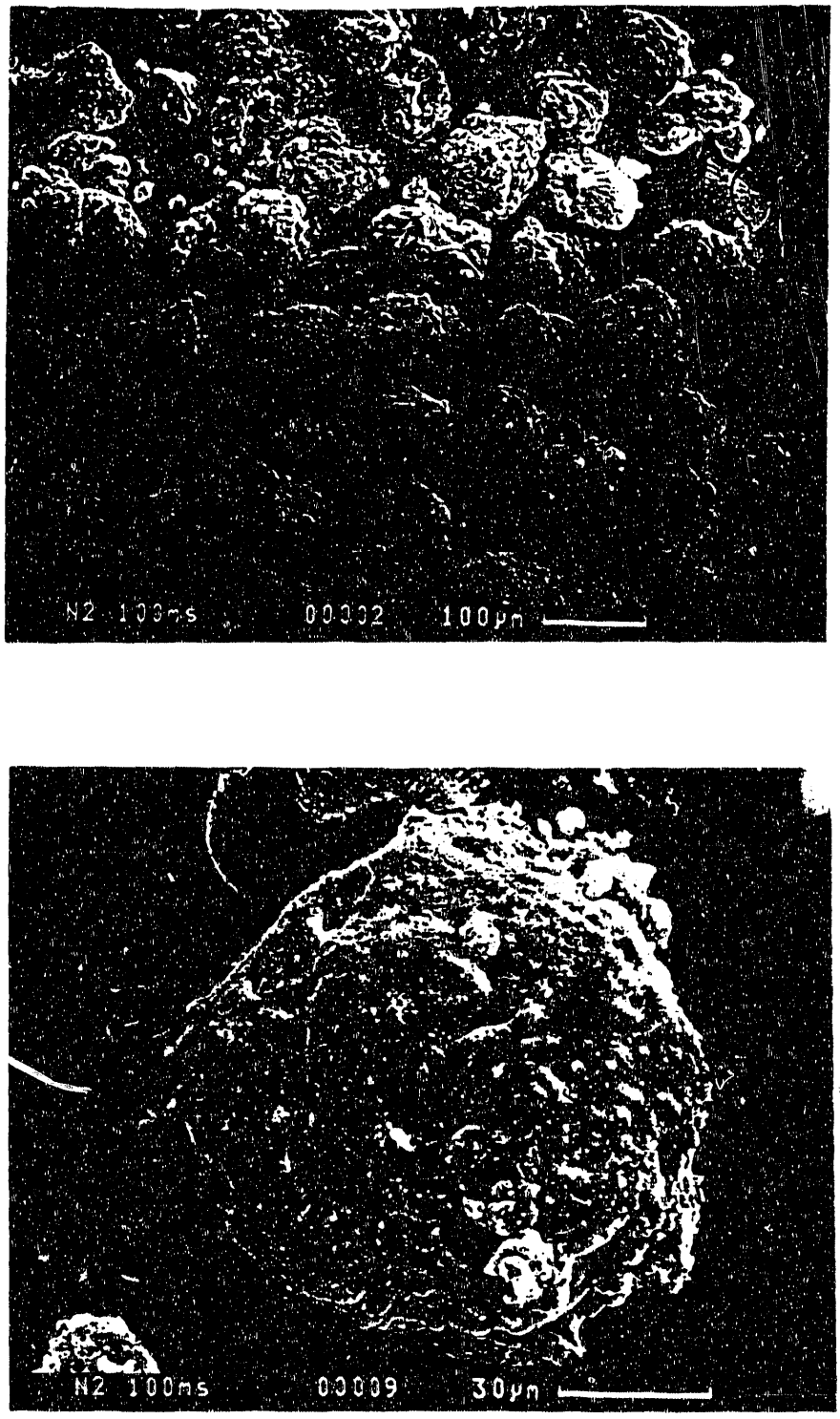

Fig. 2 Char particles produced in N_2 at 100 ms

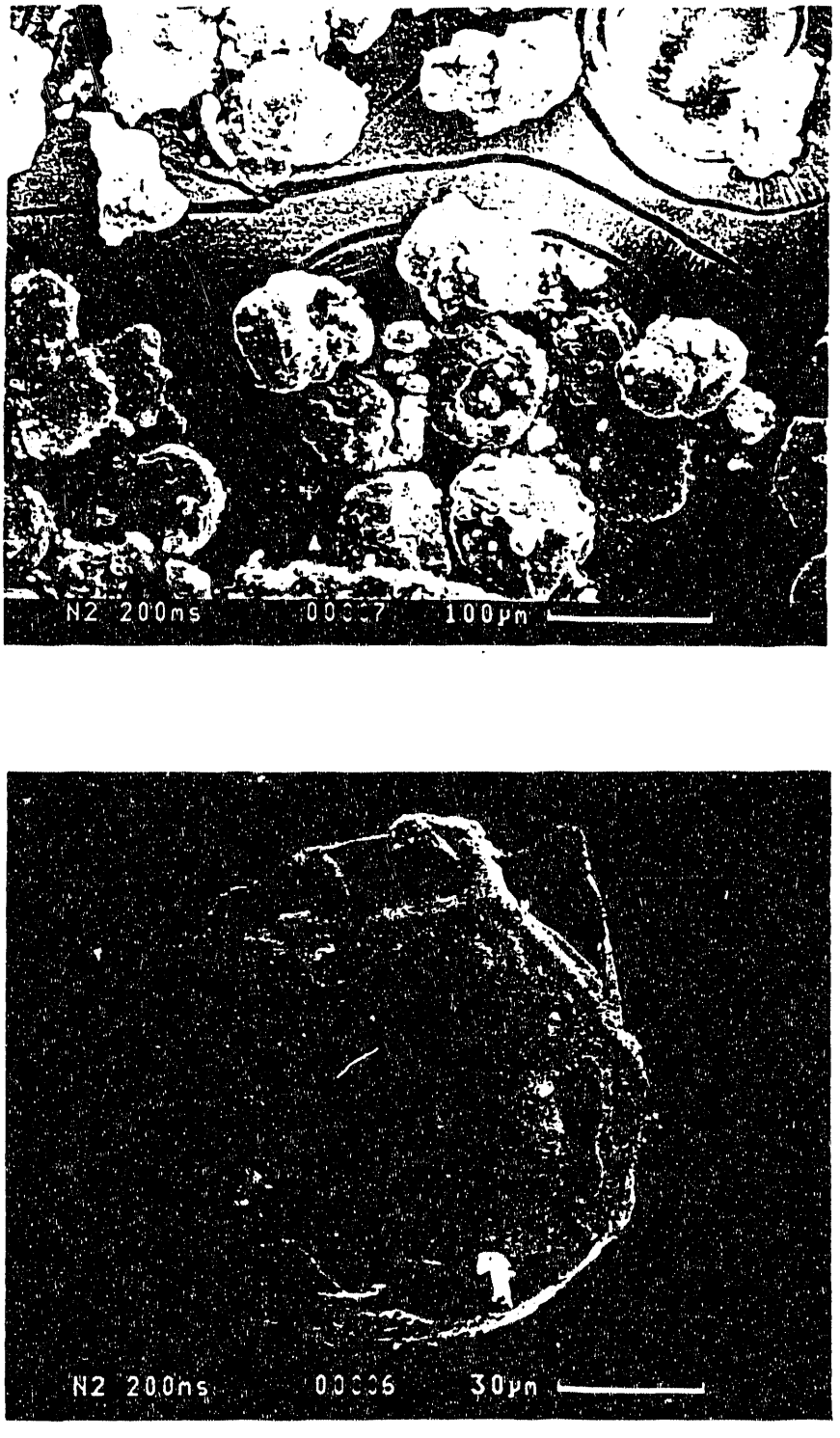

Fig. 3 Char particles produced in N_2 at 200 ms

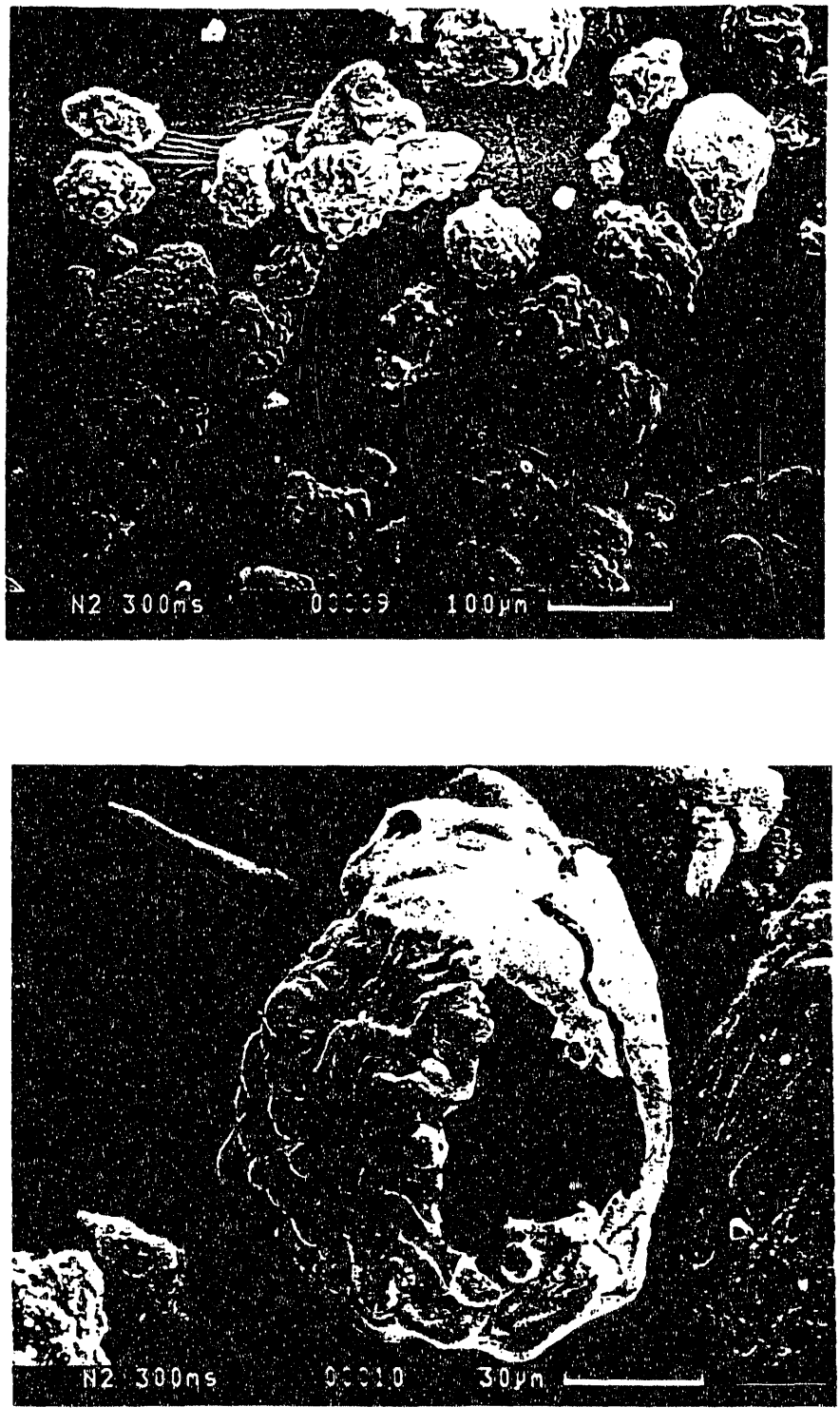

Fig. 4 Char particles produced in N_2 at 300 ms

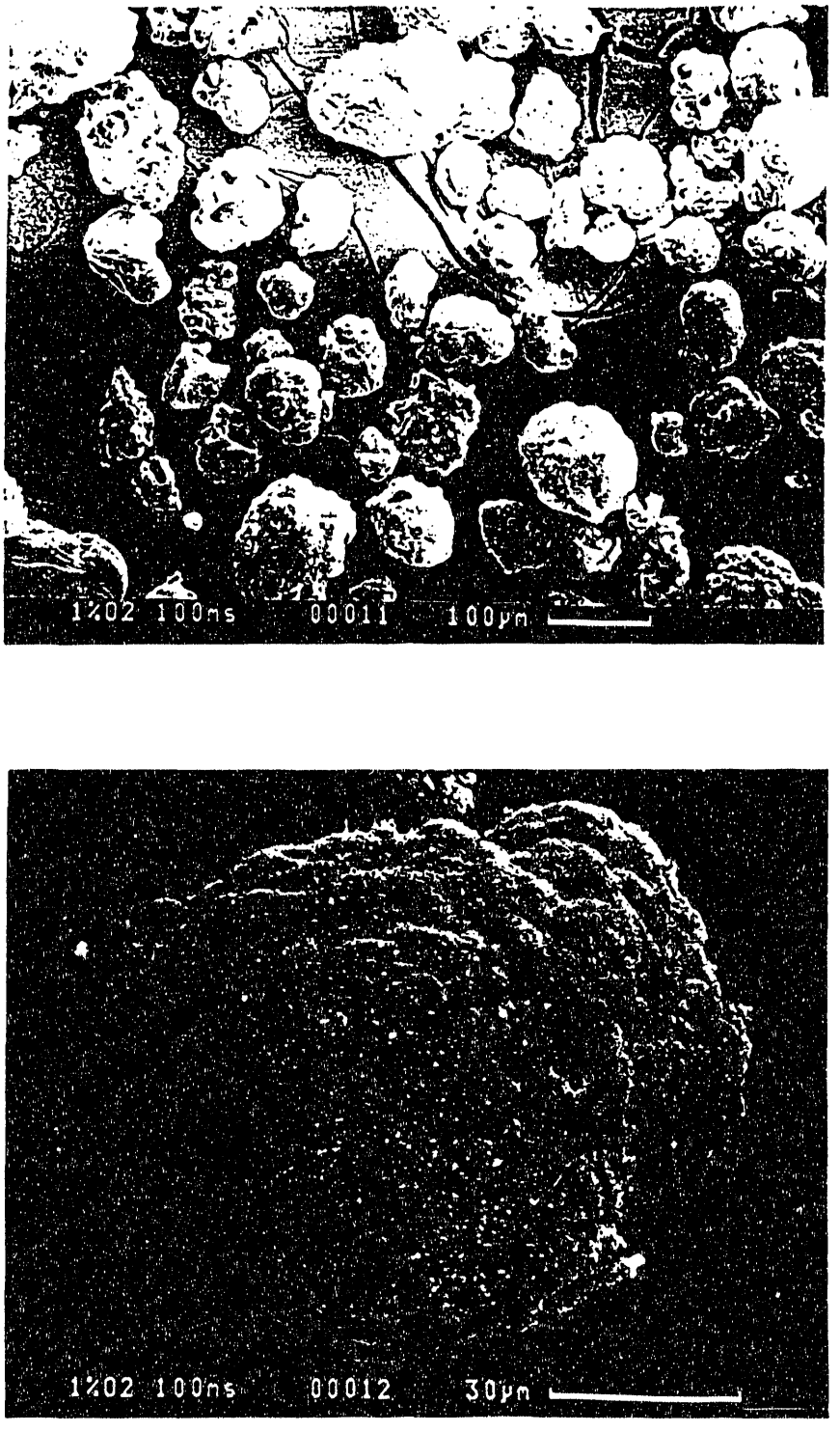

Fig. 5 Char particles produced in 1% O_2 at 100 ms

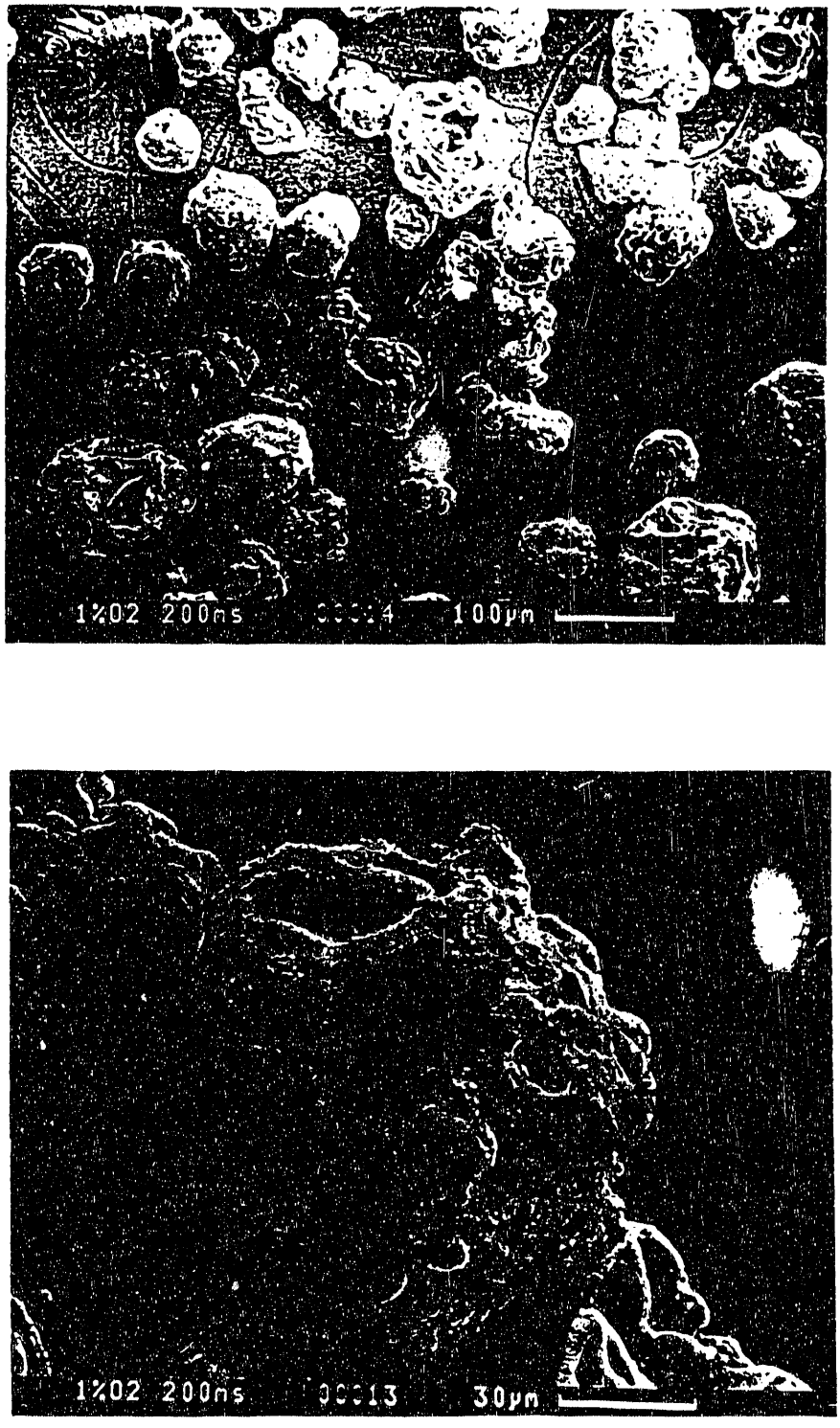

Fig. 6 Char particles produced in 1% O_2 at 200 ms

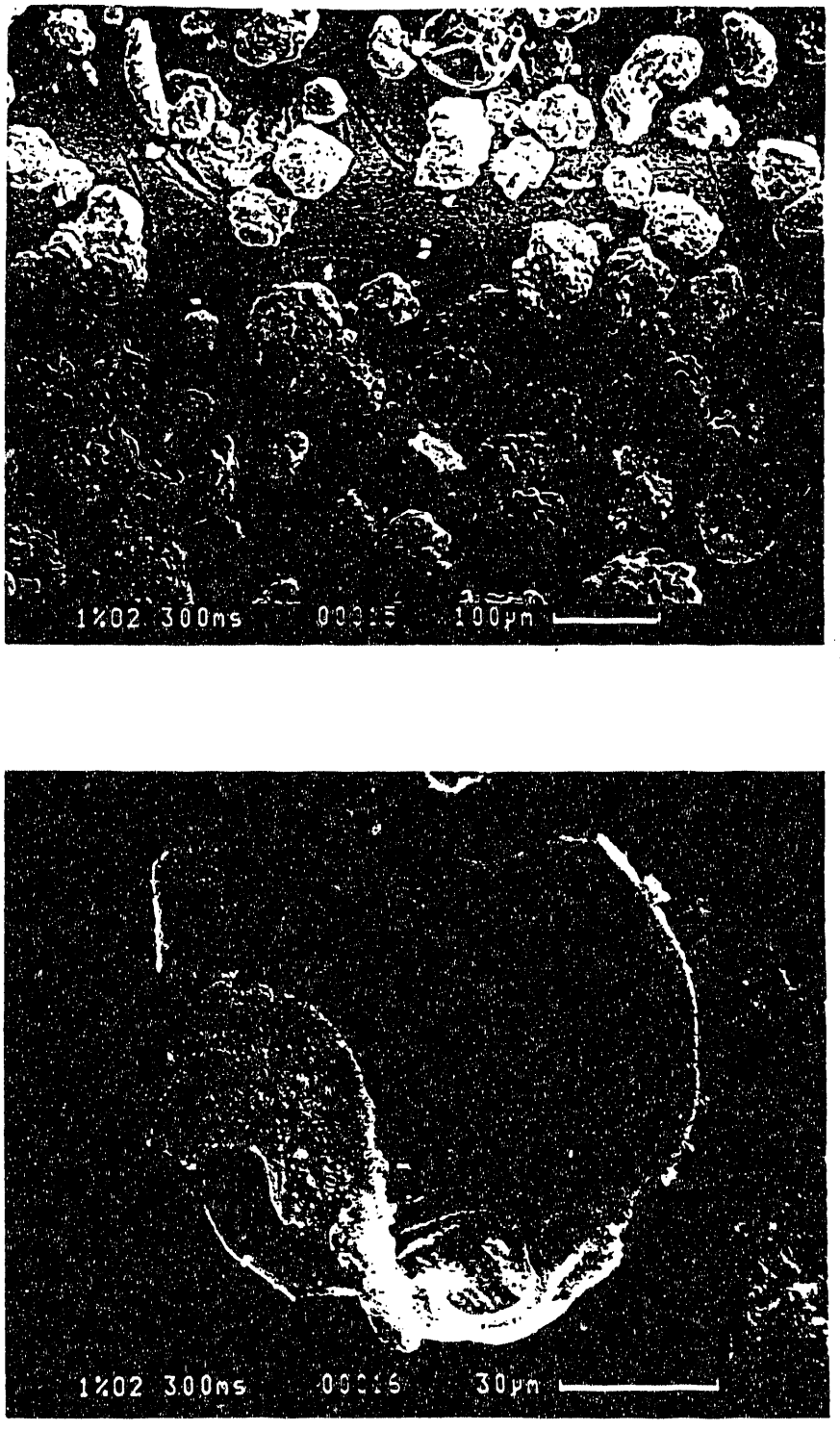

Fig. 7 Char particles produced in 1% O_2 at 300 ms

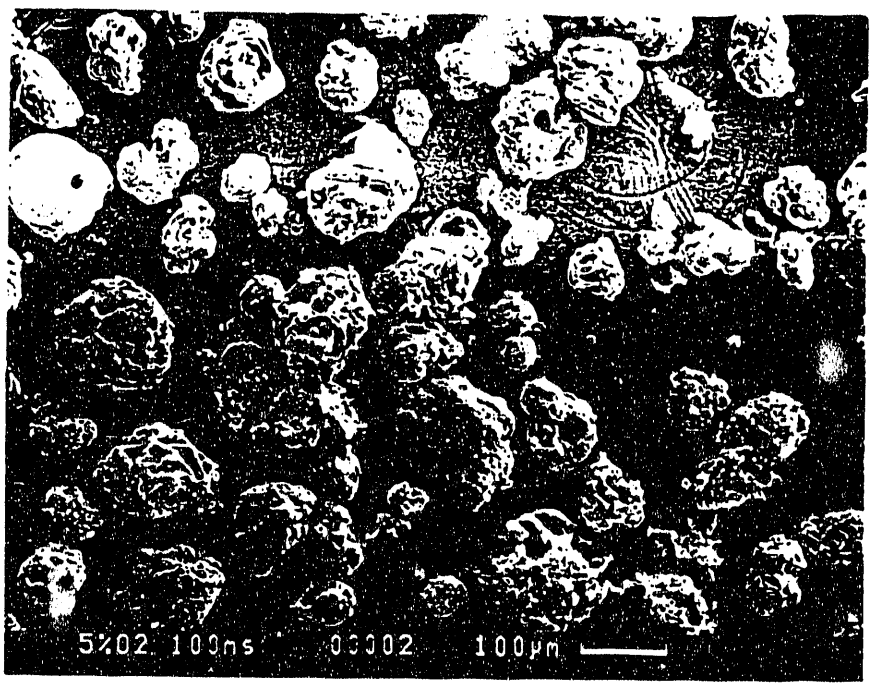

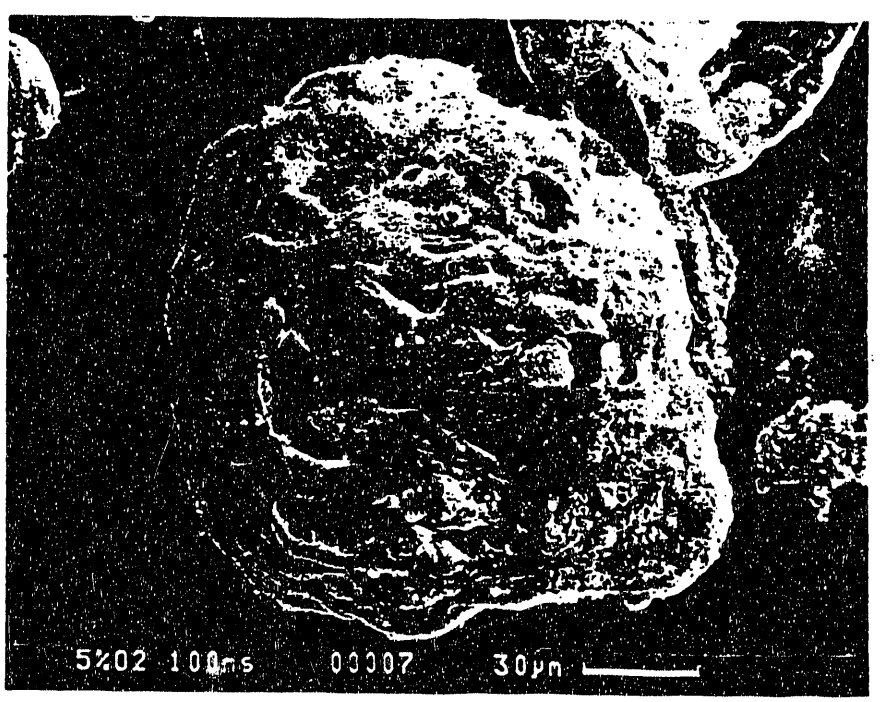

Fig. 8 Char particles produced in 5% O_2 at 100 ms

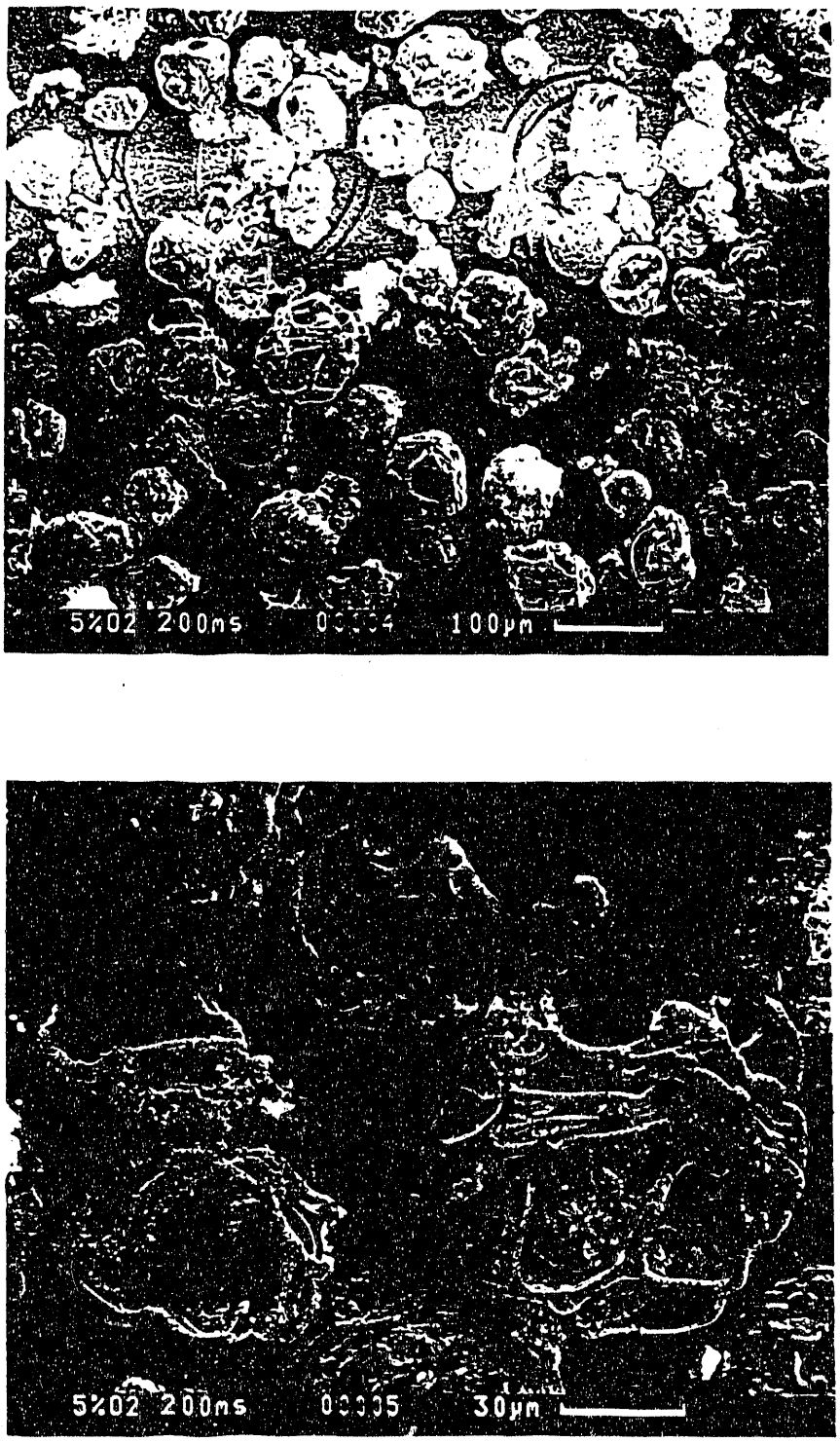

Fig. 9 Char particles produced in 5% O_2 at 200 ms

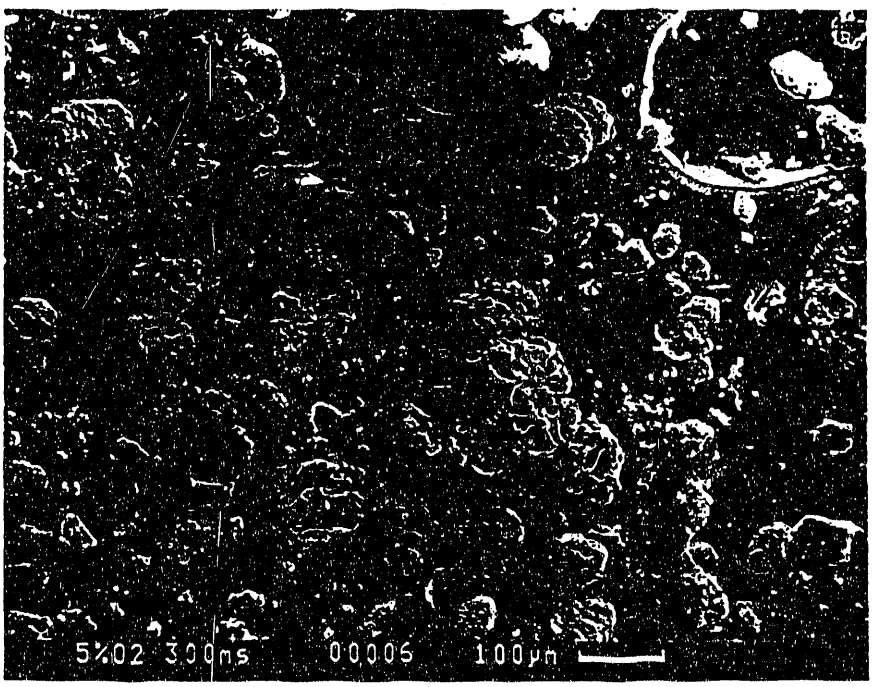

Fig. 10 Char particles produced in 5% O_2 at 300 ms

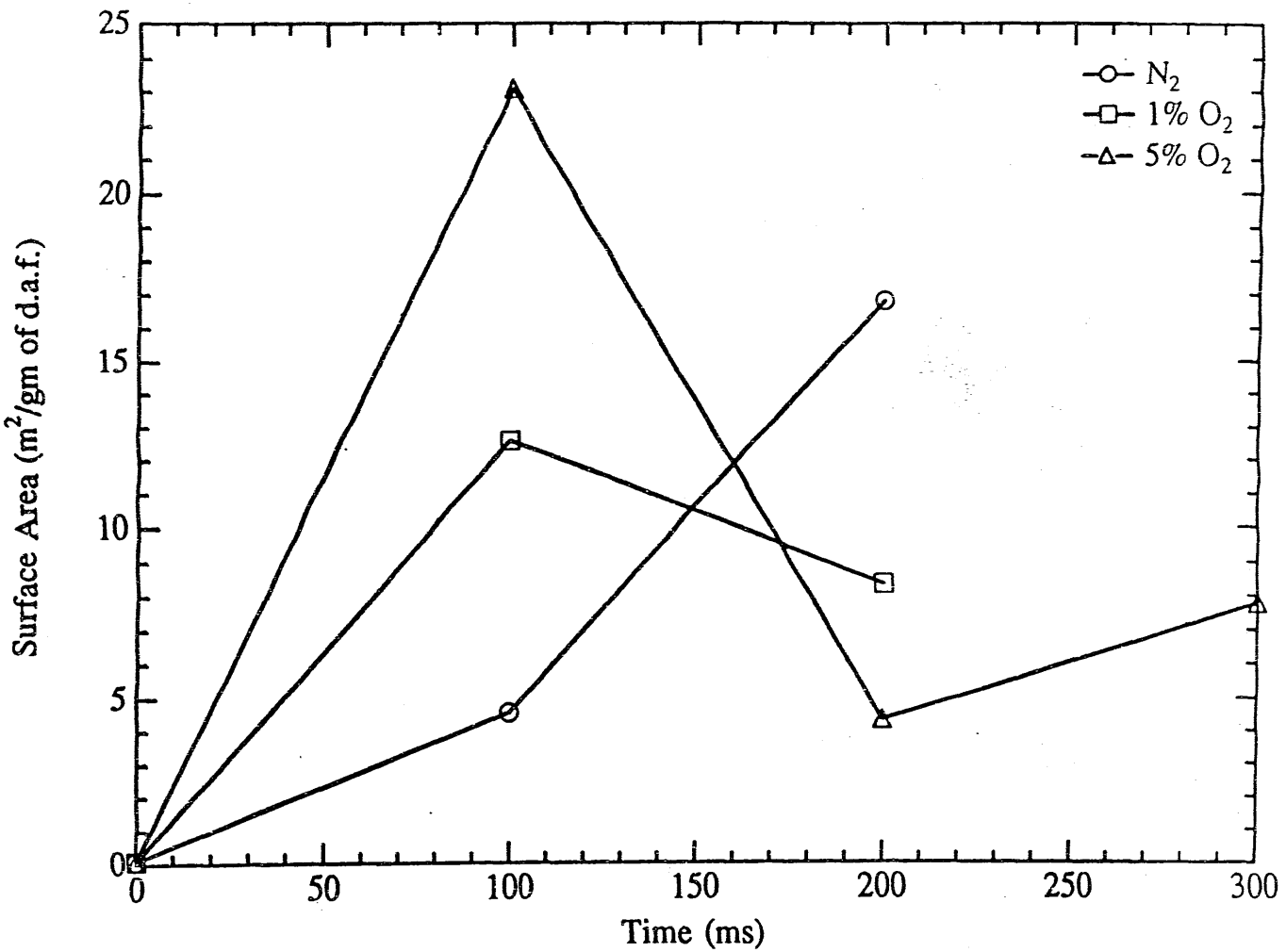

Fig. 11 Surface area of various chars at 1600K derived from drop-tube reactor experiments (dry ash free basis)

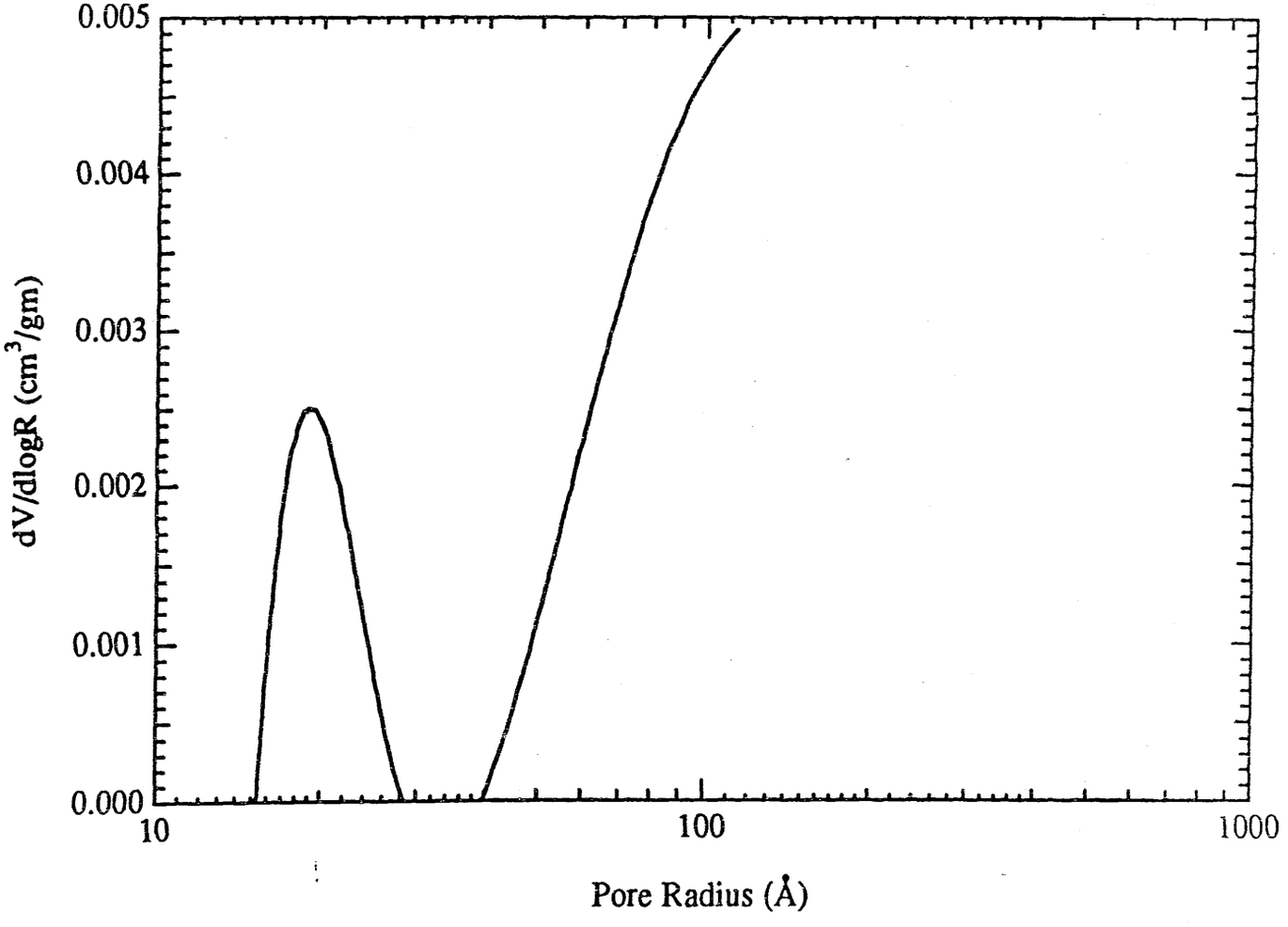

Fig. 12 Pore volume distribution of coal (PSOC 1451)

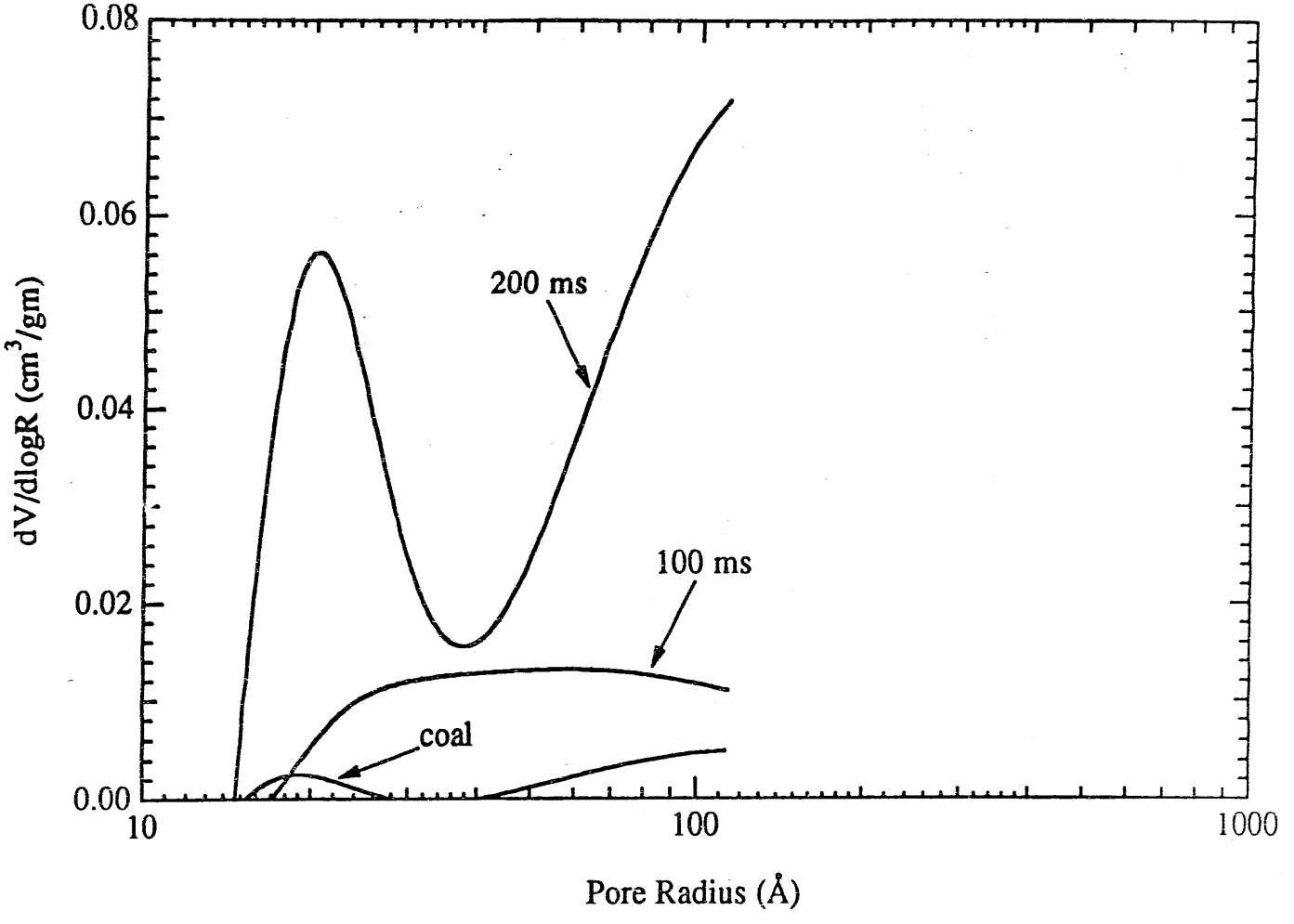

Fig. 13 Pore volume distribution of chars generated in N_2

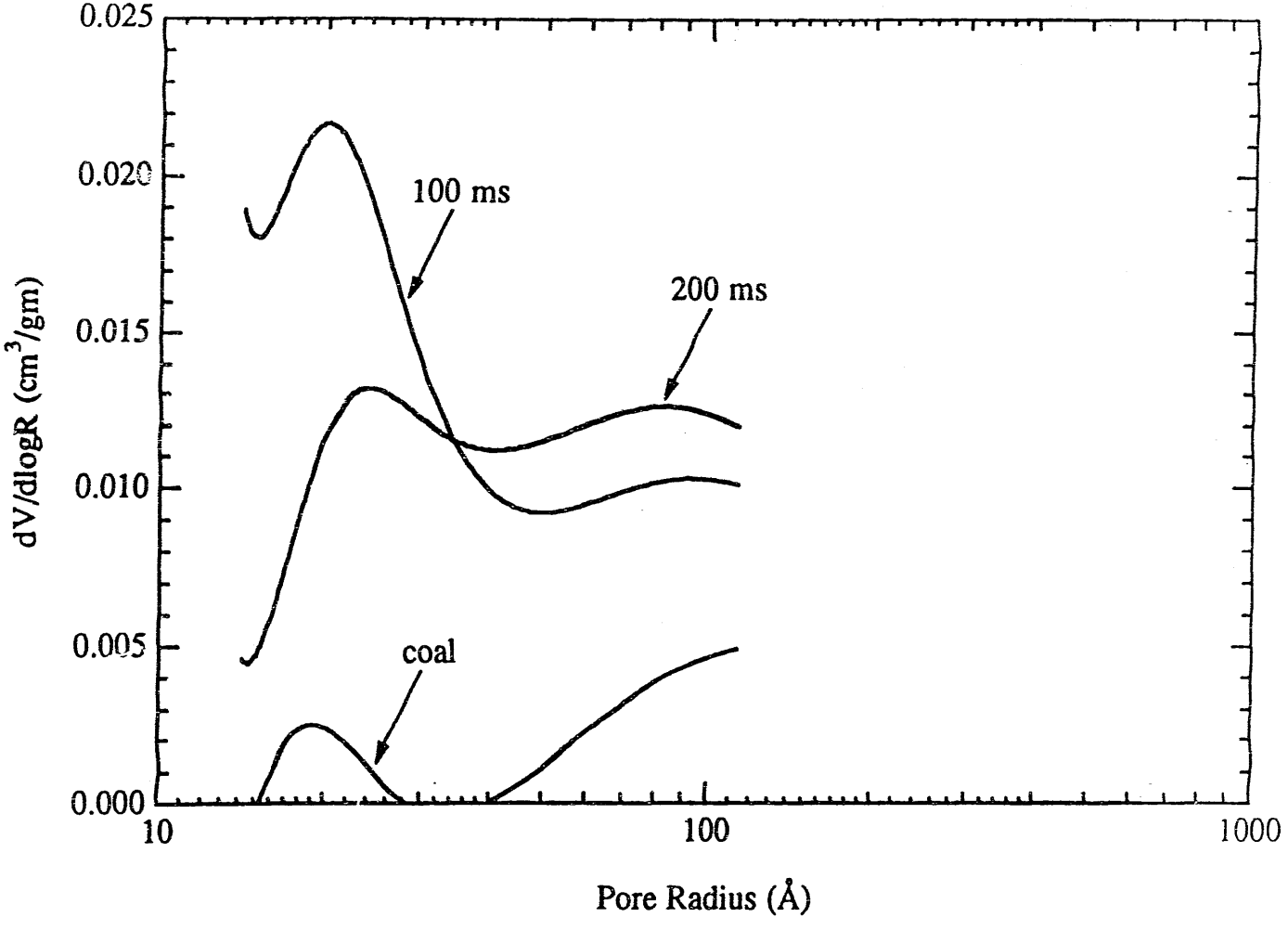

Fig. 14 Pore volume distribution of chars generated in 1% O_2

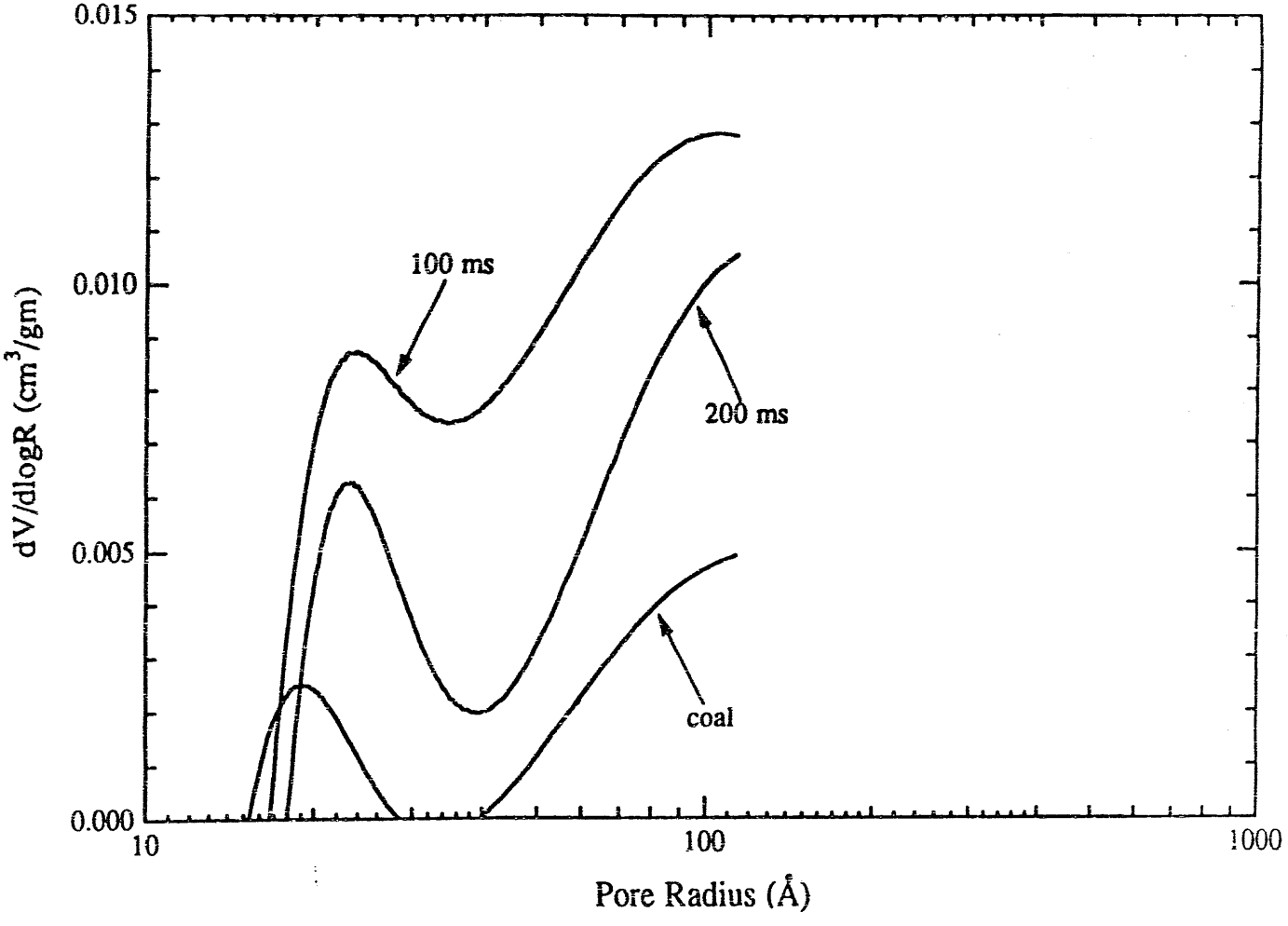

Fig. 15 Pore volume distribution of char generated in 5% O_2

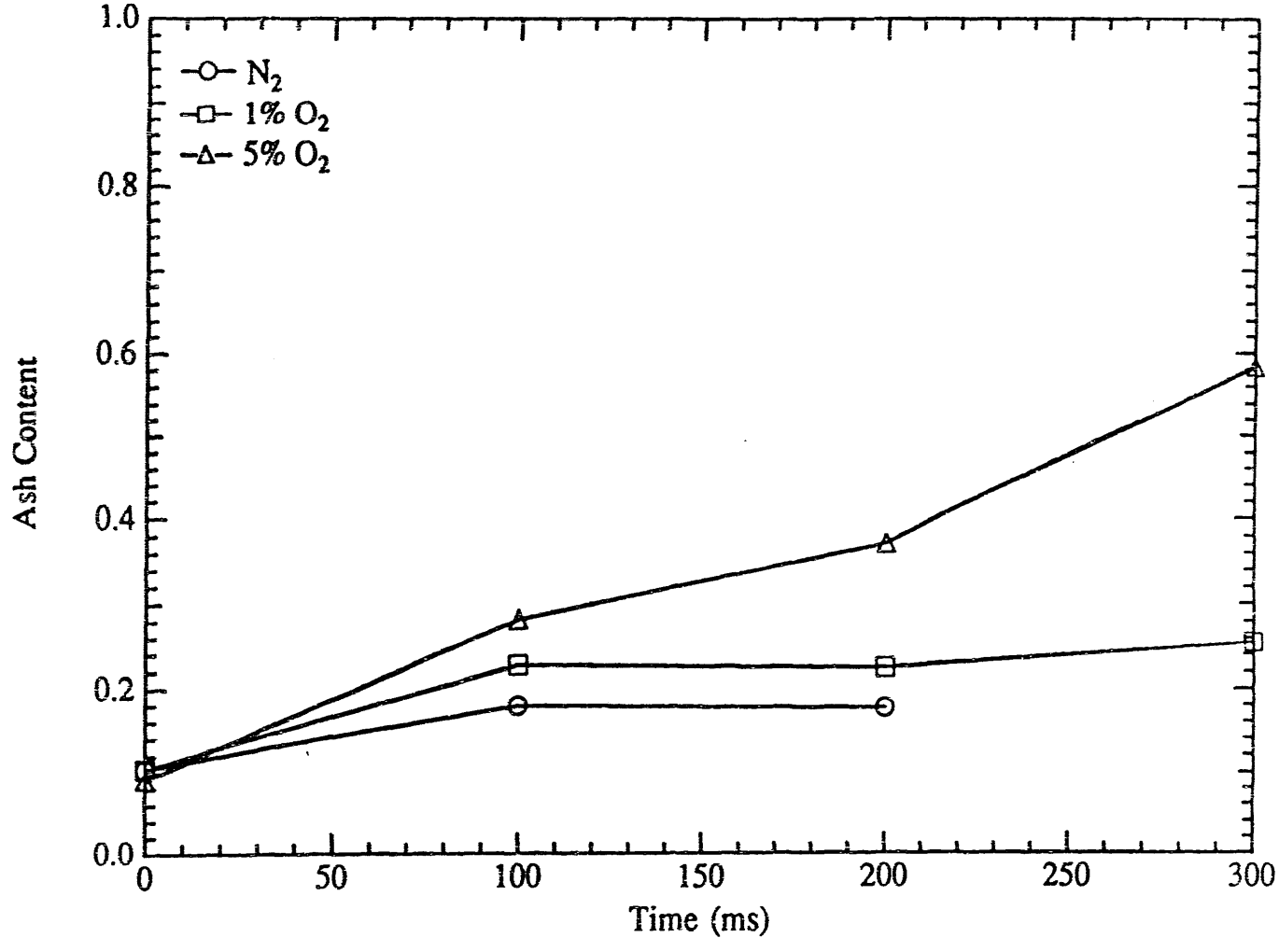

Fig. 16 Ash content of various chars at 1600K derived from drop-tube reactor experiments

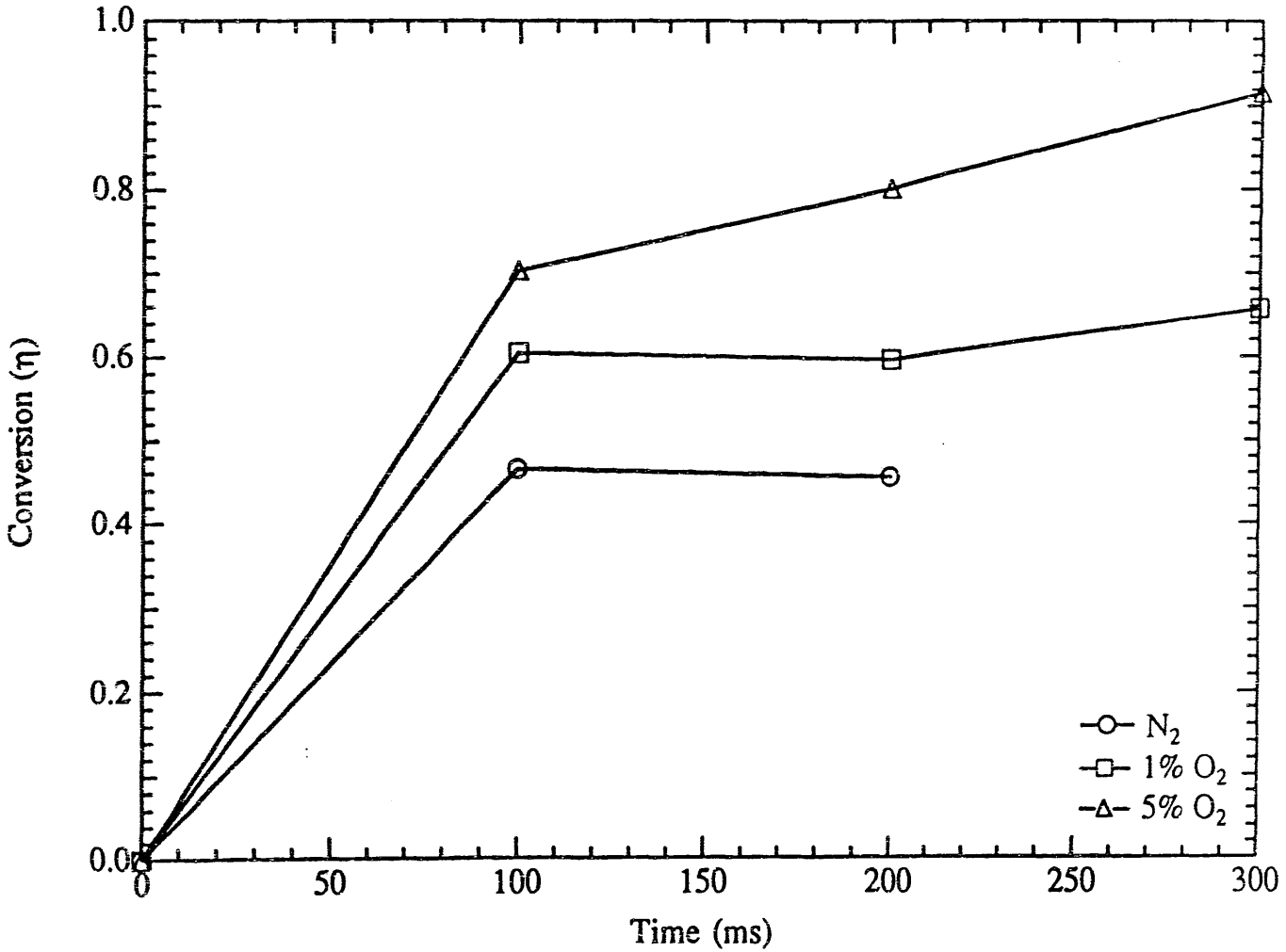

Fig. 17 Conversion of various chars at 1600K derived from drop-tube reactor experiments (dry ash free basis)

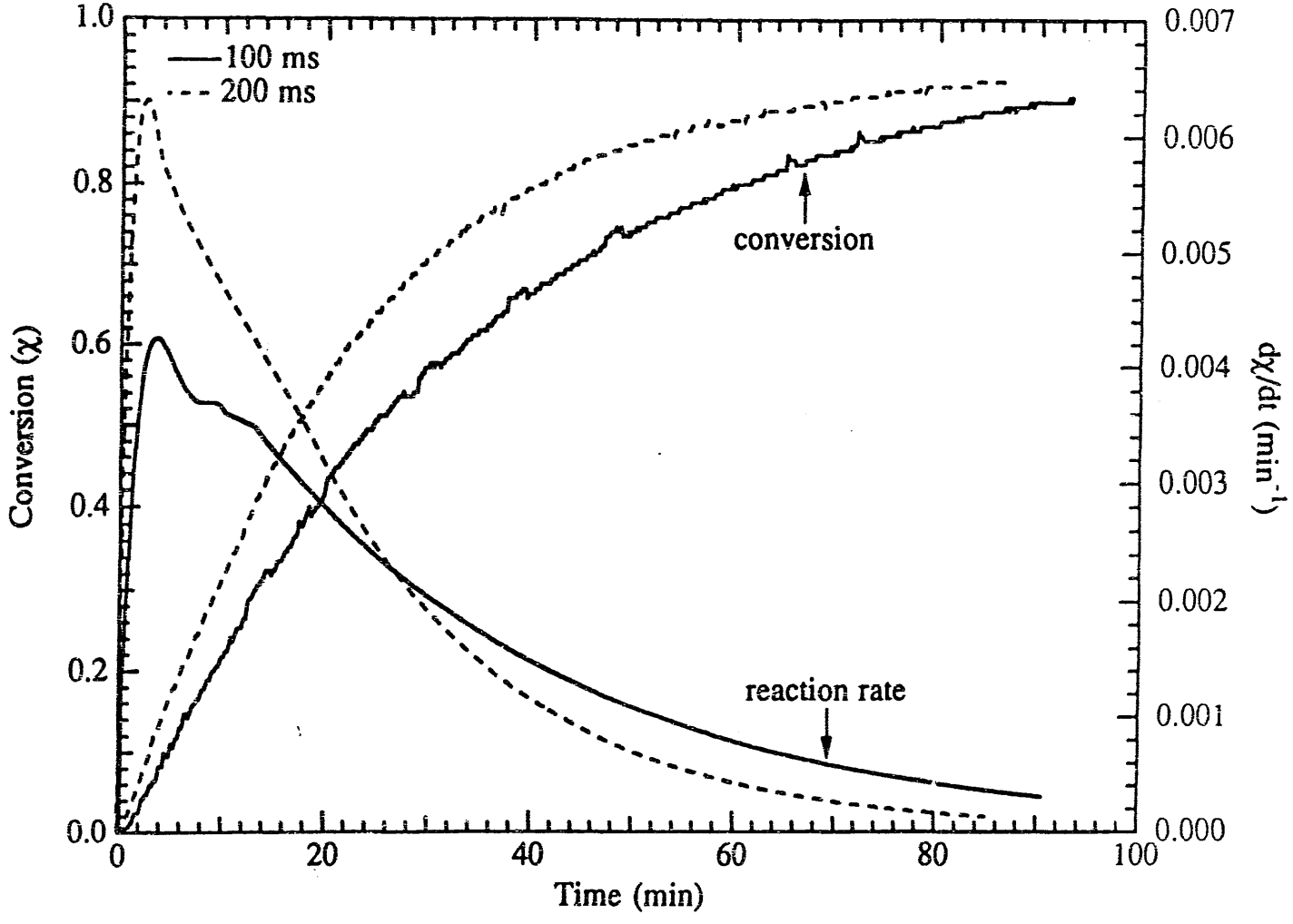

Fig. 18 TGA measurements of conversion and low temperature reactivities of chars generated at 1600K in N_2

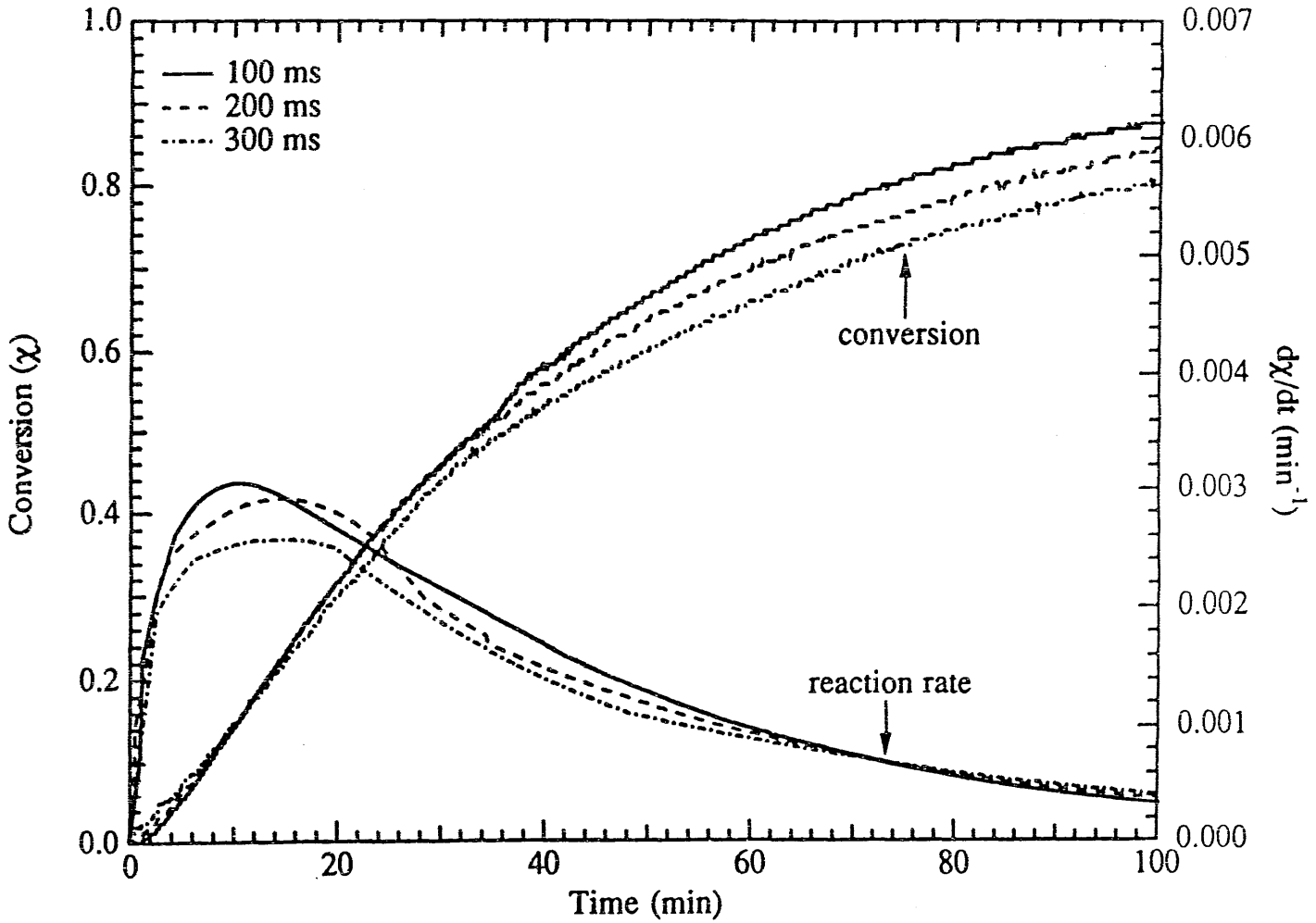

Fig. 19 TGA measurements of conversion and low temperature reactivities of chars generated at 1600K in 1% O_2

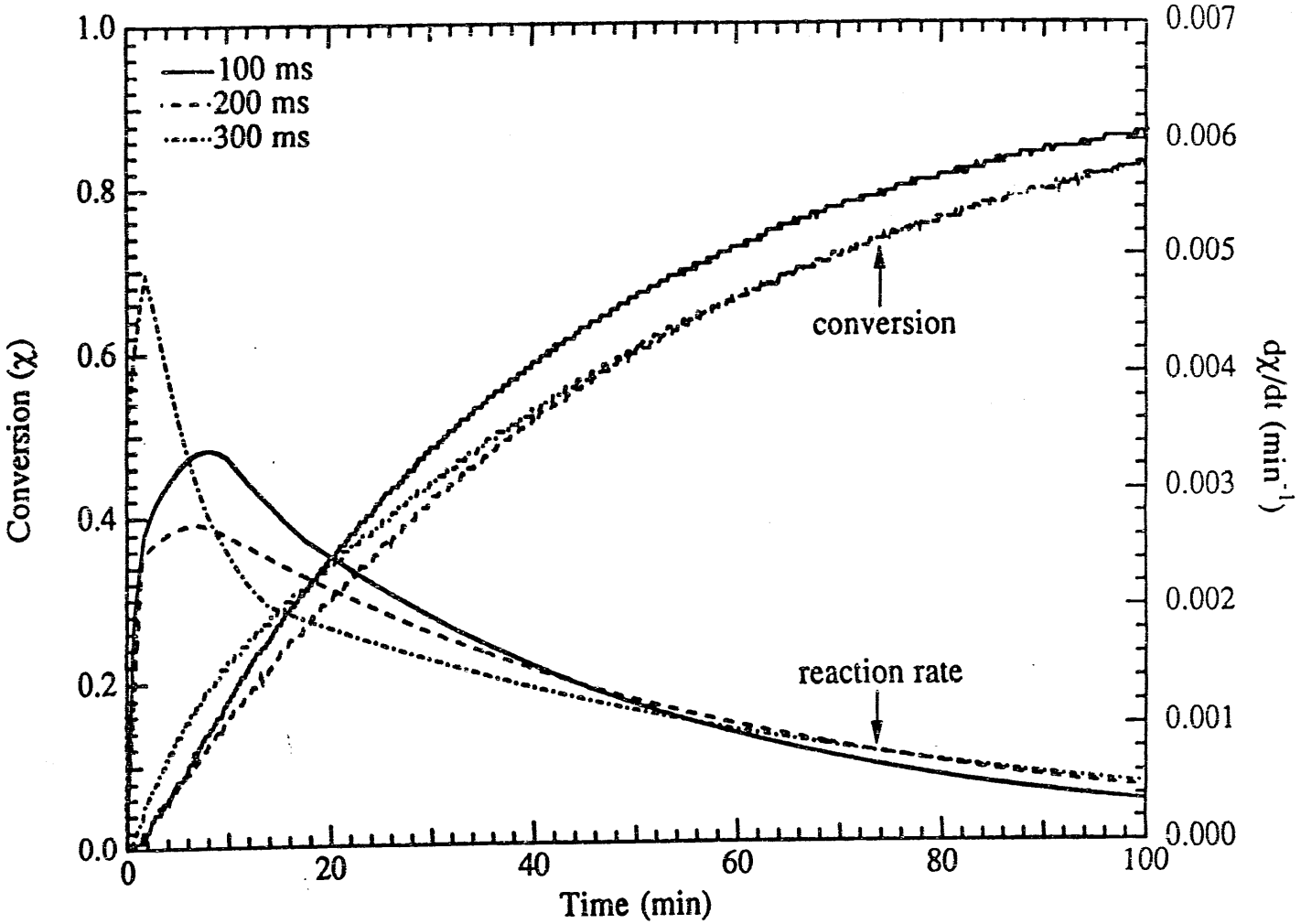

Fig. 20 TGA measurements of conversion and low temperature reactivities of chars generated at 1600K in 5% O_2

CHAPTER 3

EXPERIMENTS WITH THE ELECTRODYNAMIC BALANCE

The Effect of Char Formation Temperature on the Densification of a Bituminous Coal Char during Gasification

(Manuscript to be submitted for publication)

Laser Ignition of Levitated Char Particles

(Manuscript to be submitted for publication)

The Effect of Char Formation Temperature on the Densification of a Bituminous Coal Char during Gasification

B. A. Wong*, G. R. Gavalas† and R. C. Flagan†

*Department of Environmental Engineering Science
†Department of Chemical Engineering,
California Institute of Technology, Pasadena, CA 91125

Abstract

It has been observed that certain char particles shrink when oxidized under kinetically limited conditions, instead of reacting at constant diameter, as expected. This study was performed to determine whether or not char from PSOC 1451 coal, prepared at different temperatures would also shrink during low temperature gasification. Coal chars, formed at 1200K and 1600K, were levitated in the electrodynamic balance and heated with a carbon dioxide laser. The 1200K char did shrink, while the 1600K char reacted at constant diameter, as expected under the kinetically limited conditions. Therefore, the time and temperature history of a char is an important factor in determining how it might react during subsequent oxidation.

*Author to whom correspondance should be addressed at the Chemical Industry Institute of Toxicology, P. O. Box 12137, Research Triangle Park, NC 27709.

Introduction

The combustion of pulverized coal occurs in two steps: First, as the coal particle heats up, devolatilization occurs. Moisture and low vapor pressure organic components are first driven off, and thermal decomposition of some of the carbonaceous structure occurs (Field[1]; Smoot and Smith[2]) resulting in tar evaporation. The residual material, termed char, is enriched in carbon and mineral components. The char reacts with oxygen and burns out until only the mineral matter remains. Depending on the particle temperature, char oxidation occurs in one of three regimes. The first, at low temperatures, is the kinetically limited regime (regime I). The reaction rate is controlled by the kinetics of the surface reaction of carbon with oxygen. The oxygen can diffuse through the pores of the particle faster than it reacts, so the oxygen concentration is uniform throughout the porous particle. At higher particle temperatures, the reaction rate becomes so fast that the oxidation is controlled by the diffusion of oxygen through the porous particle as well as by the surface reaction. In this diffusion limited regime (regime II), oxygen from the bulk gas penetrates only partially through the particle, and the oxygen concentration goes to zero at the center of the particle (Walker, et al.[3]). In the third regime (regime III), boundary layer diffusion controls the oxidation rate. The reaction of carbon with oxygen is so fast that the oxygen concentration is essentially zero at the surface of the particle, and the rate is controlled by the diffusion of oxygen through the boundary layer surrounding the char particle (Smoot and Smith[2]).

If we define χ as the conversion, or the ratio of mass of carbon reacted to the initial carbon mass, m_0

$$\chi = \frac{m_0 - m}{m_0} \tag{1}$$

then

$$(1 + \frac{m_a}{m_0} - \chi) = \frac{\rho d^3}{\rho_0 d_0^3} \tag{2}$$

where m_a is the mass of the ash in the particle. Equation 2 can be divided into two equations

$$d = d_0 (1 + \frac{m_a}{m_0} - \chi)^{\alpha} \tag{3}$$

$$\rho = \rho_0 \left(1 + \frac{m_a}{m_0} - \chi\right)^{\beta} \qquad (4)$$

where $3\alpha + \beta = 1$(Smith[4]). In the kinetically limited regime, carbon loss occurs throughout the particle, provided that the temperature of the particle is uniform, and oxygen is able to penetrate through to all of the inside surface area, i.e., there are no closed pores. In regime I, the diameter stays essentially constant and $\alpha = 0$, while the density decreases linearly and $\beta = 1$, until the conversion is nearly complete. In Figure 1, showing the relative volume, $(d/d_0)^3$ as a function of conversion, the top line corresponds to regime I. If a particle burns in Regime III, carbon loss will occur only near the external surface of the particle. The density will remain constant and the diameter of the particle will decrease, so $\alpha = 1/3$ and $\beta = 0$ (constant density line in Figure 1). The area in between, then corresponds to Regime II and the transitions between I and II and between II and III. In theory, then, following the diameter or density of a particle as a function of conversion should provide information about the regime of reaction. Note that the calculations and data presented in Figure 1 describe an ash free material, i.e., Spherocarb. For a mineral-bearing material, the volume would decrease to that of the mineral residue at 100% conversion.

Smith[5] observed that for a semi-anthracite in the temperature range 1400-2200K, the particles decreased in size and density as they reacted. This was also observed by Waters et al.[6] for Spherocarb particles in the same temperature range. Smith cited the fact that the particles decreased in size and density as an indication that the particles were burning between regimes I and II. Smith and Waters calculated $\alpha = 0.25$ and $\beta = 0.25$. Neither Smith[5] nor Waters et al.[6] observed any influence of temperature on the particle size or density change because of the experimental scatter in the data.

Hurt et al.[7], observed that some chars, notably Spherocarb and sucrose char, did not gasify at a constant diameter in regime I (temperature less than 873K), as expected, but instead "shrank." At 60% conversion, the spherocarb particle diameter was about 81 to 87% of the initial diameter. For a sucrose char, the particle shrank to about 88 to 92% of the initial diameter, at 60% conversion. The particle density was not measured directly but, based on the change in size with mass loss, the density did not decrease as much as predicted, hence, the particles of both materials were said to have "densified." Other chars (Montana Lignite, Pittsburgh #8 bituminous) did not shrink, but maintained their initial diameter through 60% conversion.

The Spherocarb data of Waters et al.[6] is shown with the Spherocarb data of Hurt et al.[7] in Figure 1. The best fit line for Water's data, with $\alpha = 0.25$ is compared with the best fit line for Hurt's data, with $\alpha = 0.177$ (calculated by the authors). The line shifts towards the constant diameter line at higher temperatures, as expected. The observed shrinkage either means that the coal structure changed, as they postulated, or the particles did not burn in the kinetically limited regime. Since Hurt et al. observed, at the same low temperatures as the shrinking chars, that some chars did oxidize without shrinkage, the former possibility is the more likely. They also observed that external features, such as pore diameters, decreased in size at the same rate as the particle diameter (Hurt et al.[7]). If the reaction was occurring without shrinking, the pore diameters might be expected to enlarge as the particle reacted. In a later paper, Hurt et al.[8] presented evidence that oxygen penetrates completely into the microporous regions of the spherocarb at temperatures of 673 to 873K. The reactivity of the Spherocarb carbon was found to be independent of particle size with the calculated effectiveness factor equal to unity, indicating that all the pore surface participated in the reaction. The adsorption equilibrium time in BET gas adsorption measurements of the char surface area was much shorter for Spherocarb than for sucrose char, a completely microporous char. From this evidence, Hurt et al.[8] concluded that the oxygen penetrated completely through the micropores of the Spherocarb and reacted there under kinetically limited conditions.

Hurt observed shrinkage and densification in some but not all chars. Presumably, then, structural changes that a char may undergo during oxidation depend on the initial coal or carbon structure. Some coals, particularly bituminous coals, appear to be quite "plastic" and upon devolatilization, may swell to several times their original size (Field et al.[1]). The resulting chars may have very large macropores, and become cenospheric. It might seem, then, that chars made from such swelling coals would be prone to structural changes during subsequent oxidation. This study was undertaken to determine if a swelling coal char from the bituminous coal PSOC 1451 does indeed densify, and if so, the effect of char formation temperature on the densification phenomenon.

EXPERIMENTAL

The particles used in this study were Spherocarb and char made from a high volatile bituminous coal (Pittsburgh seam PSOC 1451). Spherocarb is a commercially available carbon material (sold as Carbosphere by Ailtech Associates, Inc.). It consists of spherical particles of high purity carbon with a high specific surface area (nominally 1000 m^3/g). Spherocarb has networks of both micro and macropores with 0.39 cm^3/g in micropores, and a porosity of 0.33 in pores > 200 Å (Floess et al.[9]).

Coal char particles were made from PSOC 1451 bituminous coal by Sahu et al.[10] Briefly, the chars were made as follows: PSOC 1451 coal was ground and sieved. Coal particles in the 104 to 125 μm fraction were entrained in a stream of nitrogen and passed through a drop tube furnace to a temperature of 1200 or 1600K for two seconds. The collected particles were washed in tetrahydrofuran and resieved. Chars in the 125 to 175 μm, 175 to 208 μm and 208 to 295 μm size ranges were selected for study.

Table 1 lists measurements by Sahu et al.[10] of the apparent density, σ_A, total porosity, ε_A, porosity of pores less than 64 Å, and pore volume and pore surface area based on mercury porosimetry for PSOC 1451 coal and chars. The apparent density decreases as char formation temperature increases, as does the total porosity. Only the 1600K char shows an appreciable microporosity, i.e., 19%. The pore volume and surface area increase as the coal is converted to char, however, there are only slight differences between chars. According to Sahu et al., chars formed at lower temperatures developed bimodal pore size distributions, while high temperature chars developed trimodal pore size distributions. The 1200K char showed a bimodal distribution of pore volume and pore area with significant volume in the macropore region and significant area in the micropore region. The 1600K char contained similar micro and macroporosity, but, additionally, showed significant area and volume in the socalled transition pore region, around a pore diameter of 500 Å (Sahu et al.[10]). For the 127 to 175 μm fraction of the 1600K char, the total porosity was 47%, while the pore volume fraction contained in pores smaller than 64 Å was 19%. The total porosity of 1200K char was 33%, with no significant microporosity. The physical properties listed for the chars are average values for the entire size range. As we chose to work with the larger char particles, it is expected that the macroporosity for these particles are even larger than that listed in the table. The large chars, particularly the 208 to 295 μm diameter particles, were cenospheres.

The use of the electrodynamic balance for studying char oxidation has been described elsewhere by Spjut et al.[11], Hurt et al.[7] and Bar-Ziv et al.[12]. A brief description of the system used in this study is presented here. The electrodynamic balance consists of two endcap electrodes with a DC voltage across the electrodes. A charged particle is suspended in the electric field against gravity. A ring at midplane between the endcap electrodes is charged with an AC voltage. If the particle deviates in any direction from the center of the cell, the particle is subject to a time-averaged force from the AC field that pushes the particle back toward the center (Davis[13]).

A microscope with a total magnification of 15x was used to view the particle. A 10x eyepiece micrometer (American Optical Co.) was used to measure the size of the particle in the horizontal and vertical directions. The suspended particles were videotaped using a catadioptric microscope (Questar QM-1) and a video camera (COHU, Inc., model 4810). The output from the video camera was shown on a monitor (Electrohome, EVM) and recorded by a videotape recorder (Panasonic AG-1830). Still photographs were obtained by photographing the monitor, or by using an adapter coupled to a standard 35mm SLR camera that fit over the viewing microscope and a standard 15x eyepiece.

The particle suspended in the EDB was heated with the radiation from a 20 Watt carbon dioxide laser emitting at 10.6m. The beam was split and directed by mirrors into the chamber vertically to heat the particle from top and bottom. The intensity of the beam intercepted by the particle was controlled by ZnSe lenses and by moving the focal point closer or farther from the particle.

The temperature of the particle was measured using a two-color optical pyrometer. Radiation emitted from the heated particle is collimated by a CaF_2 lens and split by a grating beam splitter. One arm of the split beam was focused by a CaF_2 lens through a 3.4 ± 0.0685 μm interference filter onto a liquid nitrogen cooled InSb detector. The other arm was focused through a 1.5 ± 0.037 μm interference filter onto a thermoelectrically cooled InGaAs detector. The outputs from the detectors was sent to a logratio amplifier (Analog Devices 757). The output from the logratio amplifier was monitored on an oscilloscope and sent to a data acquisition system.

A typical experimented started by trapping a single particle in the electrodynamic balance. The size of the particle was measured in the horizontal and vertical directions using the eyepiece micrometer. Photographs were taken through the viewing microscope. The CO_2 laser was allowed to stabilize with an external shutter closed. Particle heating was

then initiated by opening the shutter. The pyrometer signal was monitored on the oscilloscope and recorded by the data acquisition system. The particle position was balanced manually. The heating pulse was ended by closing the external shutter. Photographs were again taken to record any changes in particle size and shape. In many cases, after heating, the particle was rotating about a vertical axis. If the particle was very irregularly shaped, photographs were attempted when the particle rotated through its original position, if that could be determined. Particle sizing was repeated, at the same orientation, if possible.

RESULTS

The Spherocarb and char particles were heated at temperatures up to 1000K. Figures 2 and 3 show the temperature traces of a Spherocarb and a 1600K char heated in air. The particle temperature could be maintained only to within 50K. Irregular particle shape, strong photophoretic forces, and long term fluctuations in the intensity of the laser contributed to the temperature fluctuations. The primary focus of this paper is on the structural rearrangements of the char during kinetically limited oxidation. As long as the peak temperature experienced did not take the particle out of Regime I oxidation, the fluctuations should not affect the basic results.

The effectiveness factor was calculated for the Spherocarb and char particles at 1000K to verify that the oxidation reaction was occurring in the kinetically limited regime. The classical calculation of the Thiele modulus and effectiveness factor (Smith[14]) were carried out using the effective diffusivity reported by Hurt et al.[8] and Arrhenius rate parameters for the intrinsic rate coefficient reported by Floess et al.[9] A Thiele modulus of 0.15 at 1000K was calculated, which gives an effectiveness factor of unity. The method discussed by Smith[15] was used to calculate the effectiveness factor for the bituminous char particles. Based on the measured reaction rates and the effective diffusivities reported by Sahu et al.[10], the effectiveness factors for all the char particles studied were also unity at 1000K.

Photographs of the backlit particles showing their silhouettes are shown next. Figures 4a and 4b show a Spherocarb particle, before and after heating for 10 minutes in nitrogen. The particle has clearly retained its size and general surface features. Another Spherocarb particle before heating in air is shown in Figure 4c. The same particle, after 62% conversion is shown in Figure 4d. Note that the top and bottom of the particle are flattened, at the locations of the incident laser beams where the temperature was higher and

the oxidation faster. The horizontal diameter is reduced from 196 μm to 175 μm, and is indicative of the shrinking of Spherocarb.

Figures 5a and 5b show PSOC 1451 coal char made at 1200K before and after 10 minutes heating in nitrogen. This particle clearly retains its size, shape and overall features. Figure 5c shows a photograph of a 1200K char, before heating in air, while Figure 5d shows the same char, at 48% conversion. The diameter decreased from 230 m to 200 m, clearly showing some shrinkage.

Figures 6a and 6b show PSOC 1451 coal char made at 1600K before and after 11 minutes heating in nitrogen. Again, there is no change in the size or appearance of the particle after heating in nitrogen. Figure 6c shows a photograph of a 1600K char, before heating, and Figure 6d shows the same char, at 56% conversion in air. The vertical dimension remains approximately the same at 222 μm, and the horizontal dimension also remains approximately the same at 160 μm. Note also, that the particle becomes lacy and translucent. As the cenospheric chars oxidize, the thin walls become more transparent.

The experiments in nitrogen show that the shrinkage of the particles is not due simply to heating, but in some way, is related to reaction with oxygen. When the char is heated in oxygen, some particles shrink, others do not. The relative volume as a function of conversion of Spherocarb is plotted in Figure 7. Each symbol represents a different Spherocarb particle. The dotted lines connect data from experiments on one particle. The particle volume was estimated by assuming that it was an oblate spheroid with volume $\frac{4}{3}\pi a^2 b$ where a is the major axis and b is the minor axis. The relative volume and conversion for Spherocarb particles is listed in Table 2. The relative volumes determined in the present experiment appear to lie somewhat lower than the measurements of Hurt et al.[7] and approach the range of measurements of Smith[5] and Waters et al.[6]. As noted above, a comparison of the data of Hurt et al. with Smith and Waters et al. suggest that the shrinkage increases with increasing temperature. The slightly higher temperatures of the present experiments may account for the differences with the observations of Hurt et al.[7], but experimental differences cannot be ruled out. Unfortunately, the uncertainties in each data set preclude quantitative determination of this temperature dependence within each set of measurements.

Figure 8 shows the relative volume versus conversion for the bituminous char. The points for the 1200K char (the open squares) are scattered, but generally show significant shrinkage, roughly along the same line as the data of Hurt et al.[7] for

Spherocarb. The points for the 1600K char (solid circles) mostly lie very close to the constant density line along the top of the graph. In cases where the particles were irregularly shaped, the size was measured from the extreme points in the vertical or horizontal directions. Volumes were calculated assuming that the particles could be modeled as oblate or prolate spheroids. Table 3 lists the relative volumes and conversions for the char particles.

DISCUSSION AND CONCLUSIONS

The reasons for the observed shrinkage or densification of some chars are as yet unknown. It has been shown that the particles are reacting in the kinetically limited regime and not the diffusion limited regime. The 1200K and the 1600K char both contained macropores, but only the 1600K char contained significant microporosity. Hence, it might be expected that the 1600K char show some diffusion limitations, but this is not the case. The larger coal char particles that were used in this experiment were quite cenospheric in nature, and should be even more macroporous than the average values listed in Table 1. Smith[4] indicated that a cenosphere should burn at constant diameter and decreasing density, even if the reactions were limited to the outer surface. Thus, it seems unlikely that oxygen diffusion limitations would be a cause of shrinkage of the cenospheric 1200K but not the cenospheric 1600K char. Clearly then, the 1200K char is shrinking as it is reacting, while the 1600K char is reacting at constant diameter.

If diffusion limitations can be ruled out, then structural changes in the carbon must be occurring. Hurt et al.[7] speculated that as the char loses carbon, atomic rearrangements causes the loss of pore volume in the fine pores. These atomic rearrangements lead to a graphitization accompanied by an increase in the density. Sahu et al.[10] also speculated that charring at the higher temperatures led to a loss of the finer pores. They noted that as a PSOC 1451 bituminous coal char was oxidized, the total surface area increased and reached a maximum at around 60% conversion. When examined as a function of char devolatilization temperature, it was observed that the surface area at 50% conversion was greater for the chars formed at lower temperatures. They postulated that the reduction of surface area at higher charring temperatures resulted from a closure of the smaller pores due to a structural ordering of carbon. The 1600K char, then may be more graphitized and less prone to shrinking than the 1200K char. In a study of the oxidation kinetics of synthetic chars (amorphous carbon), Levendis et al.[16] observed that as the oxidation temperature increased, there was increased graphitization of the synthetic chars. Oxygen accelerated the

graphitization process. Thus, there is evidence that as chars react, the carbonaceous material undergoes graphitization. The extent to which a char shrinks during low temperature oxidation may depend on the extent of graphitization of the initial carbon particle during the devolatilization process.

The reactions that take place during devolatilization may provide some information about the difference in behavior between the 1600K char and the 1200K. Solomon et al.[17] describe a two-step devolatilization process in which the raw coal is pictured as a complex of aromatic and hydroaromatic carbon clusters linked by aliphatic bridges. In the initial pyrolysis step, the weakest bridges are broken. The lightest molecular weight fragments may vaporize, the heavier fragments may remain with the parent coal. During this time, functional group decomposition also releases CO_2 , H_2O, methane and other light gases. In the second step of pyrolysis, cross-linking between the remaining aromatic clusters occurs. Solomon et al.[18] found that there are two distinct cross-linking events, occurring at different temperatures. At a heating rate of 0.5C/s, the low temperature cross-linking occurs between about 200 and 450C, and the moderate temperature cross-linking occurs between 450 and 600C. It is conceivable that at the much higher heating rates and short exposure time (2 s) used to produce the bituminous char used in these studies, the cross-linking is less complete for the 1200K char than for the 1600K char. Thus, as a char undergoes subsequent oxidation, cross-linking also occurs, leading to the shrinkage. However, as the heating in nitrogen showed, the densification effect requires reaction with oxygen and not simply heating to elevated temperatures. Therefore, in this scenario, the cross-linking is assisted by the carbon-oxygen reaction.

There is a significant implication of these results for researchers using or producing char oxidation models. Most models assume that, as char oxidation progresses, the pores enlarge and the surface recedes, but the basic carbon structure does not change. Results from this experiment and those from the Spherocarb densification study of Hurt et al.[7] show that the models must account for changes in density which can not be characterized simply by the oxidation regimes in which the reaction is taking place. These density changes are not only dependent on the initial coal structure, but also upon on the temperature time history of char formation. Thus, a complete description of char oxidation will require both the information about the basic structure (density, porosity, surface area, etc.) and knowledge of the history of the char to account for possible carbon structural changes and shrinking during the oxidation process.

ACKNOWLEDGEMENTS

This work was supported by the U.S. Department of Energy, University Coal Research Program under grants DE-FG22-89PC89765 and DE-FG22-88PC88911.

REFERENCES

(1) Field, M. A.; Gill, D. W.; Morgan, B. B.; Hawksley, P. G. W. *Combustion of Pulverized Coal*, The British Coal Utilisation Research Association, Leatherhead, 1967.

(2) Smoot, L. D.; Smith, P. J. *Coal Combustion and Gasification.* Plenum Press, New York, 1985.

(3) Walker, P. L., Jr., Rusinko, F., Jr., Austin, L. G., *Advan. Catalysis.* **1959**, *11*, 134.

(4) Smith, I. W. *Nineteenth Symp. (Int.) Comb.* The Combustion Institute. pp. 1045-1065, 1982.

(5) Smith, I. W. *Combust. Flame.* **1971**, *17*, 421-428.

(6) Waters, B. J.; Squires, R. G.; Laurendreau, N. M.; Mitchell, R. E. *Combust. Flame.* **1988**, *74*, 91-106.

(7) Hurt, R. L.; Dudek, D. R.; Longwell, J. P.; Sarofim, A. F. *Carbon.* **1988**, *26*, 433-449.

(8) Hurt, R. L.; Sarofim, A. F.; Longwell, J. P. *Energy Fuels.* **1991**, *5*, 290-299.

(9) Floess, J. K.; Longwell, J. P.; Sarofim, A. F. *Energy Fuels.* **1988**, *2*, 18-26.

(10) Sahu, R.; Levendis, Y. A.; Flagan, R. C.; Gavalas, G. R. *Fuel.* **1988**, *67*, 275-283.

(11) Spjut, R. E.; Sarofim, A. F.; Longwell, J. P. *Langmuir.* **1985**, *1*, 355-360.

(12) Bar-Ziv, E.; Jones, D. B.; Spjut, R. E.; Dudek, D. R.; Sarofim, A. F. *Combust. Flame.* **1989**,.*75*, 81-106.

(13) Davis, E. J. In *Surface and Colloid Science* (E. Matijevic, ed.). Vol. 14. Plenum Press, New York, 1987.

(14) Smith, J. M. *Chemical Engineering Kinetics.* McGraw-Hill Book Company, NewYork, 1970.

(15) Smith, I. W. *Fuel.* **1978**, *57*, 409-414.

(16) Levendis, Y. A.; Flagan, R. C.; Gavalas, G. R. *Combust. Flame.* **1989**, *76*, 221-241.

(17) Solomon, P. R.; Hamblen, D. G.;Carangelo, R. M.; Serio, M. A.; Deshpande, G. V. *Energy Fuels.* **1988**, *2*, 405-422.

(18) Solomon, P. R.; Serio, M. A.; Deshpande, G. V.; Kroo, E. *Energy Fuels.* **1990**, *4*, 42-54.

Table 1

Properties of Chars

Coal or Char	σ_A	ε_A <7μm	ε <32 Å	V_{Hg}	S_{Hg}
	g/cm^3	%	%	cm^3/g	m^2/g
PSOC 1451 coal	1.18	17		0.14	7.9
1200K char	1.0	33	0	0.43	11.6
1400K char	0.9	40	0	0.57	11.4
1600K char53-90m from53-90m	0.98	47	2	0.46	14.7
127-147m from90-125m	0.92	47	19	0.35	14.9
Spherocarb	0.56	33[1]	.39[2]		864[3]

[1]Pores larger than 200 Å by mercury porosimetry (Floess et al., 1988).

[2]Micropore volume, cm^3/g for an average pore radius of 6.7 Å, determined by nitrogen adsorption (Floess et al., 1988).

[3]BET surface area by N_2 adsorption (Waters et al., 1988).

Table 2

Spherocarb Data

Particle	Series	Temperature K	Conversion %	Relative Volume $(d/d_0)^3$
A	TS0372	930±20	17.6	.77
		920±20	32.2	.70
		950±50	42.3	.60
		880±30	64.0	.45
		890±30	71.7	.31
B	TS0373	1000±50	60.8	.75
C	TS0374	1010±15	8.9	.94
		990±30	30.9	.79
		940±40	43.9	.62
		930±30	53.9	.54
		900±40	63.5	.47
D	TS0471	970±20	12.2	.94
		960±20	36.8	.81
		930±30	55.2	.60
		910±30	75.6	.31
E	TS0473	900±10	24.0	.79
		820±20	55.1	.63
		900±100	67.2	.41
F	TS0474	820±20	4.4	.92
		860±40	40.1	.65
G	TS0475	760±100	11.7	.88
		790±100	23.8	.86
		790±100	41.8	.80
H	TS0512	910±20	9.8	.92
		900±20	21.4	.79
		890±25	31.8	.76
I	TS0513	980±30	12.3	.90
		960±20	36.0	.80
		930±20	55.8	.54
J	TS0921	980±15	4.0	.95
		1030±30	52.1	.60
K	TS0522	920±40	78.9	.27
L	TS0523	1000±20	43.9	.82
		1000±100	82.6	.39
M	TS0524	1070±100	61.3	.62
N	TS0525	890±15	17.4	.95
		880±15	52.4	.67

Table 3

Char Data

Particle	Series	Temperature K	Conversion %	Relative Volume $(d/d_0)^3$
A (1200K)	TC0771	790±50	9.6	1 00
			42.9	.85
B (1200K)	TC0781	790±50	63.5	.46
C (1200K)	TC0782	790±50	33.6	.69
D (1200K)	TC0783	790±50	79.5	.28
E (1200K)	TC0784	790±50	70.5	.54
F (1200K)	TC0785	790±50	48.3	1 00
G (1200K)	TC0786	790±50	43.2	.72
			15.4	.82
H (1600K)	TC0861		17.9	.99
			52.1	.76
I (1600K)	TC0871		29.3	.98
J (1600K)	TC0872		19.4	.93
K (1600K)	TC0874		38.4	1 00
L (1600K)	TC0875	700±100	10.7	.95
M (1600K)	TC0881	880±100	28.3	.95
N (1600K)	TC0882	880±100	42.4	1 00
		850±100	76.0	.95
O (1600K)	TC0902	840±100	63.8	.95
P (1200K)	TC0911	780±100	51.4	.77
Q (1400K)	TC0913	840±100	51.6	.51
R (1200K)	TC1041	770±100	48.2	.64

Figure Captions

Figure 1. Graph of relative volume of particle vs. conversion. The top line is the line of constant diameter. The diagonal line is the line of constant density.

Figure 2. Temperature trace for a Spherocarb particle heated in the electrodynamic balance.

Figure 3. Temperature trace for a char particle made at 1600K from PSOC 1451 bituminous coal.

Figure 4. a. Photograph of backlit Spherocarb particle before being heated in the electrodynamic balance; b. Photograph of the same Spherocarb particle after 62% conversion. Note the flattened top and bottom, where the laser beam was heating the particle; c. Photograph of Spherocarb before reacting; d. Photograph of Spherocarb after heating in nitrogen.

Figure 5. a. Photograph of 1200K char before reacting; b. Photograph of 1200K char after heating in nitrogen; c. Photograph of 1200K char before reacting; d. Photograph of 1200K char after 48% conversion. Note the relatively uniform size change.

Figure 6. a. Photograph of 1600K char before heating; b. Photograph of 1600K char after heating in nitrogen; c. Photograph of 1600K char before reacting; d. Photograph of 1600K char after 56% conversion. The char now looks lacy or translucent. The exterior dimensions are nearly the same.

Figure 7. Relative volume of Spherocarb particles reacted at low temperatures.

Figure 8. Relative volume of bituminous char vs. conversion. The x are 1200K char, and the circles are 1600K char.

Figure 1

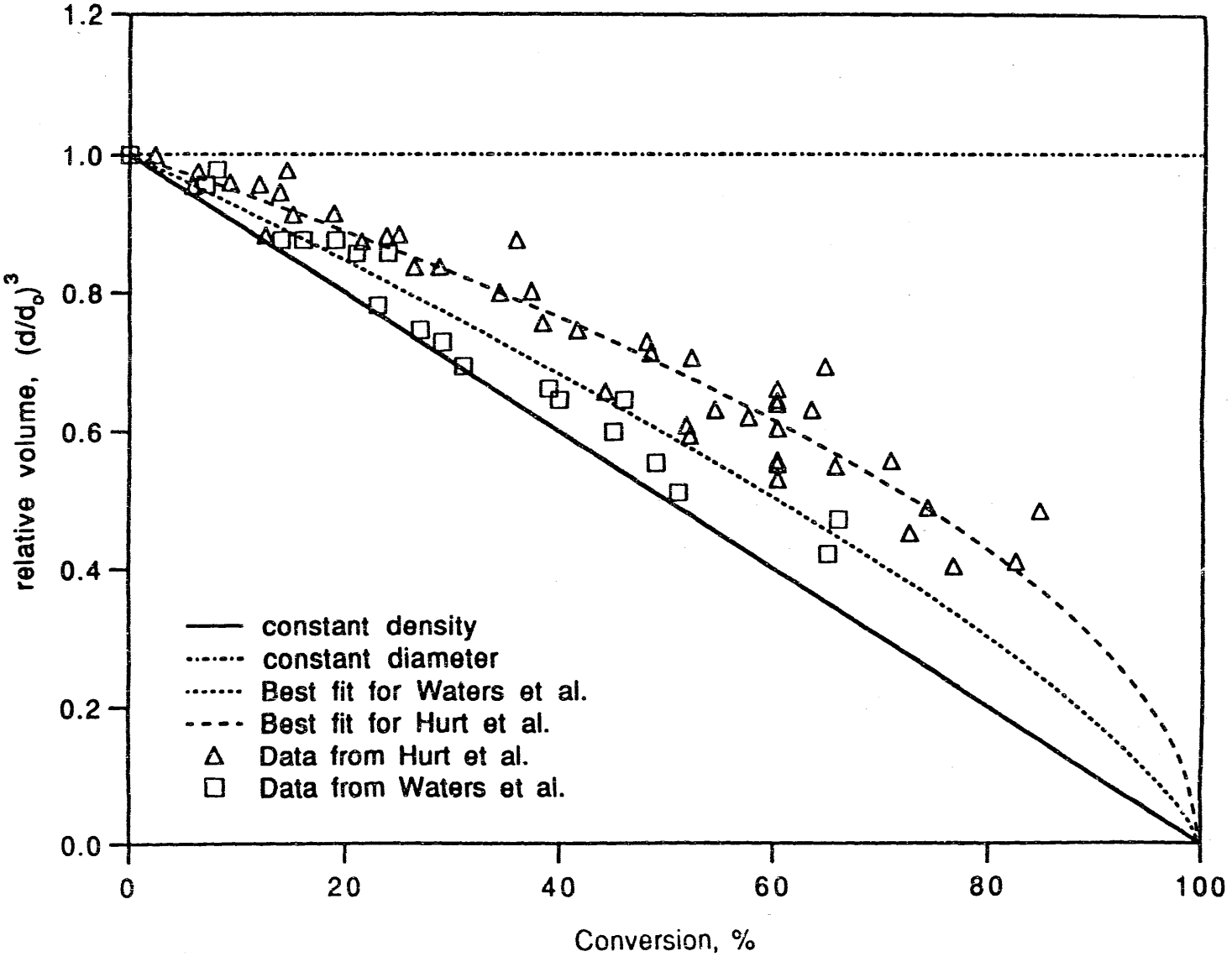
1.2
1.0
0.8
0.6
0.4
0.2
0.0
relative volume, $(d/d_o)^3$
0
20
40
60
80
100
Conversion, %
constant density
constant diameter
Best fit for Waters et al.
Best fit for Hurt et al.
Data from Hurt et al.
Data from Waters et al.

Figure 2

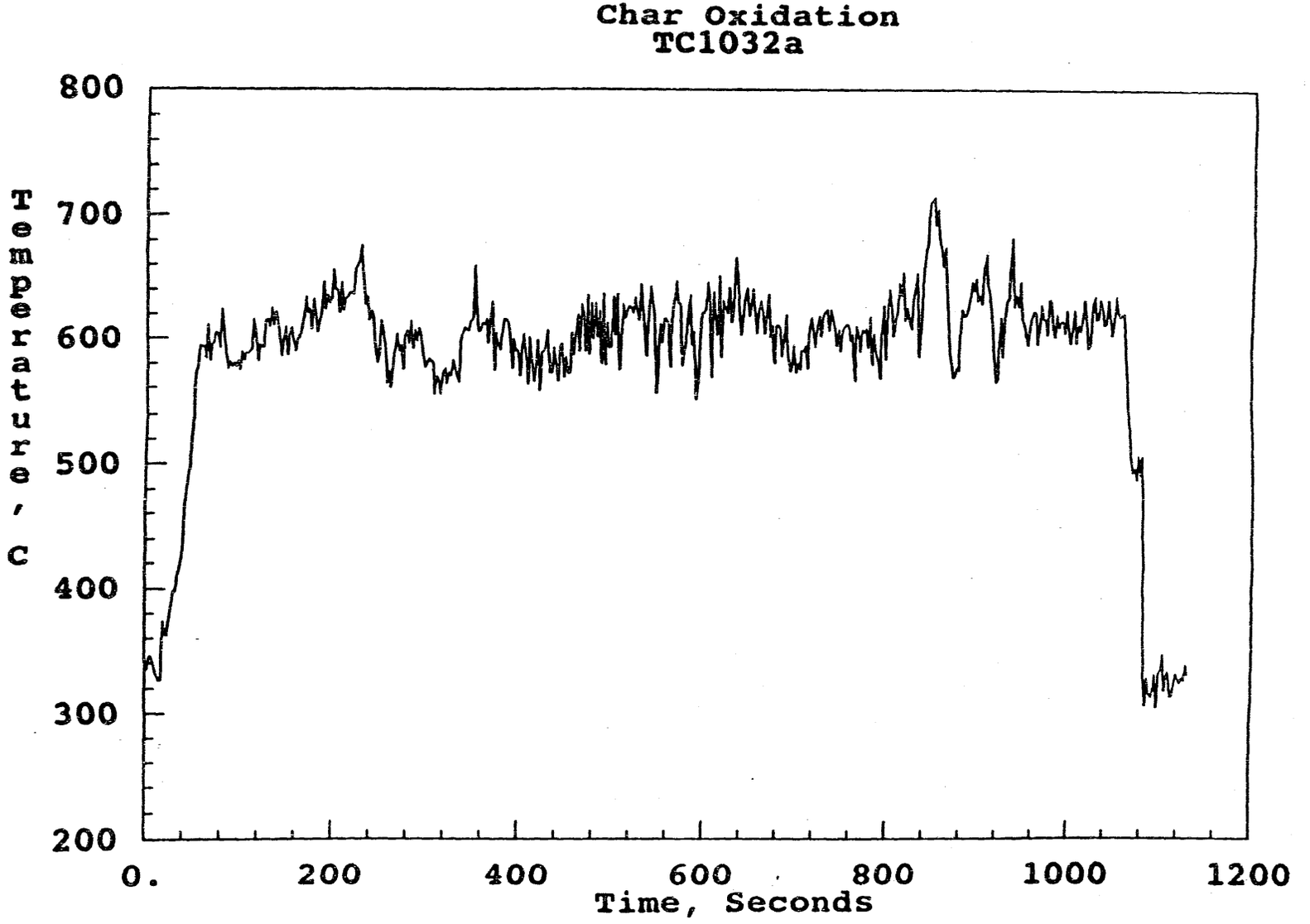
Char Oxidation
TC1032a
Temperature, C
800
700
600
500
400
300
200
0.
200
400
600
800
1000
1200
Time, Seconds

Figure 3

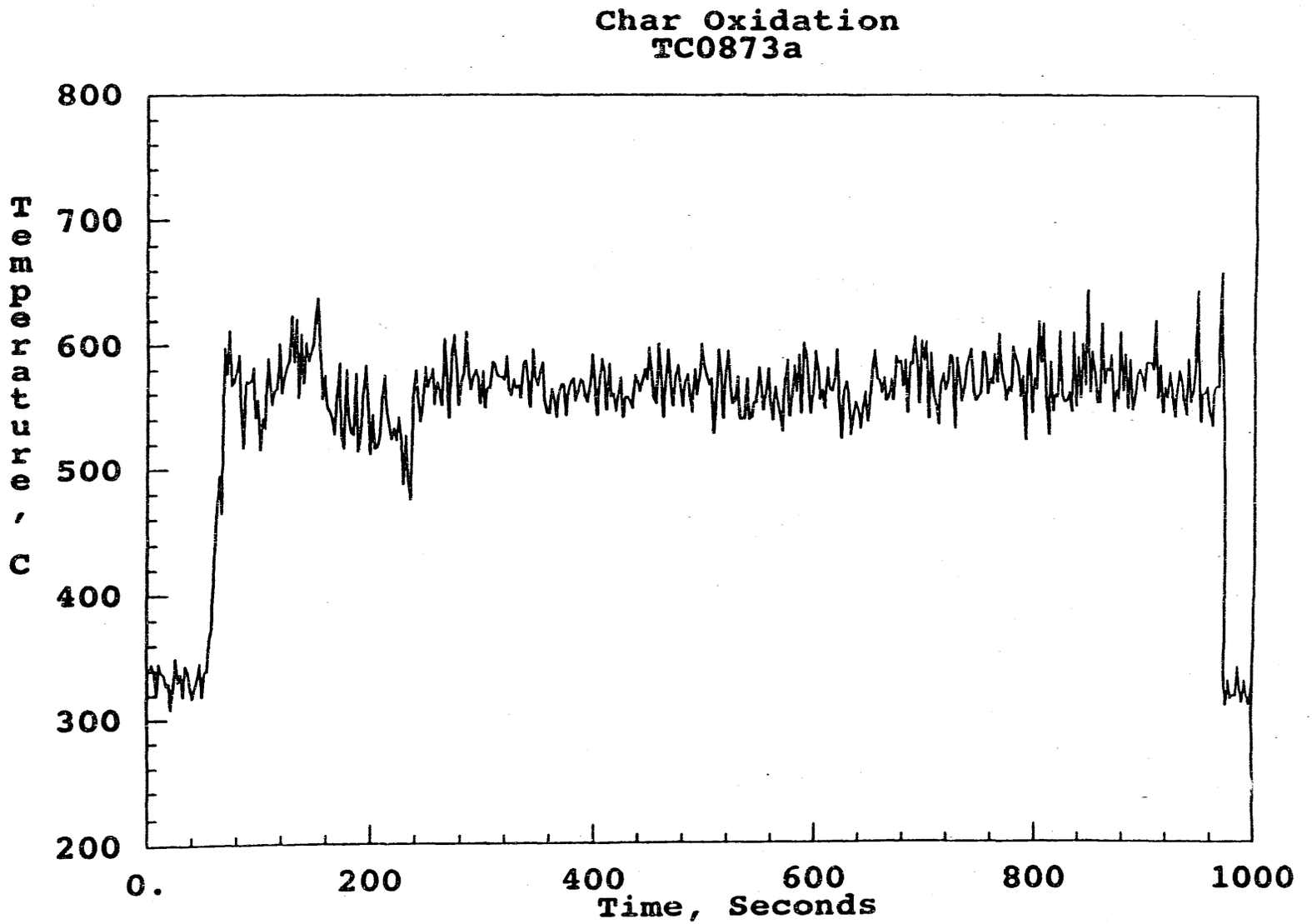
Char Oxidation
TC0873a
Temperature, C
800
700
600
500
400
300
200
0.
200
400
600
800
1000
Time, Seconds

Figure 4a. Spherocarb before heating in N_2	Figure 4c. Spherocarb before heating in air
Figure 4b. Spherocarb after heating in N_2	Figure 4d. Spherocarb after heating in air
Figure 5a. 1200K Char before heating in N_2	Figure 5c. 1200K Char before heating in air
Figure 5b. 1200K Char after heating in N_2	Figure 5d. 1200K Char after heating in air
Figure 6a. 1600K Char before heating in N_2	Figure 6b. 1600K Char before heating in air
Figure 6b. 1600K Char after heating in N_2	Figure 6d. 1600K Char after heating in air

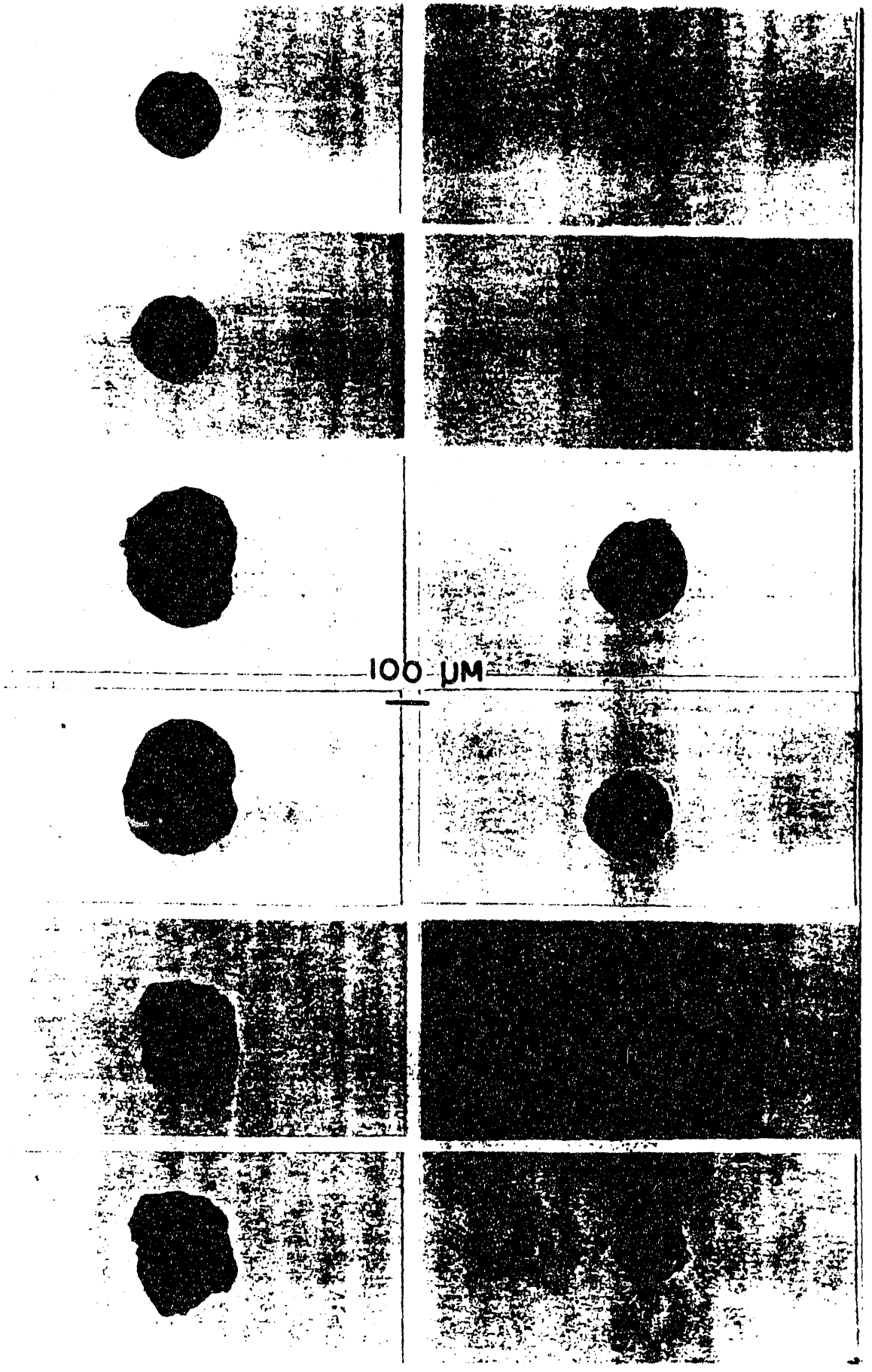
100 µM

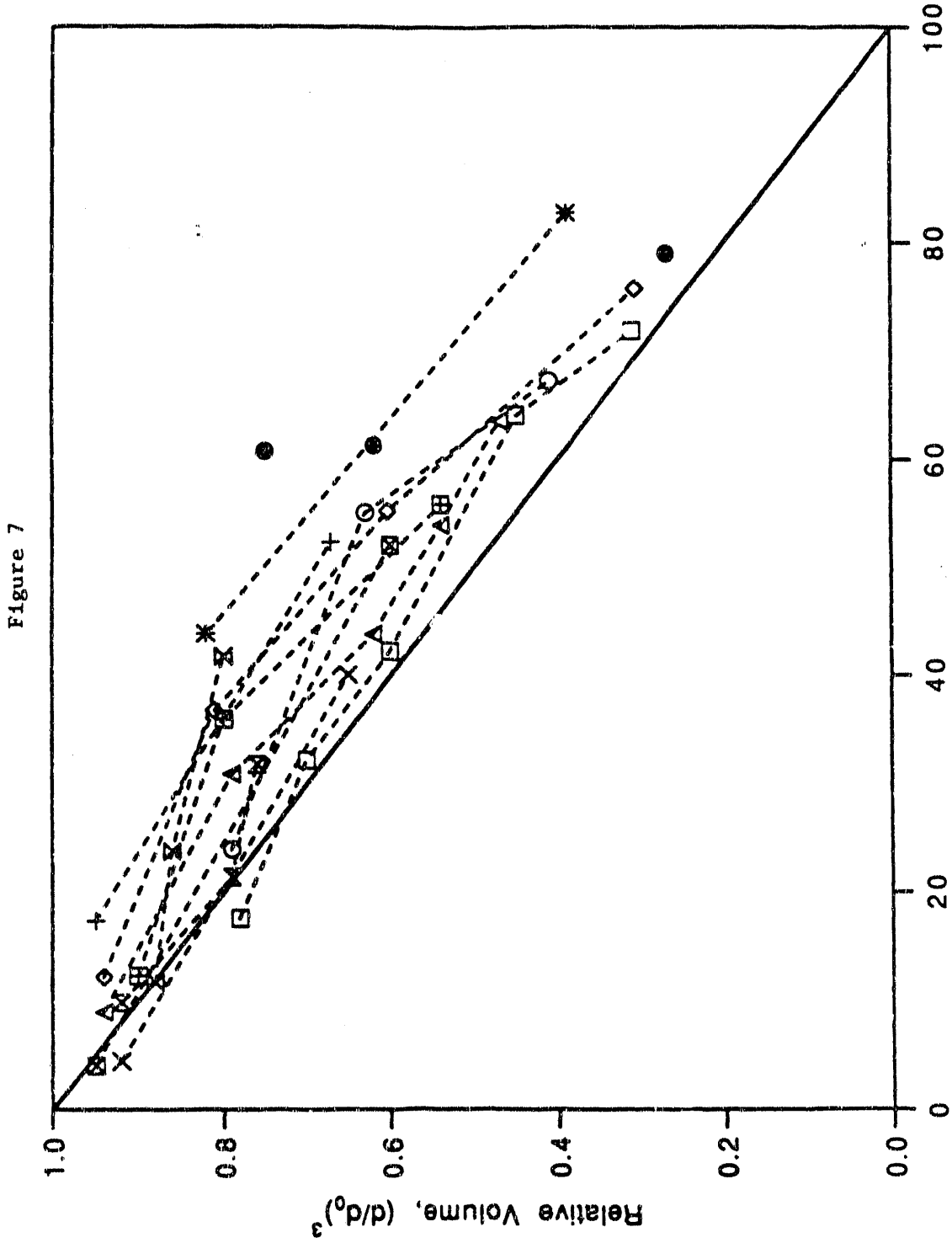
Relative Volume, $(d/d_o)^3$
1.0
0.8
0.6
0.4
0.2
0.0
0
20
40
60
80
100
Conversion, %

Figure 7

Figure 8

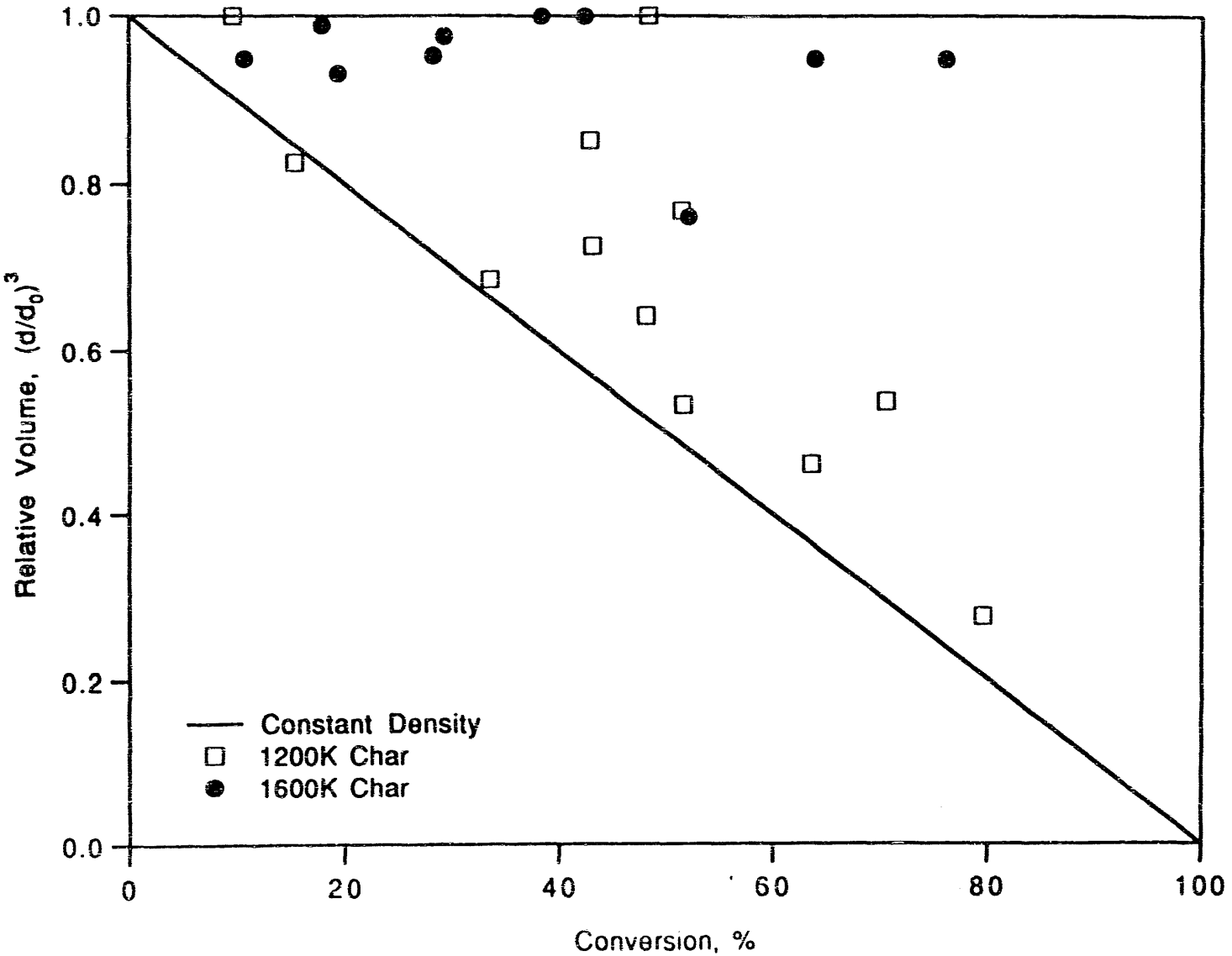
1.0
0.8
0.6
0.4
0.2
0.0
Relative Volume, $(d/d_0)^3$
0
20
40
60
80
100
Conversion, %
Constant Density
1200K Char
1600K Char

Laser Ignition of Levitated Char Particles

B. A. Wong*, G. R. Gavalas† and R. C. Flagan†

Department of Environmental Engineering Science
†Department of Chemical Engineering, California Institute of Technology,
Pasadena, California 91125

Abstract

The temperature history of a char particle heated by a carbon dioxide laser to ignition was studied in the electrodynamic balance. The experiments were conducted using Spherocarb particles, 140 to 240 μm in diameter, and char particles from a bituminous coal, 150 to 300 μm in diameter. In a typical experiment, a charged char particle was suspended in the electrodynamic balance and heated by a 500 ms pulse of radiation from a CO_2 laser. The temperature of the particle was measured with an optical pyrometer. The oxygen concentration in the ambient gas, initially only nitrogen, was slowly increased as successive laser pulses were given, until the particle ignited. Once ignition occurred, the particle lost charge and dropped from the center of the balance. The particle temperature profile at ignition shows the ignition delay predicted by Semenov's thermal explosion theory. The measured temperature traces could be described well by calculations treating the particle as a sphere and using rate parameters given in the literature.

* Present address: Chemical Industry Institute of Toxicology, P. O. Box 12137,
Research Triangle Park, NC 27709.

Introduction

In pulverized coal combustion, small particles, typically 50 μm in size are burned while entrained in the combustion gases. As a coal particle heats up, it devolatilizes and pyrolyzes. The remaining material, char, is a porous, primarily carbonaceous material. The carbon reacts with the oxygen in the surrounding atmosphere, generating heat. Ignition occurs when the heat produced by the exothermic oxidation reaction exceeds the heat loss from the system due to conduction, convection and radiation. This concept of ignition applies to an entire system, e.g., a cloud of coal particles in a furnace, as well as to an individual particle (Field et al.;[1] Essenhigh et al.[2]). Two mechanisms of ignition have been identified for coal particles, homogeneous and heterogeneous (Essenhigh et al.[2]). Homogeneous ignition occurs when the devolatilizing gases react with oxygen to ignite first, producing a flame front that initially stands off from the particle but eventually reaches the char surface as the devolatilization ceases. Heterogeneous ignition occurs directly on the particle surface as oxygen reacts with the char particle. Experimental (Howard and Essenhigh,[3]) and theoretical (Annamalai and Durbetaki[4]) results have demonstrated that the heterogeneous ignition mechanism dominates for smaller (<350 μm diameter) coal particles. The ignition characteristics of coal or char are important to the fundamental understanding of the coal combustion process. Historically, ignition was studied, not only for application in furnaces and combustors, but also because of safety concerns. Coal piles, coal dust, and dust of other materials such as grain have been known to occasionally explode and burn. Research was initiated to determine the cause of, and prevent such unplanned explosions (Essenhigh et al.[2]). Research into the ignition process continues as part of the broad area of research in coal combustion fundamentals in efforts to improve efficiency and minimize fouling, waste products and pollution in current combustor technology. The development of new technologies, such as coal-fired diesel engines, coal gasification and liquefaction and magneto-hydrodynamics will also benefit from a better understanding of coal combustion fundamentals.

The criteria used to define ignition is based on Semenov's thermal explosion theory (Essenhigh et al.[2]; Chen et al.[5]; Thomas et al.[6]). The classical conditions for ignition state that the heat loss from the particle, Q_ℓ must be equal to the heat generated, Q_g

$$Q_\ell = Q_g \tag{1}$$

and that the heat loss curve must be tangent to the heat generation curve

$$\frac{dQ_\ell}{dT} = \frac{dQ_g}{dT} \tag{2}$$

More generally, ignition occurs when the heat generation equals or exceeds the heat loss (Essenhigh et al.[2], Chen et al.[5])

$$Q_\ell \geq Q_g \tag{3}$$

The ignition limit defined by equations 1, 2 and 3 is illustrated in Figure 1 which shows the heat loss and gain for a 50 μm diameter coal particle in a hot gas as a function of particle temperature (Field et al.,[1]). The dotted lines show the heat loss and heat generation for the particle in a hot gas with 10% oxygen at 900K. At point A the curves intersect, i.e., $Q_\ell = Q_g$, but the tangency requirement is not met, so the particle reaches an equilibrium temperature without igniting. If the particle temperature increases, the heat loss is greater than the heat gain, and the particle will cool back to the equilibrium temperature. If the particle temperature undergoes a slight decrease, the heat gain becomes greater than the heat loss, and the particle warms back to the equilibrium temperature. The solid curves show the heat loss and heat generation for the particle in 10% oxygen at 1235K. Under these conditions, the reaction with oxygen causes the particle temperature to increase to about 1360K, at which point (B), the heat loss and heat gain curves are equal and, also, tangent, indicating the ignition limit. Any perturbation in temperature above this value will cause the particle temperature to increase further since the heat generation rate is greater than the heat loss rate. The final steadystate temperature of the ignited particle is attained at the point C at which the two curves again intersect. The dashed curves show the heat loss and heat generation for the particle in 10% oxygen at 1400K. The heat generation is significantly greater than the heat loss, until the boundary layer diffusion of oxygen becomes the limiting factor to any further temperature rise, and the curves intersect at point D. Mass loss has not been considered explicitly in this simple model. Instead, we have determined the steadystate temperature that would result if the particle temperature rise occurred very rapidly compared to its loss of mass by oxidation.

A detailed examination of char ignition requires solving the unsteady energy balance

$$m\, C_p \frac{dT}{dt} = Q_\ell - Q_g \tag{4}$$

in conjunction with a model of the oxidation process. Here, is the mass of the particle, is the heat capacity, is the temperature, and is the time. In Figure 2, the dotted curve shows the temperature of a 50m particle immersed in a gas at 900K. The particle temperature increases and then levels out at the temperature corresponding to the intersection of the heat loss and heat gain curve (point A) in Figure 1. For the same particle immersed in a gas at 1235K, the curve (solid line) plateaus at the ignition temperature, and then rapidly increases. The inflection point in this curve corresponds to point B in Figure 1. The length of time spent in the plateau is known as the ignition delay or induction time (Essenhigh et al.[2]; Bandyopadhyay and Bhaduri;[7] Thomas et al.[6]). The temperature rises until it plateaus at point C. The dashed curve shows the rapid temperature rise of a particle at a surrounding temperature of 1400K. At this high temperature, the particle ignites without the ignition delay (Thomas et al.[6]) and the temperature rises to a new steady-state in which oxidation is limited by the external diffusion of oxygen to the particle.

There have been many studies of the ignition process, with special interest in the ignition temperatures of coal or char particles and the relationship to particle diameter. Different techniques were devised to accomplish the three major steps in these experiments; holding or isolating the particle, heating the particle, and monitoring the transient particle temperature and identifying ignition. Bandyopadhyay and Bhaduri[7] placed a coal particle onto a fine platinum wire and inserted the wire into a furnace. The insertion step was repeated after increasing the temperature of the furnace until an ignition flash was observed. Karcz et al.[8] placed a single coal particle on the tip of a quartz needle and inserted the needle into a heated furnace. As in the experiments of Bandyopadhyay and Bhaduri, the insertion was repeated with the furnace temperature increased stepwise until ignition was observed. Ubhayakar and Williams[9] mounted a small carbon particle on the end of a glass fiber and heated the particle with a ruby laser pulse. The particle was monitored by a high-speed camera that recorded the igniting particle as a bright spot on the film. The temperature of the particle was also monitored by dual-wavelength optical pyrometry. Cassel and Liebman[10], Chen et al.[5] and Seixas and Essenhigh[11] injected particles into a heated drop-tube furnace, and observed them with a photomultiplier tube. The temperature of the furnace was gradually increased until a flash was seen, indicating ignition. Gomez and Vastola[12] injected particles into a heated gas stream, and analyzed the resultant gases for CO and CO_2. The ratio of the two gas concentrations was used to distinguish between heterogeneous and homogeneous ignition. Ignition was also confirmed by light emission measurements. Tognotti, et al.[13] placed milligram quantities of coal or char in a thermogravimetric analyzer (TGA) in an inert (N_2) or oxidizing atmosphere, and slowly

ramped the temperature. The ignition temperature was defined as the point at which the weight vs. temperature curve for the coal or char in the oxidizing atmosphere deviated from that in the inert atmosphere. In all of the above experiments, the ignition temperature was found to decrease with increasing particle size, in agreement with the thermal explosion theory. The activation energies determined from these experiments encompass a wide range of values (11 to 50 kcal/mole) because of the variety of coals and chars tested, and probably because of other differences from experiment to experiment. Essenhigh et al.[2] have reviewed early theories as well as more recent theoretical and experimental work on ignition.

These approaches have a number of drawbacks. In the experiments where a single coal particle is mounted on a thin wire (Bandyopadhyay and Bhaduri;[7] Karcz et al.;[8] Ubhayakar and Williams[9]) the effects of the physical contact on the energy balance have been assumed negligible. In the experiments which detect ignition by visual or optical detection (Chen et al.;[5] Bandyopadhyay and Bhaduri;[7] Karcz et al.;[8] Cassel and Leibman;[10] Seixas and Essenhigh;[11] Gomez and Vastola[12]) the determination of ignition is dependent on the spectral sensitivity of the selected detector. Only Ubhayakar and Williams[9] measured the actual particle temperature. Most investigators inferred particle temperature from the ambient value.

Ideally, one would like to isolate a single particle free of physical contact, rapidly heat the particle, and measure its temperature directly. In this paper we present an experimental investigation of ignition that more closely approaches this ideal. In our experiments, electrically charged char particles were levitated in an electrodynamic balance and heated with laser radiation. This type of electrodynamic thermogravimetric analyzer has been previously used in studies of char particle oxidation (Spjut et al.[14]; Bar-Ziv et al.[15]). The balance is an improved version of Millikan's oil-drop apparatus. In the electrodynamic balance, a charged particle is suspended in a DC field between two end-cap electrodes, as in the Millikan cell. In the midplane between the electrodes, a ring electrode surrounds the particle. When the particle is at the center of the cell it is not affected by the alternating field. If, however, it is displaced from that null point in any direction, the particle experiences an alternating force that increases with displacement. The particle then oscillates but lags the AC field in phase due to inertia and aerodynamic drag. The time-average force experienced by the particle drives it back toward the center of the cell. With the addition of this dynamic focussing, a particle that is levitated electrostatically can be subjected to rather strong forces without being lost. The historical background of the electrodynamic balance has been reviewed by Davis[16]. The balance has been used in

previous studies of ignition processes. Nelson et al.[17] used a form of the electrodynamic balance to suspend metal particles, which were ignited by a pulsed Nd-doped glass laser. Liebman et al.[18] also used a quadrupole levitator to suspend magnesium particles for ignition by a Nd-doped glass laser. Bar-Ziv[15] reports on some ignition studies in the electrodynamic thermogravimetric analyzer in his review article on single particle char combustion kinetics. We report here on the use of an electrodynamic balance to study laser-induced ignition of a freely levitated char particle.

Experimental

The use of the electrodynamic balance for single particle studies is well documented (Spjut et al.;[14] Davis;[16] and Monazam et al.;[19] Bar-Ziv et al.[15]). The electrode configuration in the electrodynamic balances most commonly used has a hyperboloidal geometry. The electric field in the hyperboloidal geometry balance is well-characterized (Davis[16]), but this understanding is not critical to its use. Many other electrode geometries have been used in previous applications of the electrodynamic balance (Davis;[16] Arnold and Folan[20]; Davis et al.[21]). Sloane and Elmoursi[22] have theoretically examined the characteristics of a number of electrode arrangements. We used hemispherical endcap electrodes and a right cylinder ring as illustrated in Figure 3. The electric field near the center of this balance, and therefore its operating characteristics, very closely approximates that of the hyperboloidal geometry (Sloane and Elmoursi[22]; Wong[23]). The electrode cell was housed in an evacuable stainless steel chamber with total volume of 250 cm^3. The atmosphere in the chamber was controlled by introduction of gases with the desired composition.

A 20-Watt Carbon Dioxide laser (Advanced Kinetics MIRL-20) was used to heat the particle. The laser was modified to produce a TEM-01* beam. In this mode, the cross-section of the beam appears to be doughnut-shaped rather than Gaussian shaped as in more common TEM-00 mode. The TEM-01* mode was selected because when the particle is heated, thermophoretic and photophoretic forces tend to push the particle away from the area of highest intensity (Greene[24]). In a Gaussian beam, then, the particle tends to be pushed out of the laser beam. The particle will remain trapped in a doughnut mode beam. The laser beam is directed by mirrors into the top of the chamber through a KCl window, and the beam is focused onto the particle with a ZnSe lens. The lens can be moved vertically to focus or defocus the beam with respect to the particle, changing the intensity of the beam incident on the particle.

The TEM-01* mode of the laser was very sensitive to laser temperature and power variations, therefore laser pulsing could not be controlled by pulsing the power supply. An external shutter was constructed from refractory and attached to a pneumatic piston. The laser beam was uncovered or covered in 3 to 4 milliseconds by the shutter. The length of time that the shutter was opened was controlled electronically.

A 5-mW HeNe laser (Melles Griot) was directed through the bottom of the chamber onto the particle for illumination. The particle was observed with a microscope and with a catadioptric microscope (Questar) and video camera combination. The images from the video camera were recorded on a video cassette recorder. The particle image was also focused onto a position-sensitive-detector (PSD) (Hamamatsu). The outputs from the PSD were connected to a proportional-integral- derivative (PID) controller which fed back to the DC voltage control. Thus, any force causing the particle to deviate vertically from the center in the vertical plane would cause the PID controller to adjust the DC voltage restoring the particle back to the center of the chamber.

The temperature of the particle was monitored by a two-color optical pyrometer, pictured schematically in Figure 4. Radiation from the particle was collimated by a CaF_2 lens, and then split by a coarse grating beam splitter. The two beams then passed through CaF_2 focusing lenses and interference filters at 1.48 and 3.42 μm and onto an InGaAs and an InSb detector. The output from the detectors was processed with a log-ratio amplifier, and monitored with a PC-based data acquisition system. The optical pyrometer was calibrated by inserting a type R thermocouple into the chamber with the bead placed at the center of the cell in place of the particle. The thermocouple was heated by the CO_2 laser while the thermocouple output and the pyrometer output were recorded. The pyrometer output is plotted against the thermocouple temperature in Figure 5.

The gas composition in the chamber was varied by using a 3-liter glass vessel as a continuous flow stirred tank reactor (CSTR). Nitrogen was passed through the vessel and through the chamber. At the onset of the experiment, oxygen was admitted into the CSTR. The output from the CSTR was then a N_2-O_2 mixture that was slowly increasing in oxygen. This mixture flowed through the chamber and into an oxygen analyzer (Beckman, Model 755). The TGA chamber also acted as a CSTR, but with a much shorter residence time so that concentration of oxygen was very close to that of the larger vessel.

Two materials were used in this study. The first was Spherocarb, a highly porous synthetic carbon intended for use as a gas chromatograph column packing. (Alltech purchases this material from Analabs and markets it as "Carbosphere." Because

Spherocarb is the trade name more commonly found in literature references, we shall call the material Spherocarb). Because of its high pososity, relative freedom from impurities, and highly spherical shape, this material has been used in many carbon oxidation studies (Waters et al.[25]; Floess[26]; Bar-Ziv et al.[15]). The second material studied was char from PSOC 1451 bituminous coal previously characterized by Sahu et al.[27].

Procedure

An experiment was started by presetting the AC and DC voltages of the electrodynamic balance to previously determined values. A small amount of char was placed on a small electrode and pushed under the bottom end-cap electrode. A Zerostat (Discwasher, Inc.) anti-static device was used to generate a short high voltage pulse to the electrode. Char particles on the electrode acquired charge and were repelled from the electrode through the opening in the bottom electrode into the electrodynamic cell, where some were captured by the AC field. The AC and DC voltages were manipulated to isolate a single particle. Following the suspension of an isolated particle the chamber was flushed with nitrogen. The dimensions of the particle were then measured with an eyepiece micrometer. After these preliminaries, the CO_2 laser was pulsed by opening the shutter for 500 milliseconds. During this pulse, the output from the pyrometer, the balancing voltage, and the position were recorded on a PC-based data acquisition system. The temperature rise observed in the absence of oxygen provided the data needed to calculate the laser energy absorbed by the particle. Oxygen was then admitted into the CSTR and as the N_2-O_2 mixture of increasing O_2 concentration was very slowly passed through the chamber, additional laser pulses were administered until the particle ignited.

Results

The time-temperature history of a Spherocarb particle undergoing a laser pulse in nitrogen is shown in Figure 6a. The solid line connects experimental data points. It can be seen that the particle temperature increases, reaches a steady state level and then drops when the laser pulse ends. Figure 6b shows the same particle heated in 20% oxygen. The steady state temperature is now higher, due to increased rate of carbon oxidation. At each laser pulse the oxygen concentration was about 5% higher than that present at the previous pulse. This particular Spherocarb particle ignited when the oxygen concentration reached 40%, as illustrated in Figure 6c. The temperature trace shows an ignition delay time of approximately 300 milliseconds.

The vertical position trace of a Spherocarb particle in nitrogen is shown in Figure 7a, where 0 denotes the center of the chamber. Prior to the laser pulse, the particle is oscillating with an amplitude of the order of ±15 μm. When the particle is pulsed, the oscillation changes, but the particle does not deviate from the center of the chamber. This pattern was generally observed for subsequent pulses as shown in Figure 7b. Figure 7c shows that for a particle suspended in 40% oxygen, the amplitude of the oscillations, initially very small, greatly increases during heating. Finally, when the particle reaches a temperature of 1200 to 1300K, it begins to lose charge (Dudek et al.[28]), and the particle eventually drops from the center of the chamber, as shown by the position trace.

Figure 8 shows the heat loss and heat generation curves for a Spherocarb particle exposed to different oxygen concentrations. The curves are analogous to those in Figure 1. The heat loss curve is the labeled solid line. The horizontal solid line represents the heat generation curve in nitrogen. Since the only source of heat is the laser, the particle temperature is constant, and the line is horizontal. The short-dashed line is the heat generation in 20% oxygen. This curve intersects the heat loss curve, indicating a stable temperature, without ignition. The long-dashed line shows the heat generation curve at 40% oxygen. This curve is above the heat loss curve, satisfying equations (2) and (3), so the particle ignites. The region in Figure 6c where the particle temperature rises slowly corresponds to the area where the heat generation and heat loss curves are close to each other.

The temperature trace of a 300 μm bituminous char particle laser-heated in nitrogen is shown in Figure 9a. The steady-state temperature trace fluctuates somewhat due to the more irregular shape and uneven heating of the char particle. In 10% oxygen, Figure 9b shows that the particle temperature dips slightly, then returns to a steady state level, until the laser pulse is off. The video recording shows that the dip in the temperature is due to movement and rotation of the unevenly heated particle. When the oxygen pressure reaches 15%, the particle ignites. Figure 9c shows that ignition was attained after a short induction time.

The vertical position trace of the bituminous char particle is shown in Figures 10a,b and c. When the laser is pulsed on, the particle undergoes a larger displacement from that of a Spherocarb particle, and rises in the chamber. This is evidently because of the greater buoyancy effect on the lower density char. As with the Spherocarb particles, the igniting char particle drops out of the center because of charge loss.

Discussion

In a simple analysis of particle ignition, a spherical and isothermal particle is assumed to be at rest relative to the surrounding gas. The heat loss to the gas may be written in the form of Newton's law of cooling. The heat transfer coefficient is determined from the Nusselt number, which equals 2 for spheres at low Reynolds numbers, as in this case. The contribution of radiation to the particle heat loss is small but increases as the temperature of the particle increases. The heat loss due to conduction and radiation for a sphere are:

$$H_c = \frac{k(T_p - T_g)}{r} \tag{5}$$

$$H_r = \varepsilon \sigma (T_p^4 - T_g^4) \tag{6}$$

where k is the thermal conductivity of air, T_p is the particle temperature, T_g is the gas temperature, r is the particle radius, ε is the particle emissivity, and σ is the Stefan-Boltzman constant.

The rate of carbon oxidation, R_C, is generally expressed in the simple form

$$R_C = A\, e^{(-E_a/RT_p)} P_{O_2}^n \tag{7}$$

where E_a is the activation energy, R is the gas constant, A is the pre-exponential factor, P_{O_2} is the pressure of oxygen, and n is the reaction order. The heat generation term is then given by:

$$H_g = R_C Q_{eff} \tag{8}$$

where Q_{eff} is the heat released by carbon oxidation. The time dependent equation (3) can therefore be written as

$$m C_p \frac{dT}{dt} = 4\pi a^2 (H_g + H_l - H_c - H_r) \tag{9}$$

The term H_l is the heat gain from absorption of the laser energy.

The value of the heat capacity, C_p, for Spherocarb was taken from Monazam et al.[19]. An apparent activation energy, E_a, of 20 kcal/mole and a reaction order with respect to oxygen, n, of one-half was assumed, as determined by Waters et al.[25] in their study of Spherocarb oxidation in the temperature range of 1400 to 2200K. The diffusion of oxygen through the porous char matrix becomes the limiting factor in the carbon oxidation rate at these temperatures. The particle temperatures being measured were approaching this range, hence these apparent rate parameters were selected. Also in the experiment by Waters et al.[25], it was determined that the oxidation products were CO and CO_2 in a 65% to 35% ratio, and Q_{eff} was calculated accordingly. Table I gives the values used for each parameter and the literature source.

The value of H_l was determined from the particle temperature trace when heated in nitrogen. In the absence of oxygen, H_g is zero, and at steady state, $H_l = H_c + H_r$. After H_l was determined, the time dependent equation (9) was solved using a fourth-order Runge-Kutta routine. The preexponential factor was varied until a reasonable fit of the curve to the experimental data from the ignition event was obtained.

The calculated temperature traces are shown by the dashed lines in Figures 6a to 6c and 9a to 9c. The good agreement between calculated traces and measured traces for the nitrogen atmosphere (Figures 6a and 9a) simply reflects the choice of the parameter, H_l, which was adjusted to match those two traces. The calculated laser intensity is listed in Table 2. The density parameter was adjusted to match the initial slope of the calculated trace to the measured trace in a nitrogen atmosphere. The density values are larger than the density of 600 kg/m^3 found for Spherocarb particles by D'Amore et al.[29], but they cluster around the value of 1050 kg/m^3 used by Monazam et al.[19] when he measured the heat capacity of Spherocarb.

Table 2 shows the fitted parameters for several particles. The fitted pre-exponential factors ranged from 3.6 to 6.1. The preexponential factor that was determined by Waters et al.[25] was 10.6 Kg m^{-2} s^{-1}(mole O_2 m^{-3})$^{-n}$. Although the preexponential factor is the nominal fitting parameter, Q_{eff} and $P_{O_2}^n$ can also be lumped in with the exponential factor. Therefore, the uncertainty in the fitted exponential value is also indicative of uncertainties in Q_{eff} and $P_{O_2}^n$.

The calculated trace in Figure 6b was determined using the fitted parameters from Figures 6a and 6c. It appears to overpredict the measured temperature. This discrepancy may be due to experimental error such as fluctuations in the laser power, or it may be due

to the uncertainties in the Q_{eff} and $P^n_{O_2}$ as mentioned previously. A general trend of increasing steady state temperature with increasing oxygen concentration could be detected, however, the scatter in the data was substantial, and the relationship could not be quantified.

Sahu et al.[30] determined an apparent activation energy of 17 kcal/mole for char made from PSOC 1451 bituminous coal with a preexponential factor of 107.1 g cm^{-2} s^{-1} atm^{-1}. When the apparent activation energy is used, and the preexponential factor varied to achieve a reasonable fit, Figure 9c results.

There are an number of problems with this experiment which are not apparent from the results presented. The first is related to the laser stability. The laser power, as measured on a power meter, was subject to fluctuations and occasionally drifted over a long period of time. To minimize the effect of drift, the experiments were performed only when it appeared that the laser was operating stably and the power was not drifting. However, the fluctuations were always present. Another difficulty was that the laser heated the particle from the top only. Video recordings of a Spherocarb particle during heating clearly show a thermal gradient across the particle. Thus, the model used to describe the experiments is an oversimplification. Bar-Ziv et al.[15], and Monazam et al.[19] addressed this problem for a particle heated on opposite sides and concluded that the maximum temperature difference between the surface and center of the particle was about 8K for a particle 1000°C above ambient. They concluded that this difference may be disregarded for most combustion studies. For one sided heating, however, the temperature difference is greater, although the magnitude of the temperature gradient is not known.

A particle heated on one side might lead to ignition at a point, or a very small area, as discussed by Levendis et al.[31]. Those authors used two-color pyrometry to measure the temperature of a char particle burning in a drop-tube furnace. They observed signal intensities which increased in the individual detectors while the ratio of the signal intensities remained relatively constant, indicating a relatively uniform temperature. They attributed the increase in signal intensity to localized ignition on the particle surface which gradually spread over the surface of the particle. In the present experiments we did not measure the individual signal intensities but only their ratios therefore, it is unknown whether the detector signal levels are changing while their ratio remains constant. Observations from the video recording of the particle ignition do not show localized ignition on a Spherocarb particle. The particle appears to glow uniformly as the temperature nears the ignition point (although saturation of the video camera precludes quantitative interpretation of these

images). As the particle ignites, it appears to expand to about twice its original diameter. This expansion may be due to an oscillation of the particle that is too rapid to be resolved by the video camera, or it may result from camera saturation. At this point, the particle loses a significant amount of charge, and drops from the center of the chamber. No hot spots are visible, no jetting is observed, and Spherocarb particles always move in the downwards direction. Hence, it is believed that the Spherocarb particles are igniting uniformly across the surface of the particle. In contrast, there is clear evidence of localized ignition on char particles. Video recordings show that, when a coal char particle is heated, small areas glow considerably more intensely than other areas. Since the char is irregularly shaped, this is not unexpected. Even when a char particle ignites, hot spots often are visible.

Conclusions

This experiment has shown that ignition experiments are feasible in the electrodynamic balance With the particle suspended without physical contact, heat transfer other than by conduction and radiation is avoided. The particle temperature is measured by the optical pyrometer and does not need to be calculated from the ambient temperature. There are some difficulties which need to be addressed in order to increase the utility of this experiment. The first is the temperature gradient along the particle due to heating from the top side only. When we attempted to heat from both sides, the particle bounced around excessively. The solution might be using a more powerful laser, such as used by Monazam et al.[19], in the Gaussian mode. The problem of charge loss at high temperatures also limits the usefulness of the electrodynamic balance somewhat in that the particle is lost once it reaches ignition temperatures. There are other techniques that can levitate an uncharged particle which are as yet untested for char oxidation studies.

The temperature traces of particles that ignited clearly show an induction time, or ignition time lag, as predicted by the solution of the time dependent equation for a heated particle. The effect of increasing the oxygen concentration is also seen in the increasing equilibrium temperature at sub-ignition conditions, though it was not quantifiable in this study. A simple isothermal sphere model was used with parameters obtained from the literature which adequately predicted the experimentally obtained time-temperature histories of igniting Spherocarb particles. A reasonable fit to the bituminous char data was achieved using rate parameters determined by Sahu et al.[30]. These experiments provide the first examples in which the oxidation of char during ignition is rigorously modeled and compared with existing literature data. The electrodynamic balance can be used in ignition

experiments to measure the apparent char oxidation rate parameters, and probe particle-to-particle variations in the apparent kinetics.

Acknowledgements

This research was supported by the U.S. Department of Energy, University Coal Research Program under grants DE-FG22-89PC89765 and DE-FG22-88PC88911.

References

(1) Field, M. A.; Gill, D. W.; Morgan, B. B.; Hawksley, P. G. W. *Combustion of Pulverized Coal*; The British Coal Utilisation Research Association, Leatherhead, 1967.

(2) Essenhigh, R. H.; Misra, M. K.; Shaw, D. W. *Combust. Flame.* **1989**, *77*, 3-30.

(3) Howard, J. B.; Essenhigh, R. H. *Eleventh Symp. (Int.) Comb.*, The Combustion Institute, Pittsburgh, 1967, p. 399-408.

(4) Annamalai, K.; Durbetaki, P. *Combust. Flame.* **1977**, *29*, 193-208.

(5) Chen, M.-R.; Fan, L.-S.; Essenhigh, R. H. *Proc. Twentieth Symp. (Int.) Comb.* **1984**, 1513.

(6) Thomas, G. R.; Stevenson A. J.; Evans, D. G. *Combust. Flame.* **1973**, *21*, 133-136.

(7) Bandyopadhyay, S.; Bhaduri, D. *Combust. Flame.* **1972**, *18*, 411-415.

(8) Karcz, H.; Kordylewski, W.; Rybak, W. *Fuel.* **1980**, *59*, 799-802.

(9) Ubhayakar, S. K.; Williams, F. A. *J. Electrochem. Soc.* **1976**, *123*, 747.

(10) Cassel, H. M.; Leibman, I. *Combust. Flame.* **1959**, *3*, 467-475.

(11) Seixas, J. P. S.; Essenhigh, R. H. *Combust. Flame.* **1986**, *66*, 215-218.

(12) Gomez, C. O.; Vastola, F. J. *Fuel.* **1985**, *64*, 558-563.

(13) Tognotti, L.; Malotti, A.; Petarca, L.; Zanelli, S. *Combust. Sci. and Tech.* **1985**, *44*, 15-28.

(14) Spjut, R. E.; Sarofim, A. F.; Longwell, J. P. *Langmuir.* **1985**, *1*, 355-360.

(15) Bar-Ziv, E.; Jones, D. B.; Spjut, R. E.; Dudek, D. R.; Sarofim, A. F. *Combust. Flame.* **1989**, *75*, 81-106.

(16) Davis, E. J. In *Surface and Colloid Science.* (E. Matijevic, ed.). Plenum Press, New York. Vol. 14, 1965.

(17) Nelson, L. S.; Richardson N. L.; Prentice, J. L., *Rev. Sci. Instrum.* **1968**, *39*, 744.

(18) Liebman, I.; Corry, J.; Perlee, H. E. *Combust. Sci. and Tech.* **1972**, *5*, 21-30.

(19) Monazam, E. R.; Maloney, D. J.; Lawson, L. O. *Rev. Sci. Instrum.* **1989**, *60*, 3460-3465.

(20) Arnold, S.; Folan, L. M. *Rev. Sci. Instrum.* **1987**, *58*, 1732-1735.

(21) Davis, E. J.; Buehler, M. F.; Ward, T. L. *Rev. Sci. Instrum.* **1990**, *61*, 1281-1288.

(22) Sloane, C. S.; Elmoursi, A. A. *IEEE Trans. Ind. Appl.* **1989**, *25*, 711-719.

(23) Wong, B. A. *The Oxidation of Individually Levitated Char Particles*, Ph.D. Thesis, California Institute of Technology, 1991.

(24) Greene, W. M.; Spjut, R. E.; Bar-Ziv, E.; Longwell, J. P.; Sarofim, A. F. *Langmuir*. **1985**, *1*, 361-365.

(25) Waters, B. J.; Squires, R. G.; Laurendreau, N. M.; Mitchell, R. E. *Combust. Flame*. **1988**, *74*, 91-106.

(26) Floess, J. K.; Longwell, J. P.; Sarofim, A. F. *Energy Fuels*. **1988**, *2*, 18-26.

(27) Sahu, R.; Levendis, Y. A.; Flagan, R. C.; Gavalas, G. R. *Fuel*. **1988**, *67*, 275-283.

(28) Dudek, D. R.; Wright, D. A.; Longwell, J. P.; Sarofim, A. F.; Yeheskel, J. *Combust. Sci. and Tech.* **1990**, *73*, 447-461.

(29) D'Amore, M.; Dudek, D. R.; Sarofim, A. F.; Longwell, J. P. *Powder Technol.* **1988**, *56*, 129-134.

(30) Sahu, R.; Northrop, P. S.; Flagan, R. C.; Gavalas, G. R. *Combust. Sci. Tech.* **1988**, *60*, 215-230.

(31) Levendis, Y. A.; Sahu, R.; Flagan, R. C.; Gavalas, G. R. *Fuel*. **1989**, *68*, 849-855.

Table 1

Parameters Used in Model

Parameter	Value	Source
Heat Capacity, C_p	$0.4 \frac{cal}{g\ degK}$	Monazam et al., 1989
Thermal Conductivity, k	$k_0(\frac{T_p + T_g}{2T_0})^{0.75}$ $\frac{cal}{cm\ s\ degK}$	Field et al., 1967
Emissivity	0.8	Monazam et al., 1989
Activation Energy, E_a	$20 \frac{kcal}{mole}$	Waters et al., 1988
Reaction order, n	0.5	Waters et al., 1988
Heat Release, Q_{eff}	$0.35\ Q_{CO_2} + 0.65\ Q_{CO}$ (40.82 kcal/mole)	Waters et al., 1988
Particle Density	Fitted	
Laser Intensity	Fitted	
Preexponential, A	Fitted	
Activation Energy, E_a for char	17 kcal/mole	Sahu et al., 1988b
Preexponential, A for Char	Fitted	

Table 2

Spherocarb Experiments

Series	Size μm	Laser Intensity W/m^2	Density kg/m^3	A $kg/m^2s(KPa)^{-.5}$	P_{O_2} %
1	100	$3.13x10^6$	110	3.6	50
2	98	$4.65x10^6$	1200	4.2	13
3	75	$4.11x10^6$	1000	6.1	25
4	99	$3.04x10^6$	800	3.73	40
5	99	$3.45x10^6$	1100	5.0	35
6	105	$3.46x10^6$	1000	3.6	35
7	82	$4.54x10^6$	1000	3.6	25
8	79	$3.85x10^6$	1000	5.2	30
9	95	$3.54x10^6$	1100	4.0	25

Figure Captions

Figure 1. Rate of heat loss or gain for a 50 m diameter particle at 900K (small-dashed lines), 1235K (solid lines) and 1400K (large-dashed lines). Physical parameters are from Field et al (1967). The lettered points are described in the text.

Figure 2. Curve showing ignition induction time for a 50 m particle (solid line). The curves and the lettered points correspond to the same conditions as in figure 1.

Figure 3. Schematic of the electrodynamic balance electrodes, heating system, and position monitoring system.

Figure 4. Schematic of the optical pyrometer

Figure 5. Calibration Curve for the optical pyrometer

Figure 6. Temperature trace for a 198 m diameter spherocarb particle. Experimental data are shown in open circles. a. Laser pulse in nitrogen gas. b. Laser pulse in 20% oxygen. c. Laser pulse in 40% oxygen.

Figure 7. Vertical position of the Spherocarb particle. a. Spherocarb pulsed in nitrogen. b. Spherocarb pulsed in 20% oxygen. c. Spherocarb pulsed in 40% oxygen.

Figure 8. Rate of heat generation and heat loss for a 198 m diameter spherocarb particle. The solid line shows the heat gain in nitrogen. The dash-dotted line shows the heat gain in 20% oxygen. The dashed line shows the heat gain in 40% oxygen. The dash-dot-dot line shows the heat loss curve.

Figure 9. Temperature traces for a 300 m diameter char particle produced from PSOC 1451 bituminous coal. Experimental data are shown in open circles. a. Laser pulse in nitrogen gas. b. Laser pulse in 10% oxygen. c. Laser Pulse in 15% oxygen.

Figure 10. Vertical position of the bituminous char particle. a. Char pulsed in nitrogen. b. Char pulsed in 10% oxygen. c. Char pulsed in 15% oxygen.

Figure 1

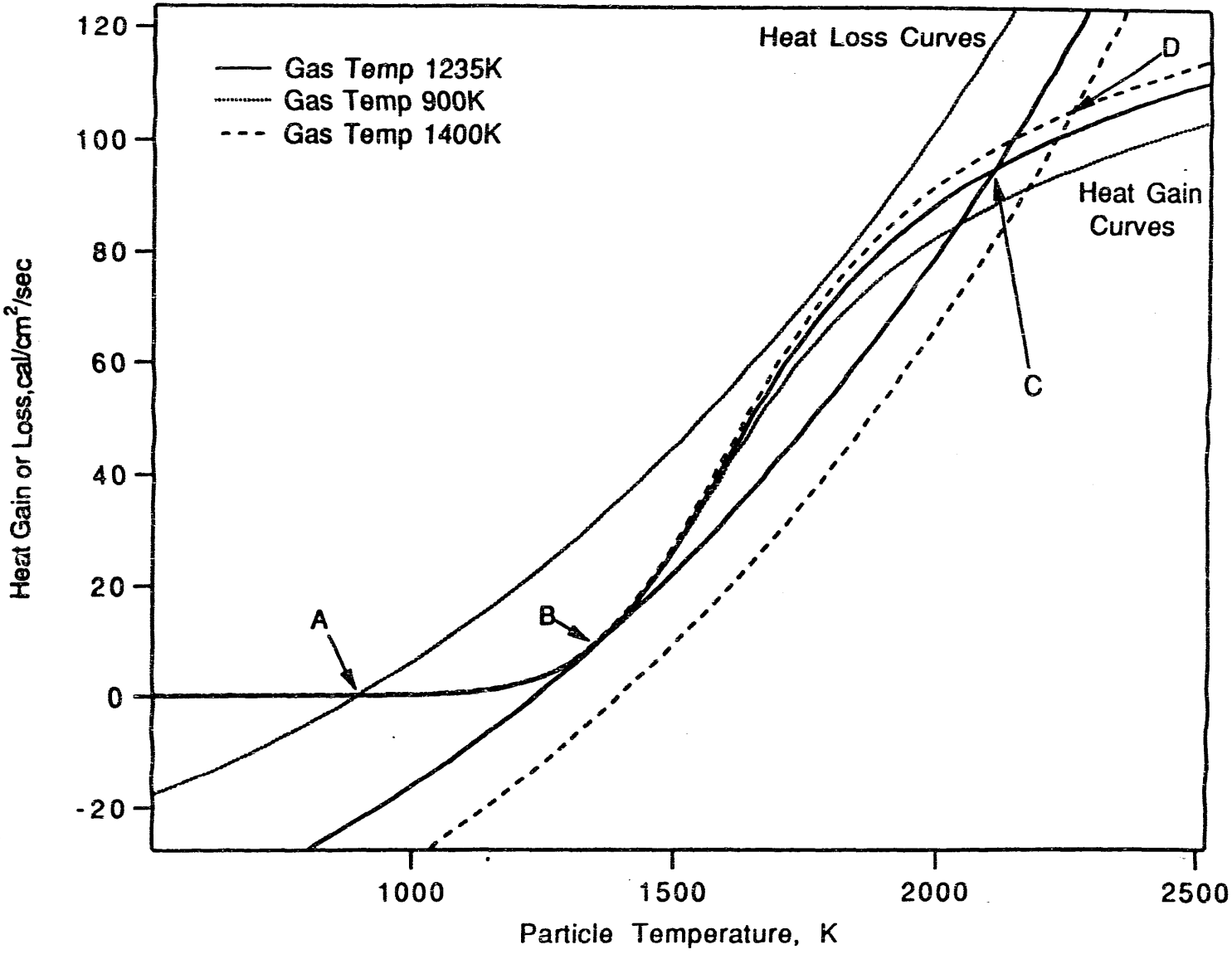
Heat Loss Curves
Gas Temp 1235K
Gas Temp 900K
Gas Temp 1400K
Heat Gain
Curves
A
B
C
D
120
100
80
60
40
20
0
-20
1000
1500
2000
2500
Heat Gain or Loss,cal/cm²/sec
Particle Temperature, K

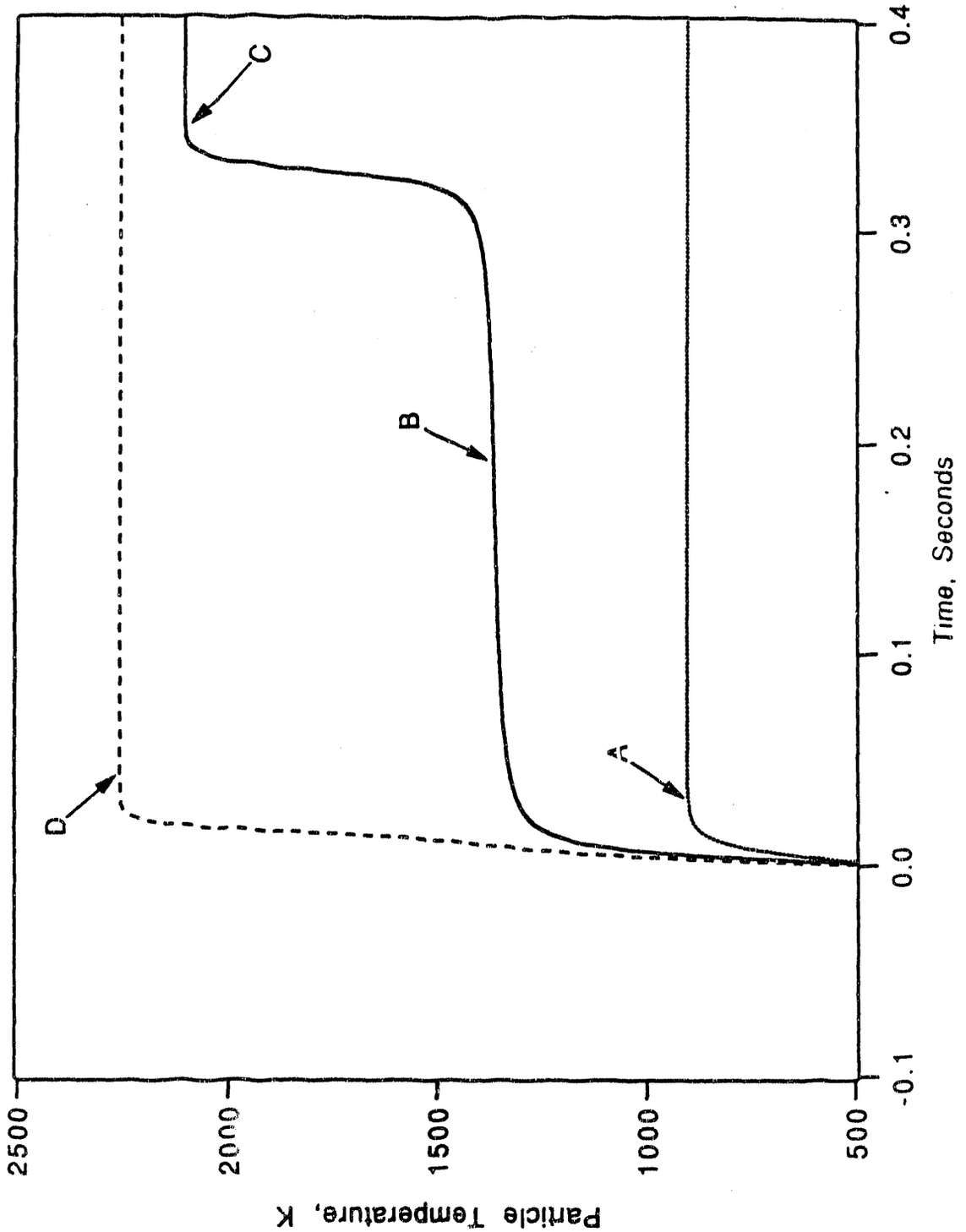
Particle Temperature, K
2500
2000
1500
1000
500
-0.1
0.0
0.1
0.2
0.3
0.4
Time, Seconds
A
B
C
D

Figure 2

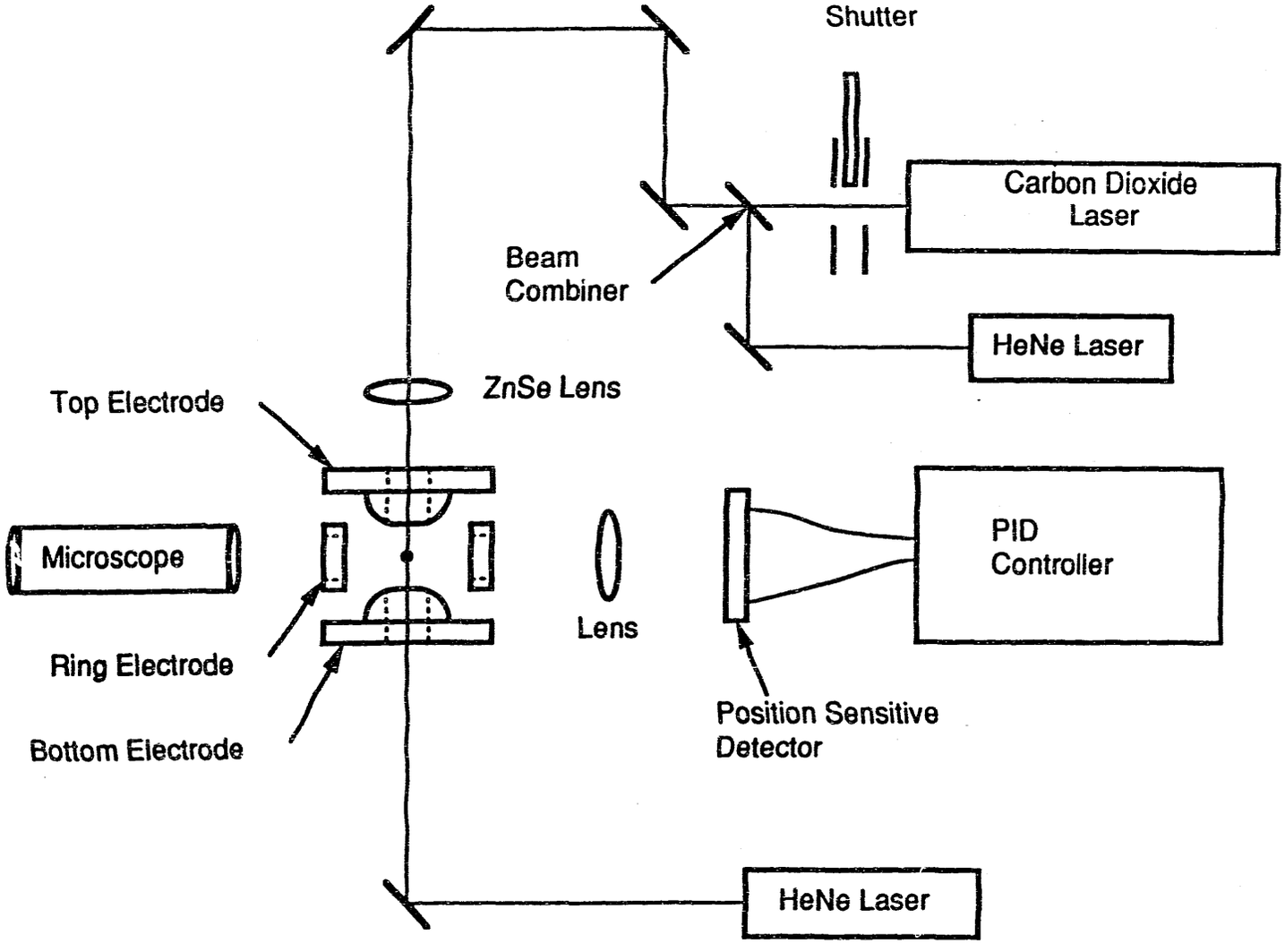

Figure 3. Schematic of the EDTGA

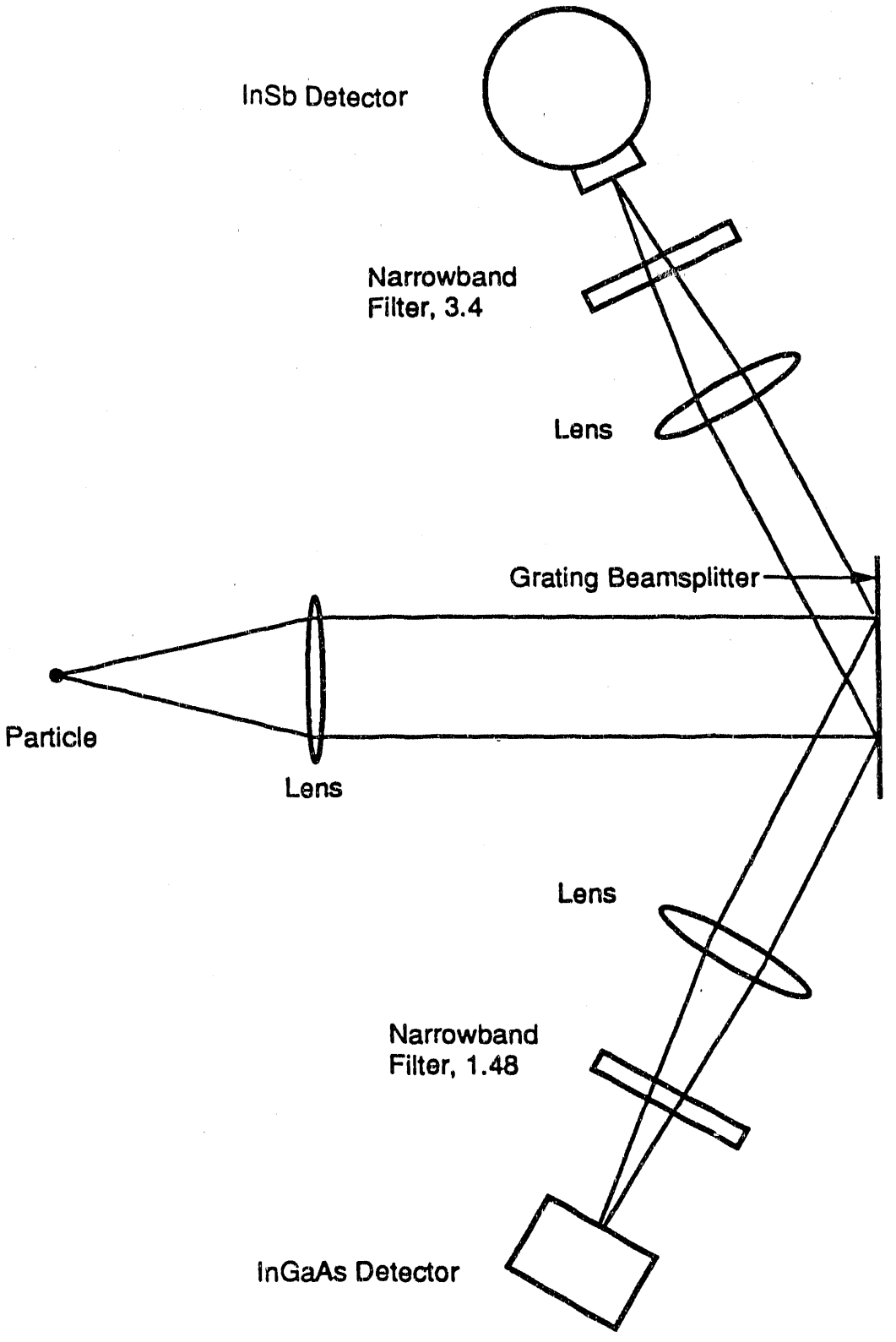

Figure 4. Pyrometer Schematic

Figure 5

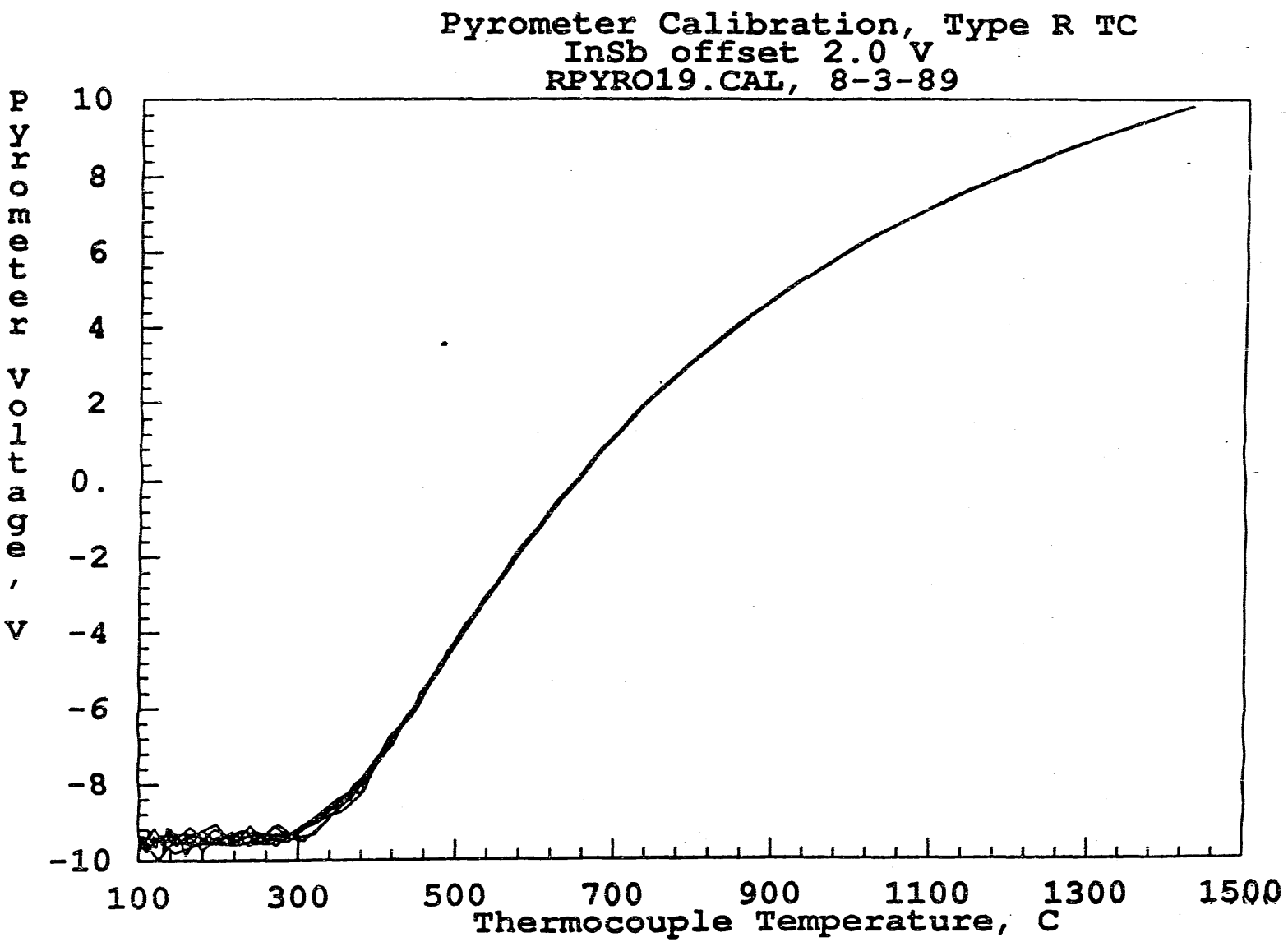
Pyrometer Calibration, Type R TC
InSb offset 2.0 V
RPYRO19.CAL, 8-3-89
Pyrometer Voltage, V
10
8
6
4
2
0.
-2
-4
-6
-8
-10
100
300
500
700
900
1100
1300
1500
Thermocouple Temperature, C

Figure 6a

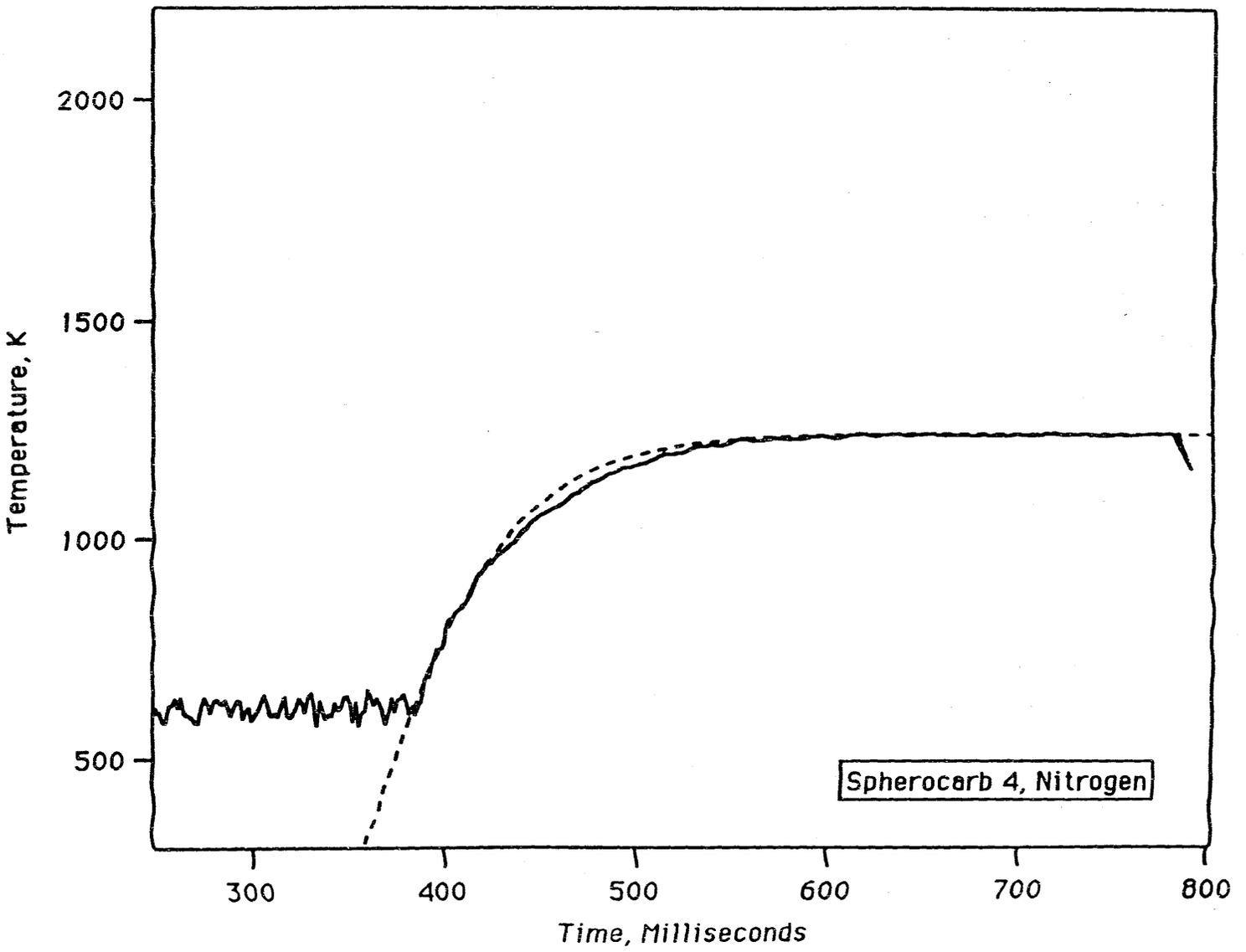
2000
1500
1000
500
Temperature, K
300
400
500
600
700
800
Time, Milliseconds
Spherocarb 4, Nitrogen

Figure 6b

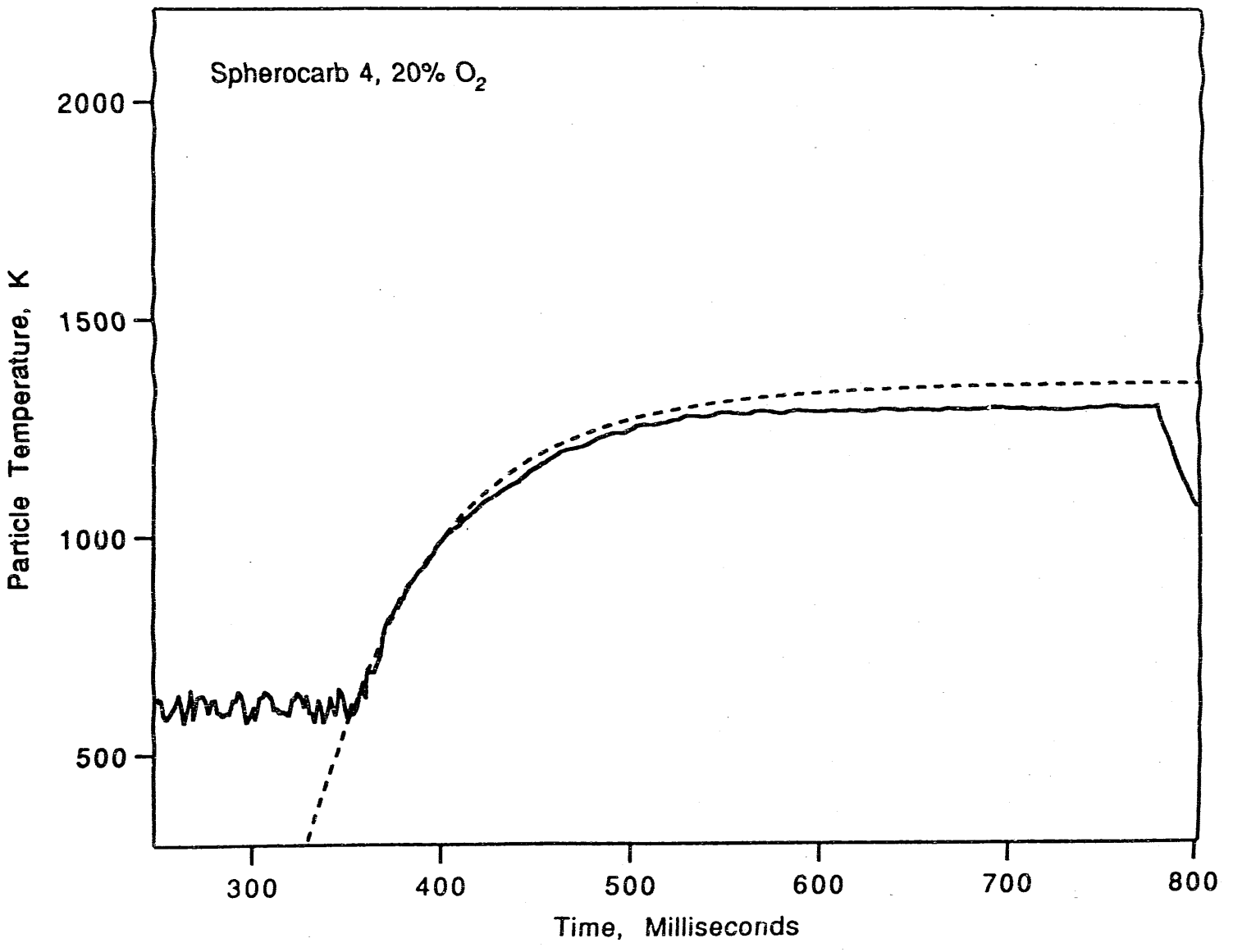
Spherocarb 4, 20% O_2
2000
1500
1000
500
Particle Temperature, K
300
400
500
600
700
800
Time, Milliseconds

Figure 6c

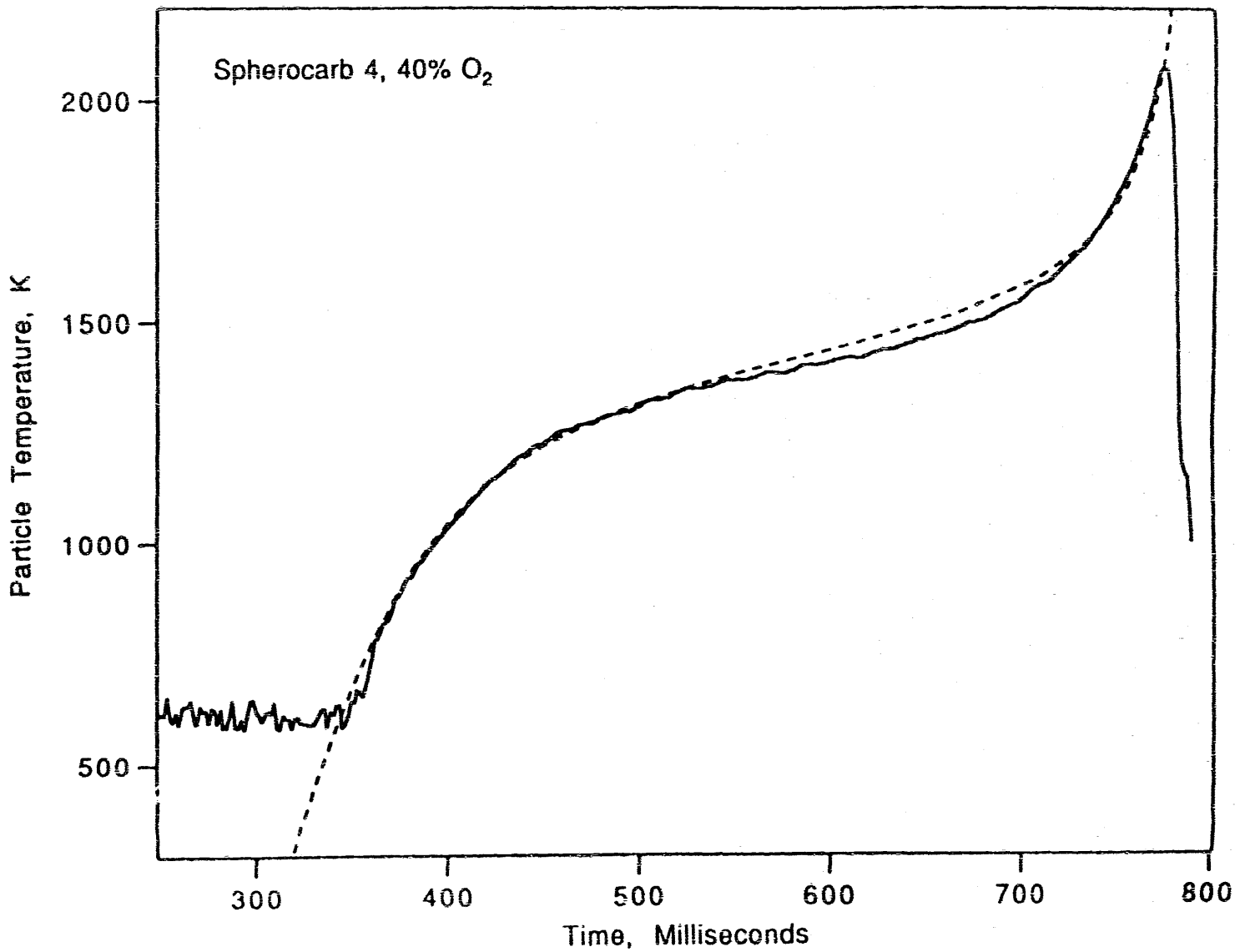
Spherocarb 4, 40% O_2
Particle Temperature, K
2000
1500
1000
500
300
400
500
600
700
800
Time, Milliseconds

Figure 7a

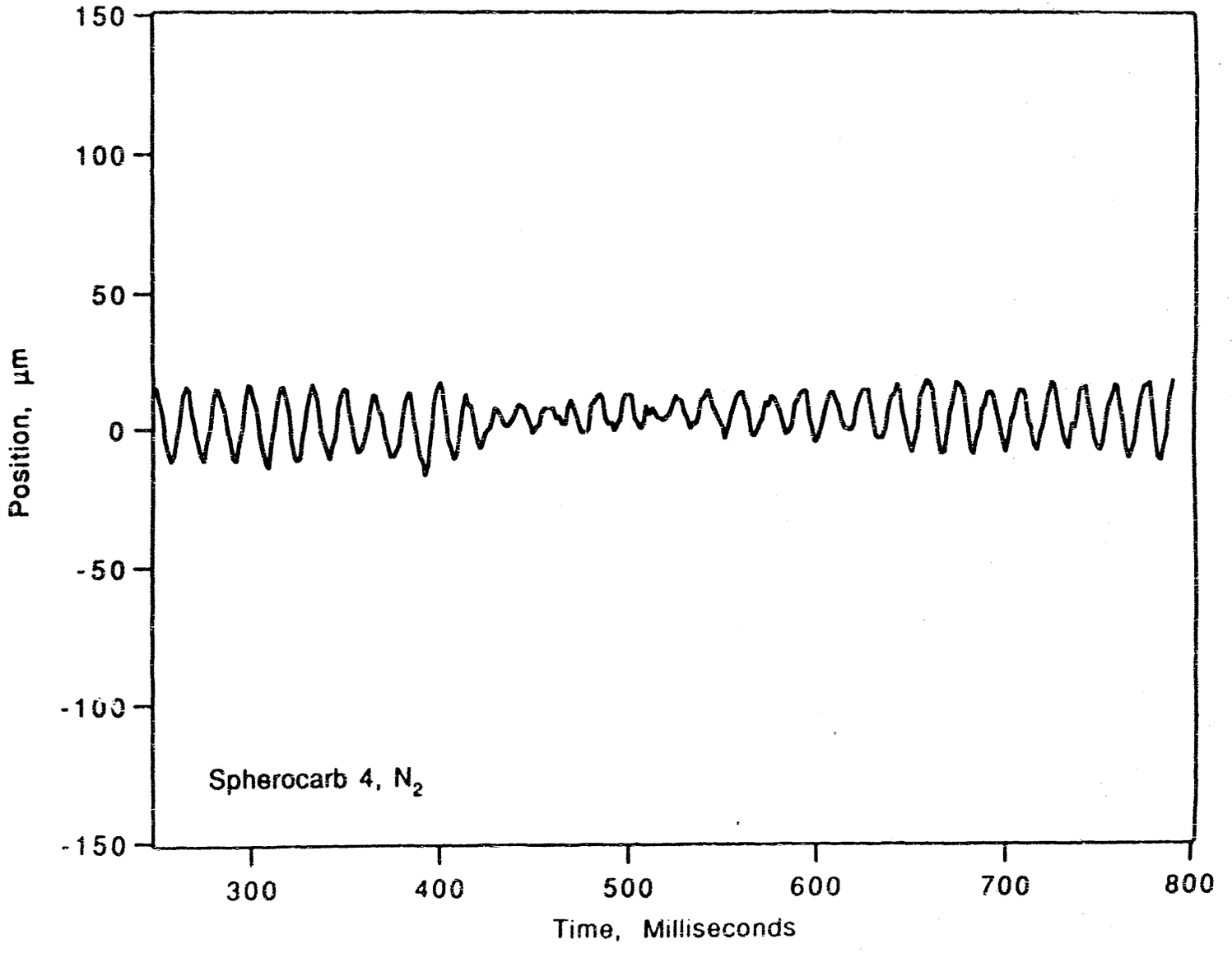
150
100
50
0
-50
-100
-150
Position, µm
Spherocarb 4, N_2
300
400
500
600
700
800
Time, Milliseconds

Figure 7b

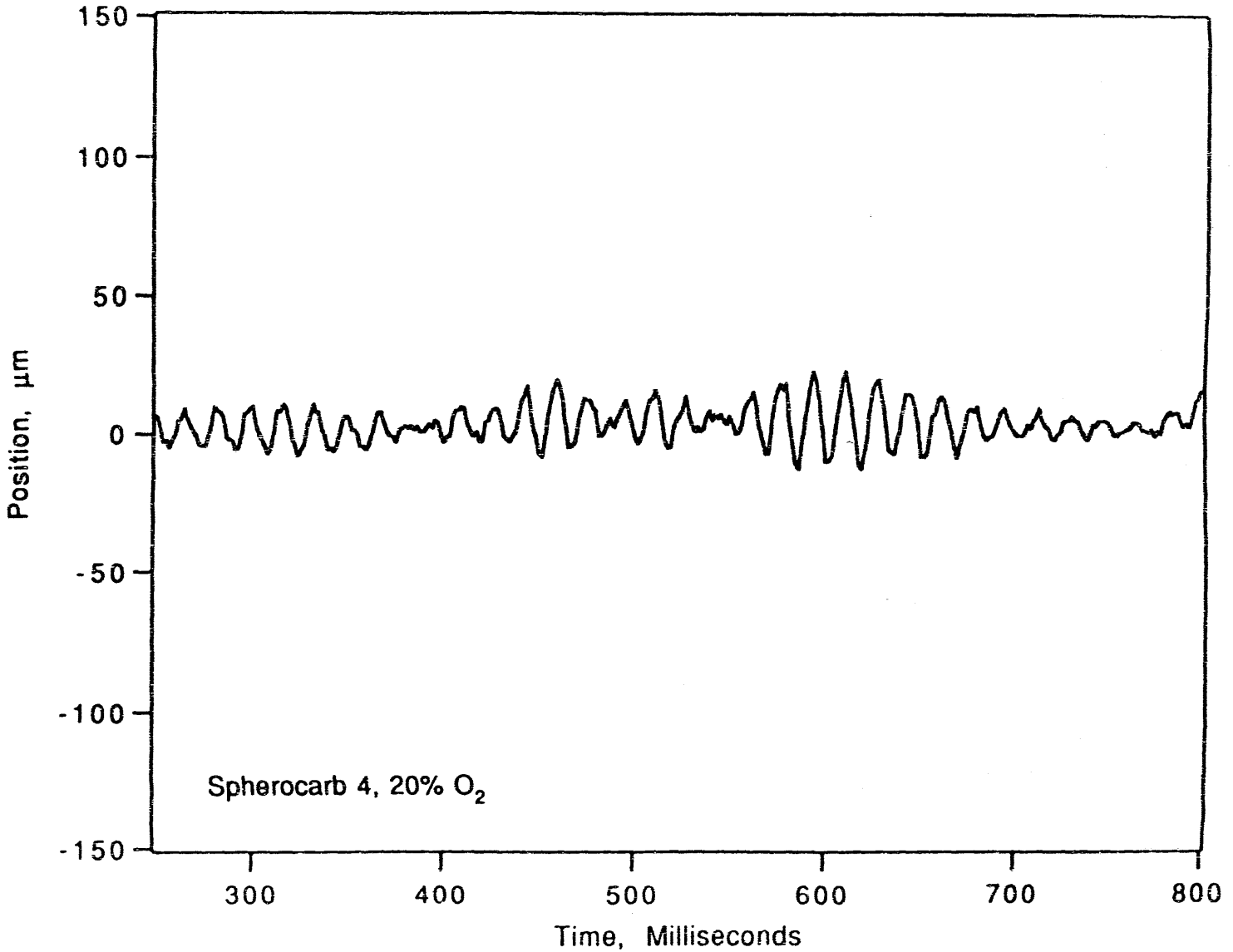
150
100
50
0
-50
-100
-150
Position, µm
Spherocarb 4, 20% O_2
300
400
500
600
700
800
Time, Milliseconds

Figure 7c

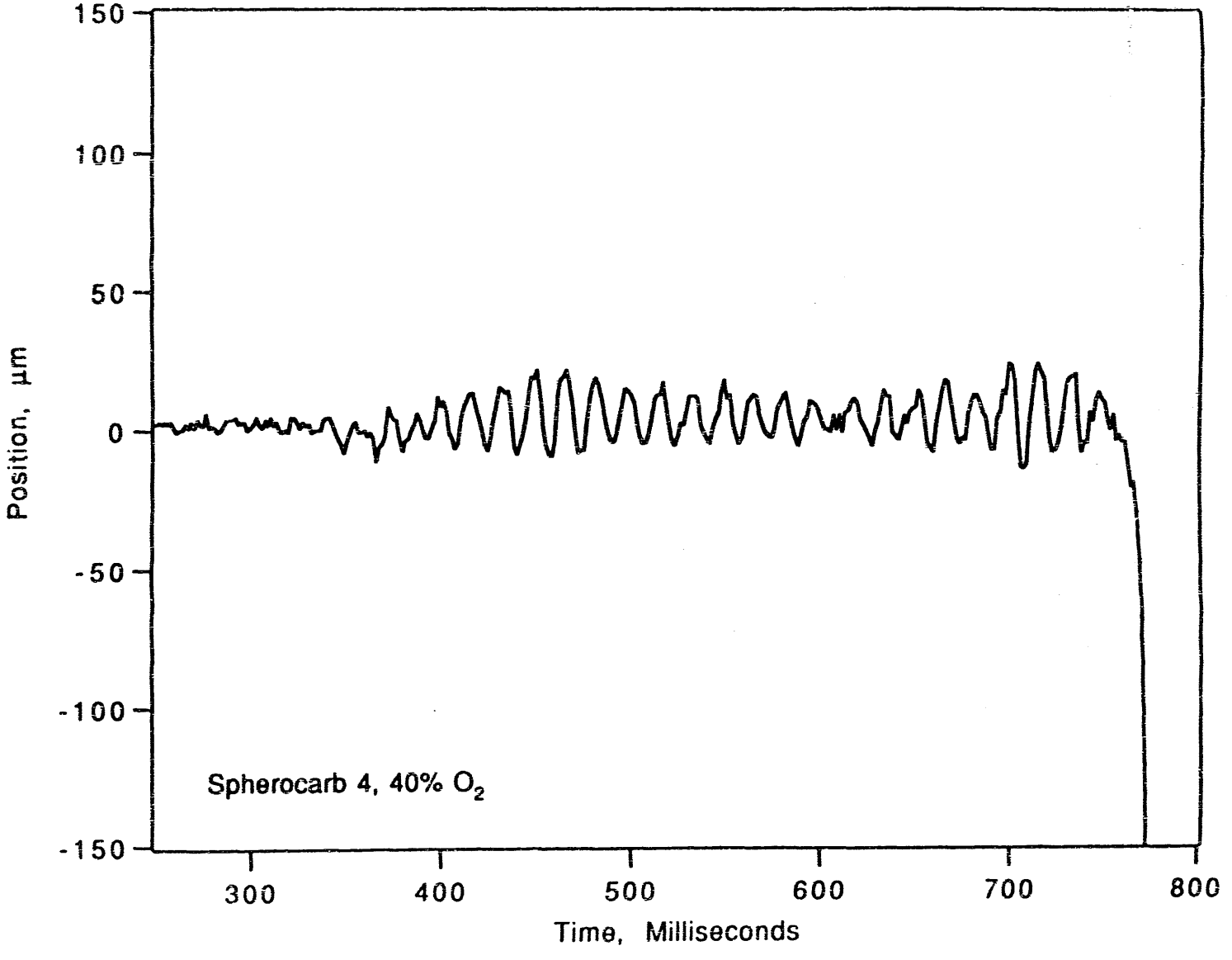
150
100
50
0
-50
-100
-150
Position, µm
300
400
500
600
700
800
Time, Milliseconds
Spherocarb 4, 40% O_2

Figure 8

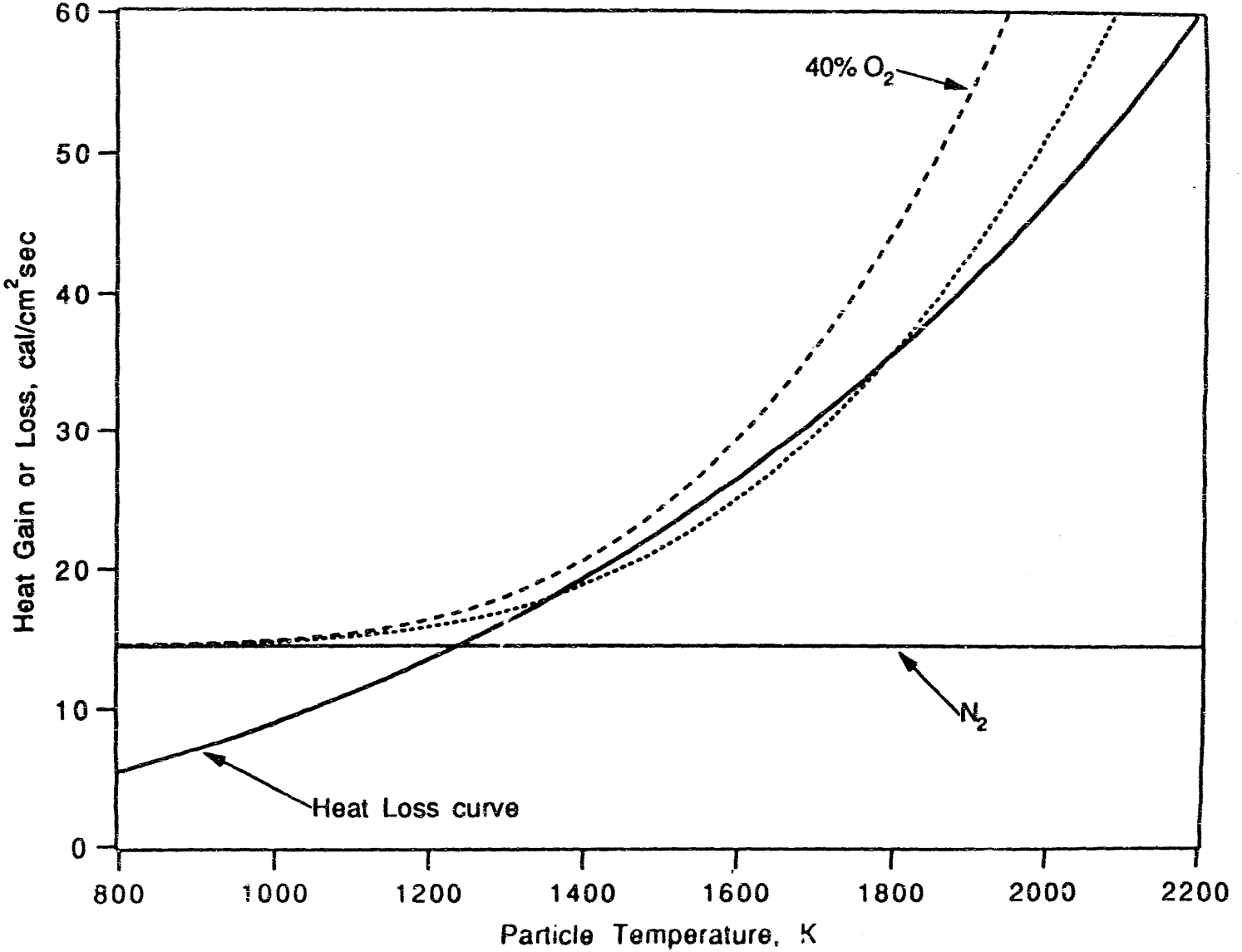
60
50
40
30
20
10
0
Heat Gain or Loss, cal/cm²sec
40% O₂
N₂
Heat Loss curve
800
1000
1200
1400
1600
1800
2000
2200
Particle Temperature, K

Figure 9a

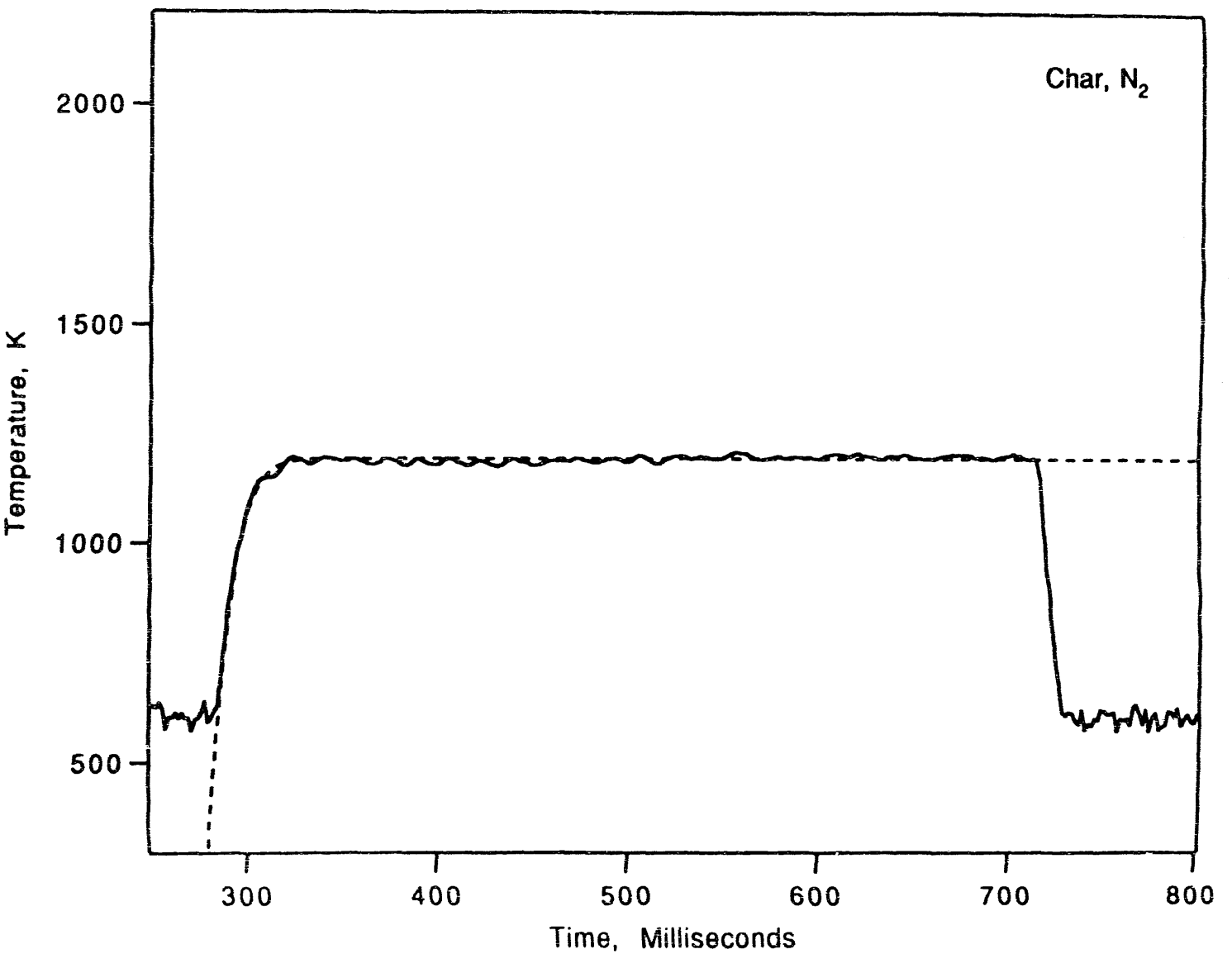
Char, N_2
2000
1500
1000
500
Temperature, K
300
400
500
600
700
800
Time, Milliseconds

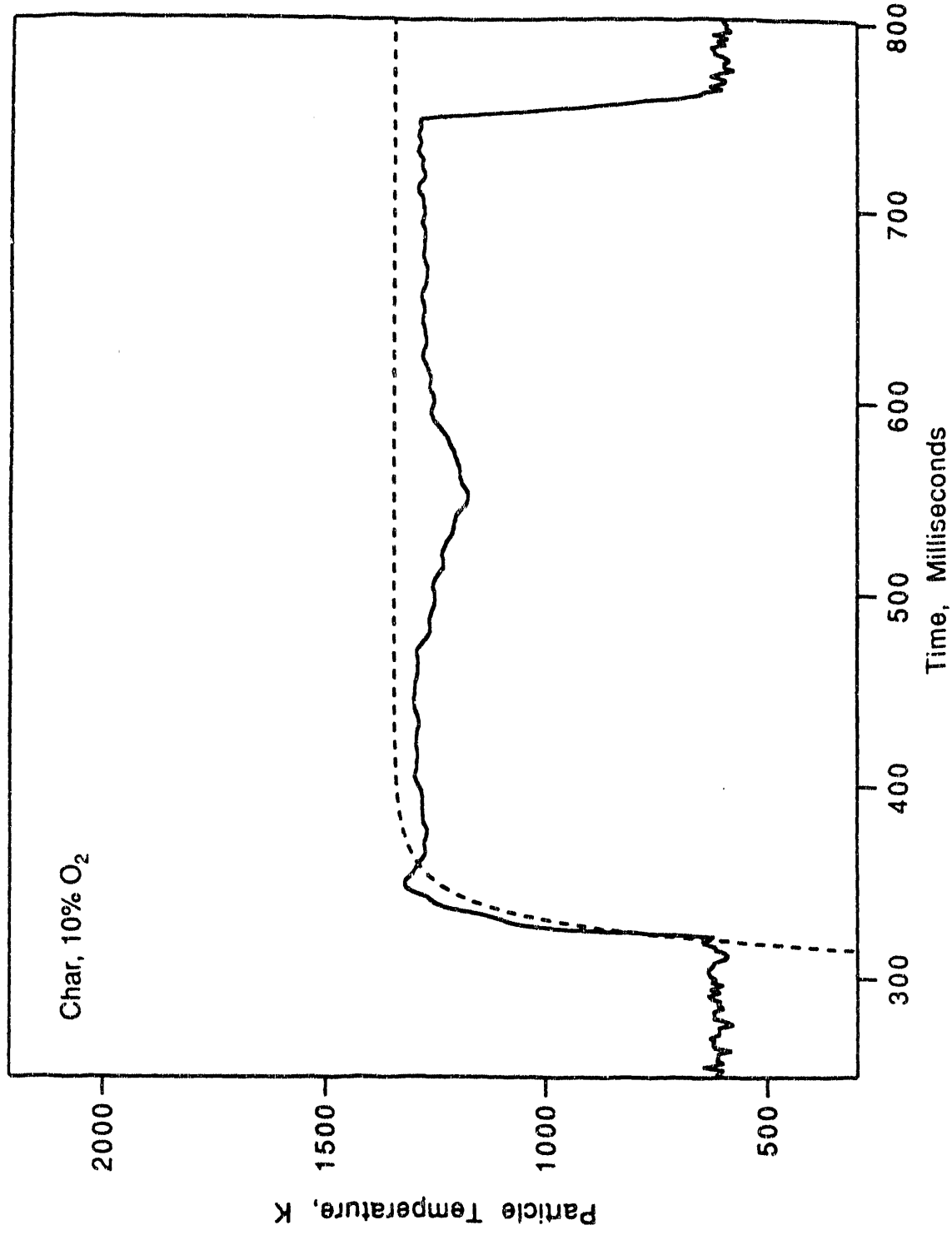
Char, 10% O_2
Particle Temperature, K
2000
1500
1000
500
300
400
500
600
700
800
Time, Milliseconds

Figure 9b

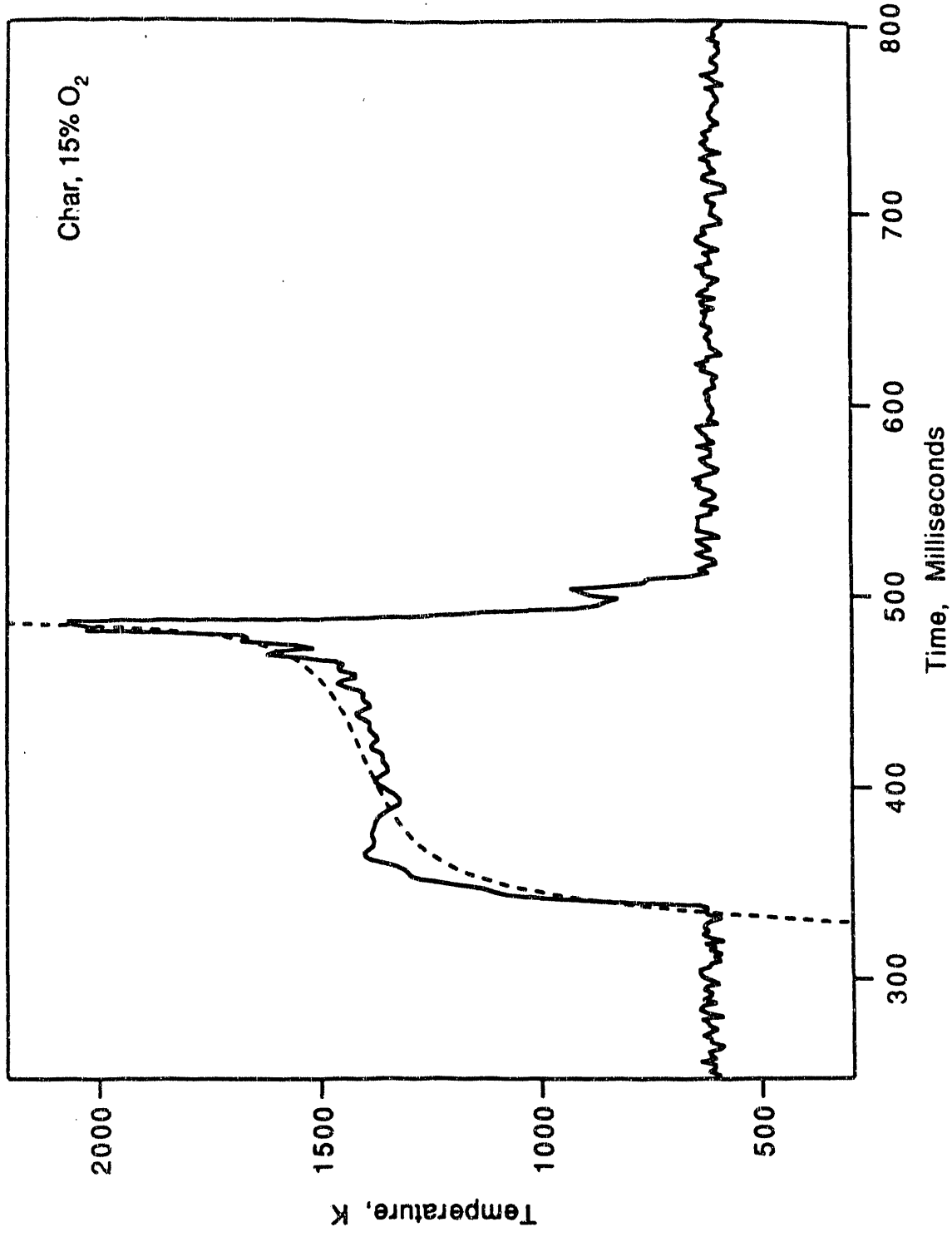
Char, 15% O_2
Temperature, K
2000
1500
1000
500
300
400
500
600
700
800
Time, Milliseconds

Figure 9c

Figure 10a

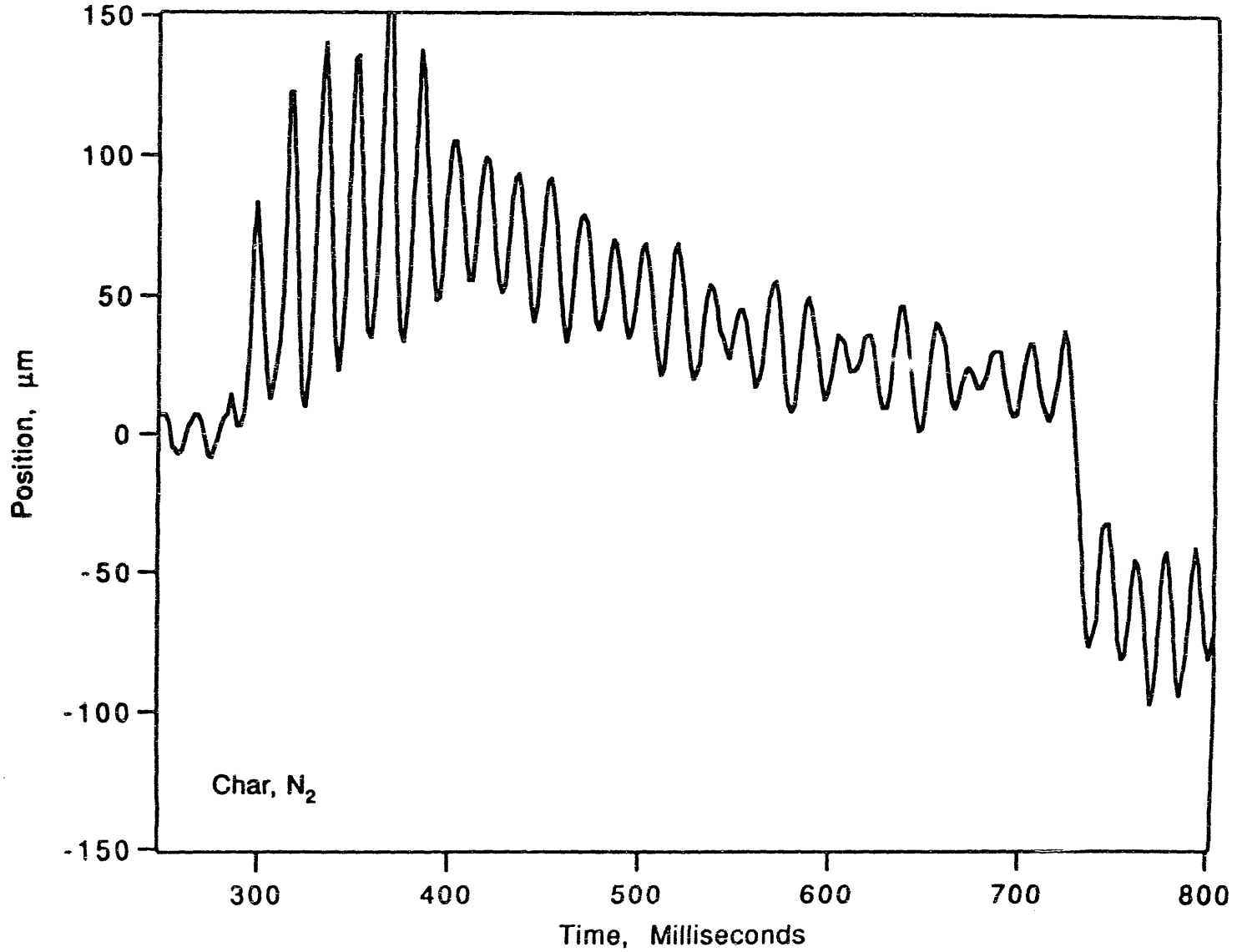
150
100
50
0
-50
-100
-150
Position, µm
Char, N_2
300
400
500
600
700
800
Time, Milliseconds

Figure 10b

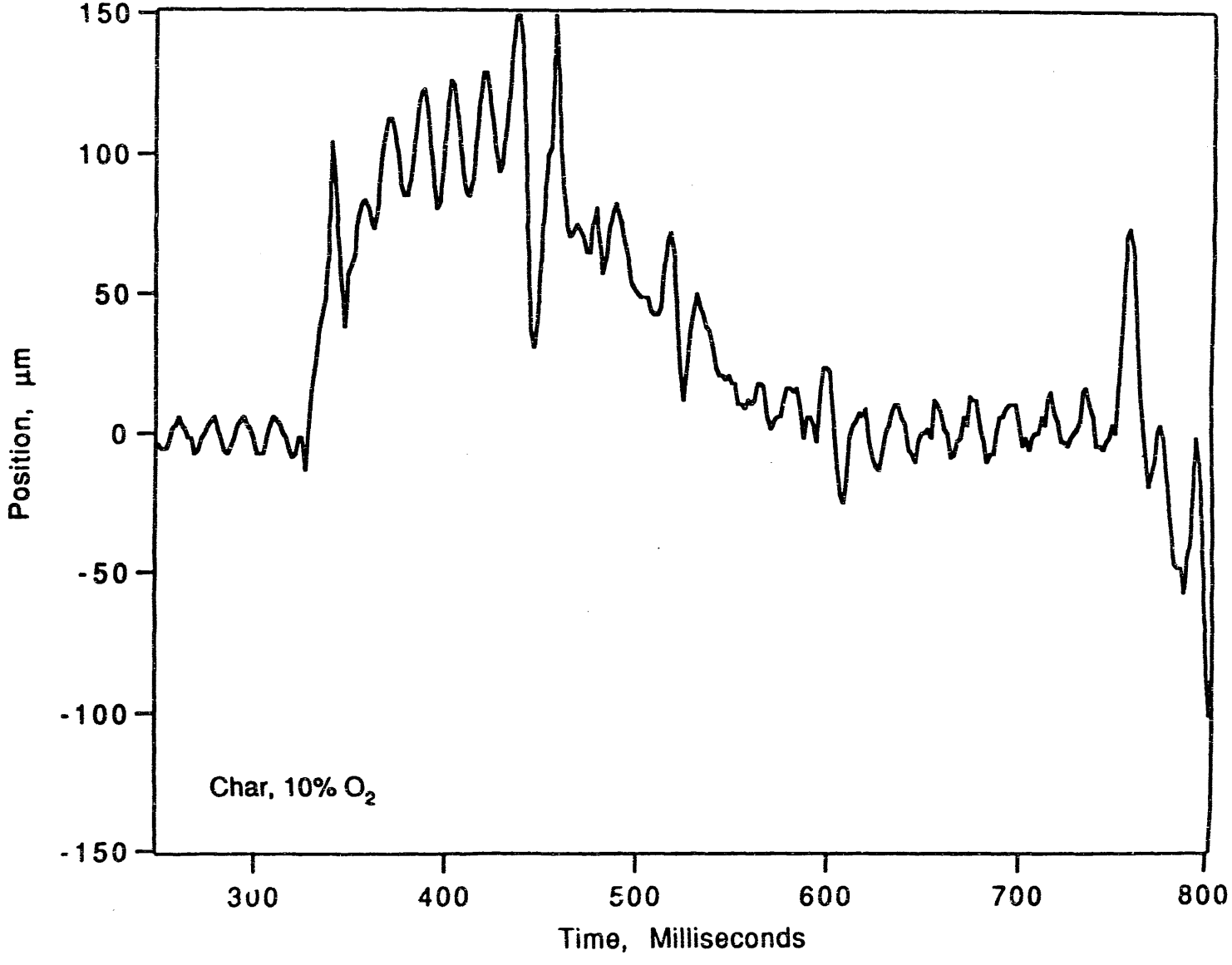
150
100
50
0
-50
-100
-150
Position, µm
300
400
500
600
700
800
Time, Milliseconds
Char, 10% O_2

Figure 10c

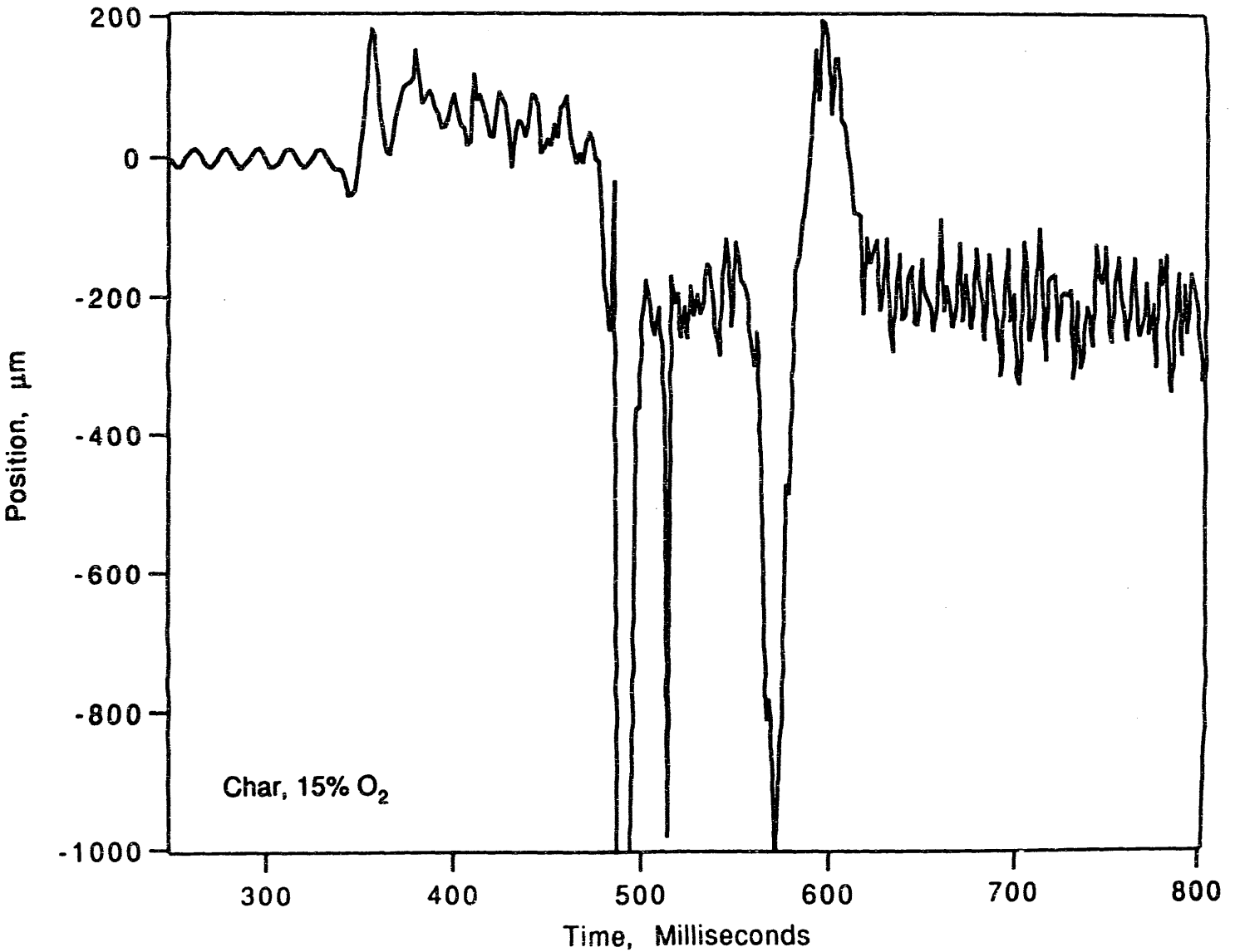
200
0
-200
-400
-600
-800
-1000
Position, µm
Char, 15% O_2
300
400
500
600
700
800
Time, Milliseconds

CHAPTER 4

A THEORETICAL STUDY OF COMBUSTION OF NONSPHERICAL PARTICLES

(Manuscript to be published in *Combustion Science and Technology*)

A Theoretical Study of Combustion of Nonspherical Particles

Moon Kyu CHOI and George R. Gavalas
Chemical Engineering 210-41
California Institute of Technology
Pasadena CA 91125

Submitted to *Comb. Sci. and Tech.*

Abstract

A theoretical study is carried out of the combustion of nonspherical carbonaceous particles in the regime of shrinking core reaction. The first problem addressed is the calculation of the pseudosteady temperature and oxidation rate for a particle of given shape. This problem involves the solution of the external diffusion and heat conduction equations with the reaction entering as a boundary condition over the particle surface. Using the boundary integral method, the problem is reformulated as a system of two coupled integral equations which are solved numerically by suitable discretization. The complete transient problem addressing the evolution of particle shape and particle temperature during burnout, is similarly formulated by the boundary integral method and solved numerically. Over a broad range of parameters, the pseudosteady particle temperature and rate of oxidation are very nearly equal to those of spherical particles of equal volume and surface area respectively. The transient solutions obtained for parameters typical of pulverized combustion show that during burnout the particle becomes increasingly nonspherical. As expected, nonspherical particles burn faster than spherical particles of the same initial volume, but the difference in burnout times is less than 20% for initial aspect ratios between one and three.

NOMENCLATURE

A_p	aspect ratio
b_1	stoichiometric coefficient
c	total concentration of gas phase
c_1	concentration of oxygen
D	diffusion coefficient of oxygen
g	Green's function for 3-dimensional Lapace's equation
k'	reaction constant
$\|\Delta H\|$	heat of reaction
n	outward normal unit vector
P_n	nth Legendre polynomial
Q	defined by Eq.(13)
q_R	heat flux by radiation
$R(\theta,\tau)$	$\frac{\tilde{R}(\theta,\tau)}{\tilde{R}_s(\tau)}$
$\tilde{R}_s(\tau)$	radius of the fictitious sphere of equal volume
r	reaction rate of oxygen
S	surface area of particle
T	temperature
t	time
x	dimensional position vector
y	mole fraction of oxygen

Greek letters

β_n	coefficients used in expanding $R(\theta, \tau)$
ϵ	emissivity of particle
λ	thermal conductivity of gas phase
ρ	radial variable
ρ_p	particle density
τ	dimensionless time variable
Ω	surface boundary of domain

Subscripts

∞	quantity evaluated using the bulk temperature
v	sphere of equal volume
s	sphere of equal surface area

INTRODUCTION

The analysis of particle(coal char, coke, etc.) combustion has undergone significant refinement over the years. Early analyses exemplified by the reports of Field *et al.*(1967) and Field(1969) employed simple heat and mass transfer coefficients and assumed shrinking core reaction. The analysis was later extended to include a detailed account of external heat and mass transfer while retaining shrinking core oxidation(Ubhayakar,1976 ; Libby and Blake,1979 ; Annamalai and Durbetaki,1979). Further extensions invoked considerations of intraparticle diffusion, reaction and pore growth. A comprehensive review of work up to 1984 has been published by Sotirchos *et al.*(1984). Regardless of the treatment afforded to internal and external diffusion, all previous investigations treated the reacting particles as spherical thus

avoiding the mathematical and computational complications entailed by nonspherical geometry. In the present paper we explore the effect of nonspherical shape on the reaction rate, particle temperature and other combustion charateristics.

Grinding coal, coke, etc. produces particles of widely varying size and shape. Upon heating and devolatilization, bituminous coal particles tend to become smoother and more spherical, while particles of other coals retain their original shape. The nonuniformity of shape and size arising from grinding and devolitilization can cause a spread in the time for complete burnout, the maximum particle temperature, and the size distribution of flyash, all important properties for coal combustion practice. In this paper we explore the effect of the initial shape on the combustion history of a particle. We consider the instantaneous temperature and oxidation rate for a given particle shape, and the evolution of the particle shape as reaction progresses. We also examine the degree to which the combustion of nonspherical particles can be approximated by that of spherical particles of appropriate size.

As we relax the assumption of spherical shape we are forced to make other simplifications or restrictions in order to contain the mathematical-computaional effort. The analysis is thus restricted to shrinking core combustion, spatially uniform transport coefficients and negligible Stefan flow. Furthermore, we only consider particle shapes which are rotationally symmetric and choose the initial shape to be a prolate or oblate spheroid. With these simplifications and restrictions the problem becomes one of external diffusion and heat conduction with the reaction entering as a boundary condition on the particle surface. We treat this problem numerically using the boundary integral method which converts the spatial differential equations to integral equations over the particle surface and thereby reduces the computational

effort. Although not explicitly considered, the case of negligible pore diffusion resistance, such that the particle size and shape remain constant during burnout, is also subsumed in the analysis developed here.

THE PSEUDOSTEADY PROBLEM

In this section we formulate the pseudosteady problem, i.e., for a given particle shape and free stream conditions, calculate the particle temperature and the reaction rate. In a strict sense, these pseudosteady properties are not exactly realized, because the particle shape evolves with oxidation. However, except for a brief initial transient, the thermal inertia is negligible and the particle temperature approaches and remains close to the pseudosteady temperature corresponding to the instantaneous particle shape. Having established that pseudosteady relation, in the next section we examine the evolution of particle shape due to the reaction.

Figure 1 shows a rotationally symmetric particle with O being the particle center and Oz the axis of symmetry. Although not essential, we shall also assume that the particle has a plane of symmetry perpendicular to Oz. The particle surface Ω is then defined by some equation

$$\rho = F(\theta, t), \quad 0 < \theta < \pi \tag{1}$$

where ρ is the distance from the center O and, because of the plane of symmetry, $F(\pi - \theta, t) = F(\theta, t)$.

Physical parameters such as the thermal conductivity and the diffusivity are functions of temperature with an approximate power dependence (Hirschfelder *et al.*, 1954),

$$\lambda \propto T^{0.5}, \quad D \propto T^{1.5}.$$

Thus the thermal conductivity λ and the product cD are represented as

$$\lambda = \lambda_\infty \left(\frac{T}{T_\infty}\right)^{0.5}, \quad cD = c_\infty D_\infty \left(\frac{T}{T_\infty}\right)^{0.5}$$

with the subscript ∞ denoting free stream properties.

In a further approximation, the product cD_{ij} of total concentration and any diffusion coefficient will be taken as spatially uniform, equal to its value at the particle surface Ω. Moreover, the flux of oxygen will be described by the approximate expression $-Dc\nabla y$, where y is the oxygen mole fraction and D is the binary diffusion coefficient for the $O_2 - N_2$ pair. This simple flux expression neglects the minor convective contribution due to the relative velocity between particle and free stream, the "Stefan flow" terms induced by multicomponent diffusion, and the direct contributions of pressure and temperature gradients included in the Stefan-Maxwell equations.

The approximation of spatially uniform cD was evaluated for a spherical particle where the exact and approximate problems could be solved in closed form(see Appendix). Even when surface and free stream temperatures differed by 640°C, the error in the reaction rate was less than 8%. The error committed by neglecting the Stefan flow depends mainly on the magnitude of the surface reaction rate. The analytical solution available for a spherical particle suggests that this error is less than 10% for the range of parameters used in the numerical calculations. In view of the modest magnitude of these errors we believe that the two approximations are reasonable for evaluating differences in the combustion rate, burnout time, etc., between a spherical and a nonspherical particle.

With the above approximations, the oxygen mole fraction y and the temperature T satisfy the equations

$$\nabla^2 y = 0 \tag{2}$$

$$\nabla \cdot (\lambda \nabla T) = 0 \tag{3}$$

with boundary conditions at the free stream

$$\rho \to \infty \ : \ y \to y_\infty \ ; \ T \to T_\infty . \tag{4}$$

The boundary conditions on the particle surface will be based on two additional assumptions : uniform particle temperature and shrinking core reaction(high Thiele modulus). The relevance of the latter assumption depends on several factors among which particle temperature, particle size, and porous structure. A particle initially burning in the shrinking core mode(decreasing size, constant density) after a certain reduction in size will switch to a mode of decreasing size and density.

On the basis of the last two assumptions, the boundary condition for the oxygen mole fraction becomes

$$\rho \in \Omega \ : \ cD\frac{\partial y}{\partial n} = r(p_1, T) \tag{5}$$

where $p_1 = yP$ is the partial pressure of oxygen on the surface. There are two boundary conditions for the temperature

$$\rho \in \Omega \ : \ T = T_s \tag{6}$$

where T_s is the unknown particle temperature, and

$$\int_\Omega \left[\lambda \frac{\partial T}{\partial n} - q_R + r|\Delta H| \right] dS = 0 \tag{7}$$

where q_R is the net radiative flux, r is the rate of oxygen consumption per unit external area of the particle. This latter condition is simply a thermal energy balance for the whole particle between heat generated by the reaction and heat lost

by radiation and conduction. It must be noted that whereas T_s is uniform over the surface, $p_1 = yP$ and $\frac{\partial T}{\partial n}$ are variable. The radiative flux q_R will be taken as

$$q_R = \sigma\epsilon(T_s^4 - T_\infty^4) \tag{8}$$

where the temperature of the surrounding surfaces is taken equal to that of the free stream, and a common emmisivity is used for all radiating surfaces.

For a spherical particle of radius a, Eqs. (2)-(7) can be reduced easily to the solution of two equations in the unknowns, y_s, T_s,

$$\frac{PD(T_s)}{R_g T_s a}(y_\infty - y_s) = r(Py_s, T_s) \tag{9}$$

$$\frac{\lambda(T_s - T_\infty)}{a} + \sigma\epsilon(T_s^4 - T_\infty^4) = |\Delta H_r| r(Py_s, T_s). \tag{10}$$

If the reaction is first order with Arrhenius temperature dependence,

$$r = k' p_1 = A\exp(-E/R_g T_s) Py_s, \tag{11}$$

Eqs. (9) and (10) can be combined in a single equation for T_s :

$$\frac{\lambda(T_s - T_\infty)}{a} + \sigma\epsilon(T_s^4 - T_\infty^4) = |\Delta H_r| \frac{A\exp(-E/R_g T_s) Py_\infty}{1 + Q(T_s)} \tag{12}$$

where

$$Q(T_s) = \frac{k'(T_s) R_g T_s a}{D(T_s)} = \frac{A R_g T_s a}{D(T_s)} \exp(-E/R_g T_s). \tag{13}$$

Equation (12) exhibits the well-known multiplicity and ignition phenomena.

BOUNDARY INTEGRAL METHOD

For nonspherical particles the problem defined by Eqs.(2)-(7) can be reformulated using single layer and double layer potentials(Stakgold,1972) into two integral

equations for the surface values of y and $\frac{\partial T}{\partial n}$. Once the two integral equations are solved numerically, the particle temperature, the total reaction rate, and the values of T and y outside of the particle can be computed, if desired. This approach, which is known as the "boundary integral method", involves a much smaller number of unknowns than the finite difference method and is, accordingly, much more computationally economical. The boundary integral method has been used extensively in low Reynolds number hydrodynamics.

The integral form of Eq.(2) with boundary conditions (4) and (5) can be derived by standard potential theory, using a double layer potential. For any $\mathbf{x}_s \in \Omega$ we have

$$y(\mathbf{x}_s) = 2y_\infty - \frac{1}{2\pi}\int_\Omega \left[-y(\xi)\frac{\partial g}{\partial n} + g\frac{r(Py(\xi), T_s)}{(cD)_s}\right] dS_\xi \qquad (14)$$

where $\frac{\partial}{\partial n}$ is the outward normal derivative and

$$g = \frac{1}{|\mathbf{x}_s - \xi|}. \qquad (15)$$

For axially symmetric particles, integration over the azimuthal angle converts the double integral in Eq.(14) to a single integral over the angular variable θ :

$$y(\mathbf{x}_s) = 2y_\infty - \frac{1}{2\pi}\int_0^\pi \left[-y(\theta')\frac{\partial G}{\partial n} + G\frac{r(Py(\theta'), T_s)}{(cD)_s}\right] v(\rho)\sin\theta' d\theta' \qquad (16)$$

where

$$\rho = F(\theta, t)$$

and

$$v(\rho) = \rho^2\left[1 + \frac{1}{\rho^2}\left(\frac{dF}{d\rho}\right)^2\right]^{1/2} \qquad (17)$$

$$G = \int_0^{2\pi} g d\phi \qquad (18)$$

$$\frac{\partial G}{\partial n} = \int_0^{2\pi} \frac{\partial g}{\partial n} d\phi. \tag{19}$$

Equation (16) is an integral equation in the unknown function $y(\theta)$, with T_s appearing as an unknown parameter to be determined in conjunction with the energy equation.

An integral equation equivalent to (3), (4) and (6) can be derived using a single layer potential after introducing a new variable defined by

$$\psi = \frac{(T/T_\infty)^{1+a} - 1}{(T_s/T_\infty)^{1+a} - 1}. \tag{20}$$

It is

$$-\int_\Omega g \frac{\partial \psi}{\partial n} dS_\xi = 4\pi. \tag{21}$$

Integration over the azimuthal angle now yields

$$-\int_0^\pi G \frac{\partial \psi}{\partial n} v(\rho) \sin\theta' d\theta' = 4\pi. \tag{22}$$

This is an integral equation in the unknown function $\frac{\partial \psi}{\partial n}(\theta)$ with the unknown T_s appearing as a parameter. For any given T_s, Eq.(16) can be solved for $y(\theta)$, and Eq.(21) for $\frac{\partial \psi}{\partial n}(\theta)$, or $\frac{\partial T}{\partial n}(\theta)$. The unknown T_s can then be determined from Eq.(7).

THE TRANSIENT PROBLEM

The transient problem is a conceptually simple extension of the pseudo-steady problem. It is still assumed that the oxygen mole fraction y and temperature T satisfy the pseudosteady equations (2) and (3) and boundary conditions (4)-(6). However, boundary condition (7) does not apply any more since the particle temperature is variable ; it is replaced by

$$\rho_p C_p V_p \frac{dT_s}{dt} = \int_\Omega [\lambda \frac{\partial T}{\partial n} - q_R + r|\Delta H|] dS \tag{23}$$

where ρ_p, C_p and V_p are the density, specific heat, and volume of the particle. An additional equation is needed governing the changing particle shape on account of carbon consumption. This is

$$\frac{\partial F(\theta,t)}{\partial t} = -\frac{b_1}{\rho_p} r(p_1, T_s)\sigma(\theta,t) \tag{24}$$

$$t = 0 \; ; \; F = F_0(\theta) \tag{25}$$

where the shape function F was introduced by Eq.(1). F_0 is the initial value of F, b_1 is the stoichiometric coefficient between grams of carbon and moles of oxygen ($b_1 = 24$ if CO is the only product), ρ_p is the particle density and r is the reaction rate in moles of oxygen per unit surface area per unit time. The factor $\sigma(\theta,t)$ converts a displacement of the surface perpendicular to itself due to the reaction to a displacement along OP (see Figure 1). One can easily derive

$$\sigma(\theta,t) = \left[1 + \left(\frac{1}{F}\frac{\partial F}{\partial \theta}\right)^2\right]^{1/2}. \tag{26}$$

As before, Eqs.(2)-(6) are equivalent to the two integral equations (16) and (21), therefore the transient problem is governed by Eqs. (16), (22) supplemented by (23)-(25).

NUMERICAL RESULTS FOR THE PSEUDO-STEADY PROBLEM

As a preliminary to the solution of Eqs. (16) and (22) it is necessary to evaluate the functions G and $\frac{\partial G}{\partial n}$ defined as integrals of the Green's function g and its normal derivative $\frac{\partial g}{\partial n}$(Eqs. (18),(19)). Carrying out these integrations yields G and $\frac{\partial G}{\partial n}$ in terms of three complete elliptic integrals which were evaluated by the approximating polynomials given in Abramowitz and Stegun(1972). Next, equations (16) and (22)

were discretized using the values of the unknowns y, and $\frac{\partial \psi}{\partial n}$ at 2N+1 discrete points over $0 < \theta < \pi$ and evaluating the integrals by an 8-point Gaussian quadrature. By this discretization, Eq.(22) was converted to a system of 2N+1 linear equations for the values of $\frac{\partial \psi}{\partial n}$ at the discrete points in $0 < \theta < \pi$. This linear system was decoupled from the rest of the equations and had to be solved only once.

The other integral equation, Eq.(16), was discretized into a system of 2N+1 nonlinear equations(or linear equations for a first order reaction) in the 2N+1 unknown values of y. This system contained the unknown surface temperature T_s as a parameter and was solved in conjunction with Eq.(7) by successive substitutions. To this end, Eq.(7) was rewritten as

$$\int \left(q_R - \lambda \frac{\partial T}{\partial n} \right) dS = \int r |\Delta H| dS$$

But on the surface

$$r = cD \frac{\partial y}{\partial n} = c_\infty D_\infty \left(\frac{T_s}{T_\infty} \right)^{1.5} \frac{\partial y}{\partial n}$$

so that

$$\left(\frac{T_s}{T_\infty} \right)^{1.5} = \frac{\int \left(q_R - \lambda \frac{\partial T}{\partial n} \right) dS}{c_\infty D_\infty \int \frac{\partial y}{\partial n} |\Delta H| dS} \tag{27}$$

Starting from an initial guess of T_s, Eq.(16) was solved for $\frac{\partial y}{\partial n}$ and Eq.(22) gave $\frac{\partial T}{\partial n}$. The values of $\frac{\partial y}{\partial n}$ and $\frac{\partial T}{\partial n}$ were introduced into the right side of Eq.(27) to yield an improved value for T_s, and the procedure was repeated until successive values of T_s differed by less than one degree. Convergence took 5 to 10 iterations depending on the shape of the particle.

Table I gives the values used in the calculations. With the exception of the oxygen concentration in the free stream, these values were taken from a paper by Sahu *et al.*(1988). These authers had estimated the oxidation rate for shrinking

core combustion of a bituminous coal char as

$$R_a = 107.1 \exp(-17,000/RT)\ \mathrm{gcm^{-2}s^{-1}atm^{-1}},$$

which yields the value of k'_∞ listed in Table 1.

Numerical results for the pseudosteady problem are presented in Figures 2-4. Figure 2 shows the particle temperature vs. Q_∞. At each value of Q_∞, various prolate and oblate spheroids of equal volume but different aspect ratios are considered. The temperature varies significantly with Q_∞ but is insensitive to the shape, with the curves for both prolate and oblate spheroids of different aspect ratios essentially coinciding. This insensitivity on particle shape seems to be due to the approximate cancellation of two opposite effects. Increasing the aspect ratio decreases the local mass transfer coefficient on the particle surface, thereby decreasing the heat release. The same increase of the aspect ratio decreases the local heat transfer coefficient as well, thereby decreasing the heat loss. The sensitivity of the particle temperature to the particle shape may be higher in other operating regions, e.g., at higher gas temperatures or oxygen contents where the effect of radiative heat transfer would be more pronounced. It should be further noted that for the set of parameters used here(Table I), all particle temperatures shown in Figure 2 correspond to the upper(ignited) branch of the usual ignition diagram.

Figure 2 also shows the normalized reaction rate vs. Q_∞ for particles of different shapes. For any given particle shape, the normalized rate initially decreases with increasing Q_∞, then levels off and remains constant as Q_∞ increases beyond 1. At low values of Q_∞ the normalized rate is equal to the ratio of the surface area of the particle to that of a sphere of equal volume. As Q_∞ increases, the rate ratio falls below the surface area ratio, and eventually reaches a limiting value as the reaction

becomes mass transfer limited. For fixed Q_∞, the rate ratio increases significantly with the aspect ratio, with the oblate spheroids yielding higher reaction rates than the corresponding prolate spheroids. For aspect ratios between 1 and 3.2 the rate for the prolate and oblate spheroids was no more than 20 % and 28 % higher than that of a sphere of equal volume.

Figure 3 shows the surface area normalized with respect to that of a sphere of equal volume as a function of aspect ratio for prolate and oblate spheroids. Oblate spheroids have a somewhat higher surface area than prolate spheroids of the same aspect ratio. At the highest aspect ratio of 3.2 used in most calculations the prolate and oblate spheroids have surface area 20 and 29 % higher than a sphere of the same volume. Figure 4 shows the total rate normalized by the total rate of a sphere of equal surface area vs. A_p for different values of Q_∞. For the whole range of Q_∞ and A_p examined, the rate is within 3 % of the rate of a sphere of equal surface area. From the standpoint of the instantaneous total reaction rate, therefore, a nonspherical particle can be closely represented by a spherical particle of equal surface area. The curves for a few of the prolate spheroids show oscillatory behavior, which seems to be due to numerical errors, but in these curves the normalized total rate is very close to unity.

NUMERICAL RESULTS FOR THE TRANSIENT PROBLEM

The transient problem consists of Eqs. (23) and (24) with the respective initial conditions. Eq.(24) was written at M discrete points of $\theta, \theta_1 = 0, \cdots, \theta_M = \pi/2$ which were more densely distributed at the points of higher curvature, i.e., near $\theta = 0$ for prolate spheroids. M was chosen in the range 25 - 50. Each evaluation of the right side of these equations required solving the pseudosteady equations (16),

(22) for y and $\frac{\partial \psi}{\partial n}$(giving $\frac{\partial T}{\partial n}$). Equations (23) and (24) become increasingly stiffer with decreasing Damköhler number Q_∞ because small Q_∞ implies rapid change of shape in terms of the dimensionless time, τ defined by

$$\tau = \frac{b_1 (k'_\infty)^2 y_\infty}{\rho_\infty c_\infty D_\infty}. \tag{28}$$

In view of the lack of explicit expressions for the right sides of the differential equations, we could not conveniently use a stiff equation solver. Instead we used the explicit fourth order Runge-Kutta method with step size control, decreasing the step size as integration progressed to compensate for the gradually increasing aspect ratio. In the calculations reported below, the time increment $\Delta\tau$ varied from 0.1 to 0.01.

Figure 5 shows the fractional conversion vs. dimensionless time for particles of the same initial volume but different initial aspect ratios. The conversion curves for different aspect ratios are quite close to each other. For example, the dimensionless time to 0.95 conversion changes from 3.1 for $A_p(0) = 1$ to 2.7 for $A_p(0) = 3.2$. Figure 6 shows the aspect ratio as a function of dimensionless time for particles of different initial aspect ratios. The aspect ratio increases with time for all particles and this increase accelerates with increasing A_p. Thus, a particle with initially nearly spherical shape will change little during burnout(curve for $A_p(0)$=1.667) while a particle with initial $A_p(0)$=3.2 will become much more elongated($A_p \simeq 4.3$) when the dimensionless time reaches 2.5, i.e., at 0.95 conversion. Figure 7 shows the evolution of particle temperature during burnout. The temperature transients of particles of different initial aspect ratios, but equal volume, nearly coincide. Although not portrayed in Figure 7, the calculations also show that for any given initial particle shape, the transient temperature rapidly approaches and remains

close to the pseudosteady temperature corresponding to the instantaneous particle volume.

CONCLUSIONS

An analysis of nonspherical particle combustion was carried out using the boundary integral method. For particles of equal volume, the pseudosteady temperature is nearly independent of shape, but the combustion rate increases with increasing aspect ratio. The local combustion rate varies moderately over the particle surface increasing with the distance from the particle center. The total combustion rate depends on the particle surface area alone, i.e., particles of equal surface area but different volumes and shapes have the same rate. This dependence on the surface area is less than linear, becoming linear only in the limit of low Damköhler numbers.

The effect of initial particle shape on the burnout transient was explored for a set of parameters typical of a bituminous coal char burning in the shrinking core regime. The calculations show the particle shape to become increasingly nonspherical with the progress of combustion and this change to be more pronounced for particles with larger initial aspect ratios. For particles of equal initial volume, the burnout time decreases slightly with the initial aspect ratio. For example a particle of initial aspect ratio 3.2 requires 12 % less time to reach 80 % burnout compared to a spherical particle of the same initial volume.

APPENDIX

The purpose of this appendix is to estimate the error made by treating the quantity cD as temperature independent in the derivation of Eq.(2) from the equa-

tion

$$\nabla \cdot (cD \nabla y) = 0. \qquad (A1)$$

This evaluation is carried out by comparing the approximate solution with the exact solution for a spherical particle. In the case of a spherical particle, Eq.(3) can be easily integrated to obtain

$$\frac{T}{T_\infty} = \left[1 + \frac{(T/T_\infty)_s^{1.5} - 1}{\rho/a}\right]^{\frac{1}{1.5}}. \qquad (A2)$$

Equations (A1),(4),(5) can now be solved along with Eq.(A2) to obtain the dimensionless surface concentration as

$$y_s = \frac{y_\infty}{1 + Q(1.5)\frac{(T_s/T_\infty)^{1.5} - (T_s/T_\infty)^{0.5}}{(T_s/T_\infty)^{1.5} - 1}}. \qquad (A3)$$

The approximate dimensionless surface concentration obtained from Eqs. (2), (4) and (5) is

$$y_{s,\text{approx}} = \frac{y_\infty}{1 + Q}. \qquad (A4)$$

Eqs.(A3) and (A4) are the exact and approximate solutions to Eqs. (A1) and (3) for a sphere. The relative error between exact and approximate solutions is

$$\left|\frac{y_s - y_{s,\text{approx}}}{y_s}\right| = \frac{Q}{1 + Q}\left|(1.5)\frac{(T_s/T_\infty)^{1.5} - (T_s/T_\infty)^{0.5}}{(T_s/T_\infty)^{1.5} - 1} - 1\right|. \qquad (A5)$$

The quantity

$$F(T_s/T_\infty) = \left|(1.5)\frac{(T_s/T_\infty)^{1.5} - (T_s/T_\infty)^{0.5}}{(T_s/T_\infty)^{1.5} - 1} - 1\right|, \qquad (A6)$$

is an increasing function of T_s/T_∞ starting from zero at $T_s = T_\infty$ and remaining small. For example at $T_s/T_\infty = 1.4$, $F(T_s/T_\infty) = 0.08$ and the error is less than 8%, in as much as the factor$Q/(Q+1)$is less than one.

Acknowledgements

This research was supported by the U.S. Department of Energy, University Coal Research Program under grant DE-FG22-88PC88911.

REFERENCES

Abramowitz, M. and Stegun, I.A.(1972). *Handbook of Mathematical Functions*, 8th ed., Dover, New York, pp.590-591.

Annamalai, K. and Durbetaki, P.(1979). Combustion Behavior of Char/Carbon Particles, *Seventeenth Symposium(International) on Combustion*, 169.

Field, M.A., Gill, D.W., Morgan, B.B. and Hawksley, D.W.G.(1967). *Combustion of Pulverized Coal*, BCURA, Leatherhead pp.189-208.

Field, M.A.(1969). Rate of Combustion of Size-Graded Fractions of Char from a Low-Rank Coal between 1200 K and 2000 K. *Combustion & Flame*, **13**, 237.

Hirschfelder, J.O., Curtiss, C.F. and Bird, R.B.(1954). *Molecular Theory of Gases and Liquids*, Wiley, New York, pp.533-591.

Libby, P.A. and Blake, T.R.(1979). Theoretical Study of Burning Carbon Particles. *Combustion & Flame*, **36**, 139.

Mon, E. and Amundson, N.R.(1980). Diffusion and Reaction in a Stagnant Boundary Layer about a Carbon Particle. 4. Dynamic Behavior. *Ind. Eng. Chem. Fund.*, **19**, 243.

Sahu, R., Northrop, P.S., Flagan , R.C., and Gavalas, G.R.(1988). Char Combustion : Measurement and Analysis of Particle Temperature Histories, *Comb. Sci. and Tech.*, **60**, 215.

Sotirchos, S.V., Srinivas, B. and Amundson, N.R.(1984). Modelling of the Combustion of Single Char Particles. In Amundson, N.R. and Luss, D., *Reviews in Chemical Engineering*, D. Reidel Publishing Co., London.

Stakgold, I.(1972). Boundary Value Problems of Mathematical Physics, vol.II, Macmillan, New York, pp.88-193.

Ubahyakar, S.K(1976). Burning Charateristics of a Spherical Particle Reacting with Ambient Oxidizing Gas at its Surface. *Combustion & Flame*, **26**, 23.

Table I. The parameter values used in the calculations.

Physical Parameters	Values Used
bulk temperature, T_∞	1600 K
initial radius of equivalent sphere, $\tilde{R}_s(0)$	25 μm
bulk mole fraction of oxygen, y_∞	0.1
heat of reaction, $-\Delta H_r$	2.32 x 10^8 J/kgmol O_2
solid density, ρ_p	800 kg/m^3
solid emissivity, ϵ	1
diffusion coefficient of oxygen at T_∞, D_∞	2.80 x 10^{-4} m^2/s
thermal conductivity of gas at T_∞, λ_∞	5.38 x 10^{-2} J/m-s-K
activation energy, E	17,000 cal
heat capacity of gas, C_p	2.5 x 10^4 J/kgmol-K
total molar concentration at T_∞, c_∞	7.62 x 10^{-3} kgmol/m^3
1st order reaction constant at T_∞, k'_∞	0.2119 kgmol O_2/m^2-s-atm
dimensionless time, τ	63.135sec^{-1} t

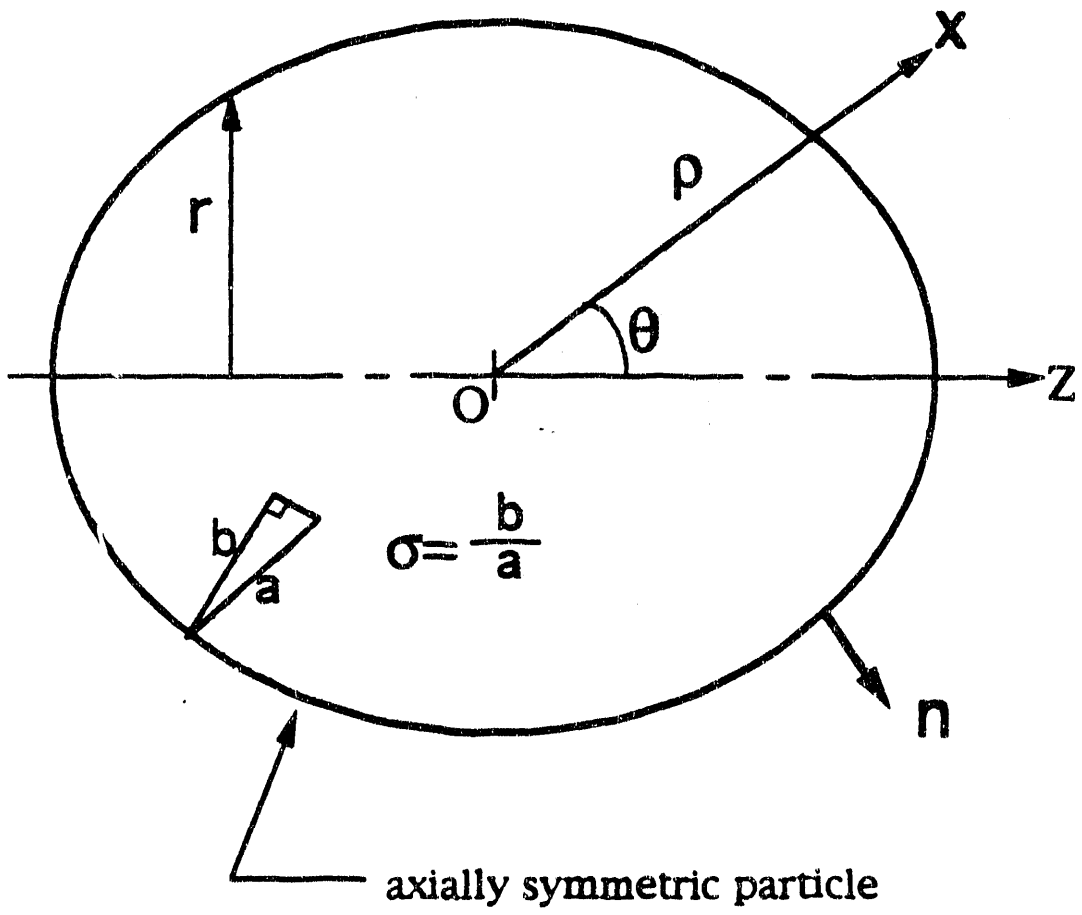

Figure 1. Geometry and notation for a nonspherical particle.

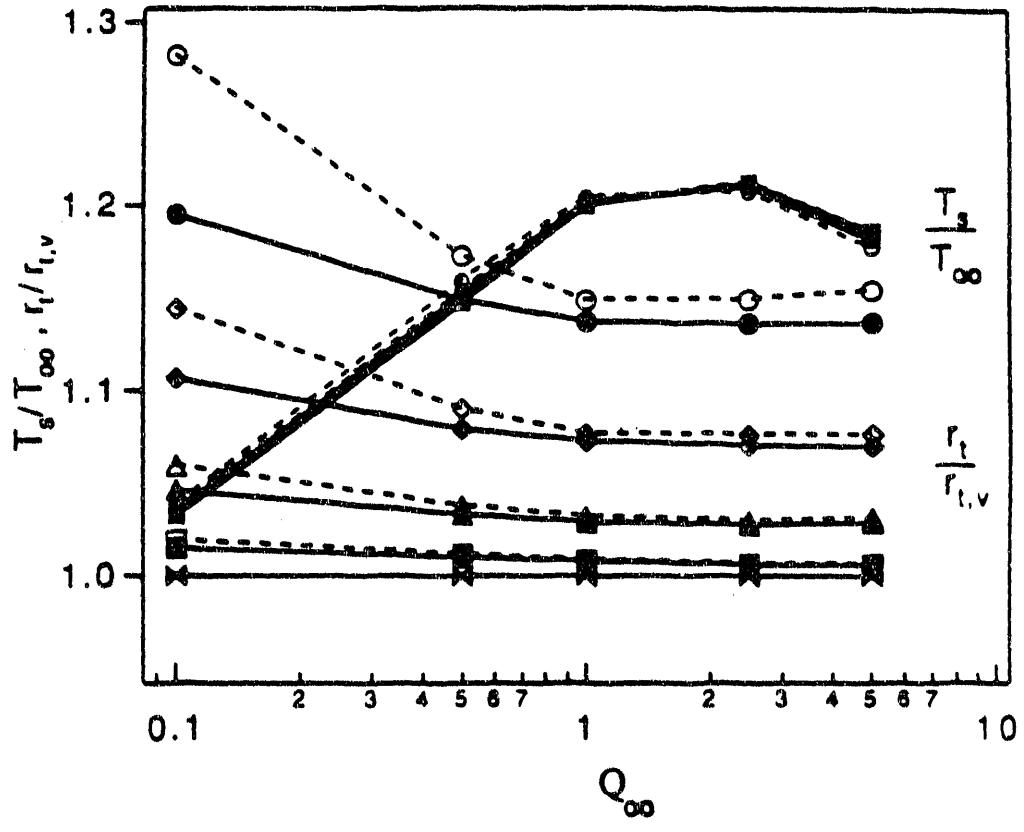

Figure 2. Pseudosteady particle temperature normalized by free stream temperature and reaction rate normalized by that of a sphere of equal volume vs. Damköhler number(⋈:A_p = 1.,□: A_p = 1.25,△:A_p = 1.667,○:A_p = 2.294, ◯:A_p = 3.2026 ; solid lines : prolate spheroids, dashed lines : oblate spheroids).

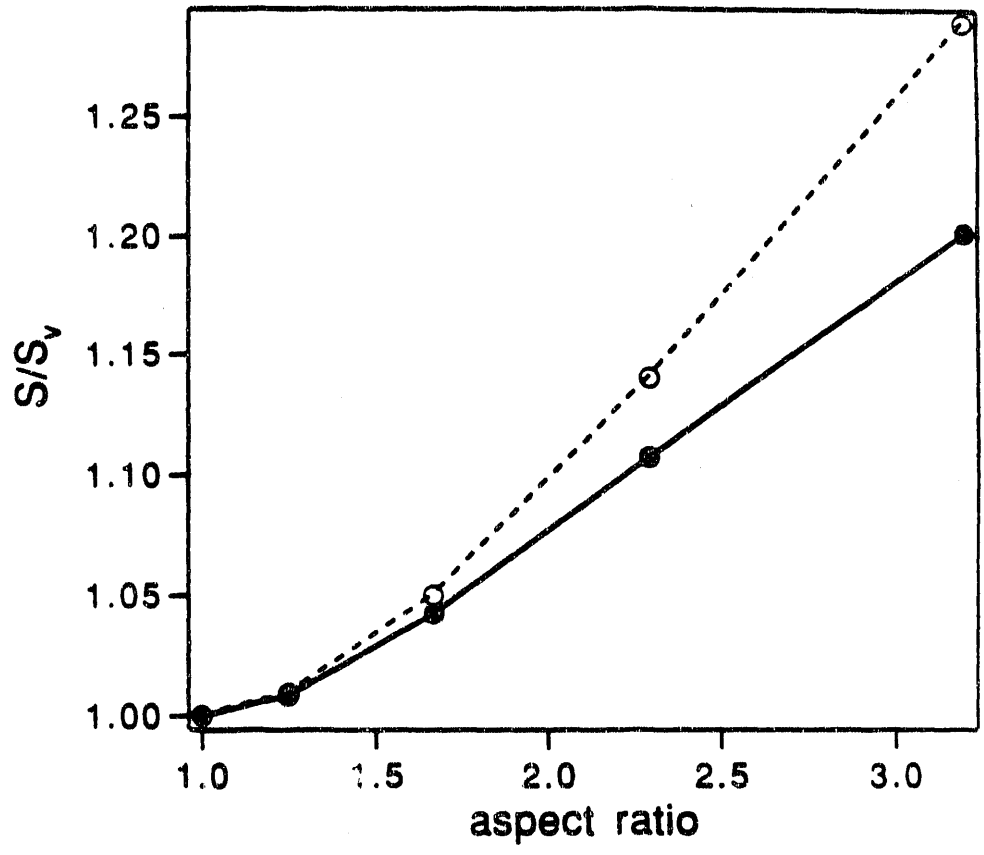

Figure 3. Surface area normalized by that of a sphere of equal volume vs. aspect ratio(solid lines : prolate spheroids, dashed lines : oblate spheroids).

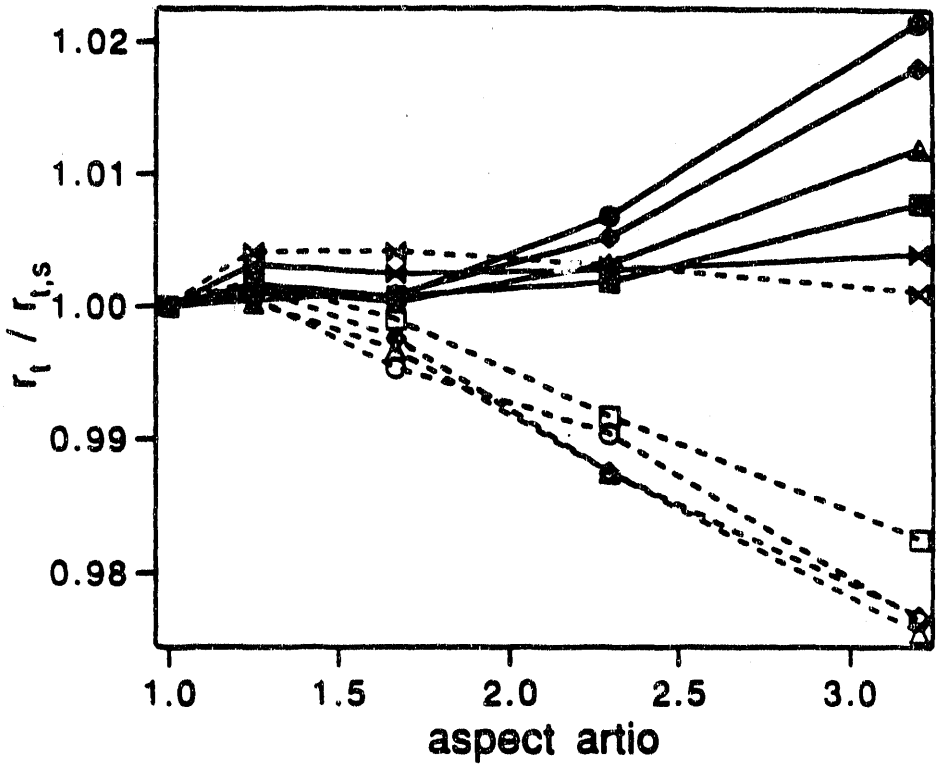

Figure 4. Total reaction rate normalized by that of a sphere of equal surface area vs. aspect ratio(⋈:$Q_\infty = 0.1$,□: $Q_\infty = 0.5$,△:$Q_\infty = 1$,◇:$Q_\infty = 2.483$, ○:$Q_\infty = 5$; solid lines : prolate spheroids, dashed lines : oblate spheroids).

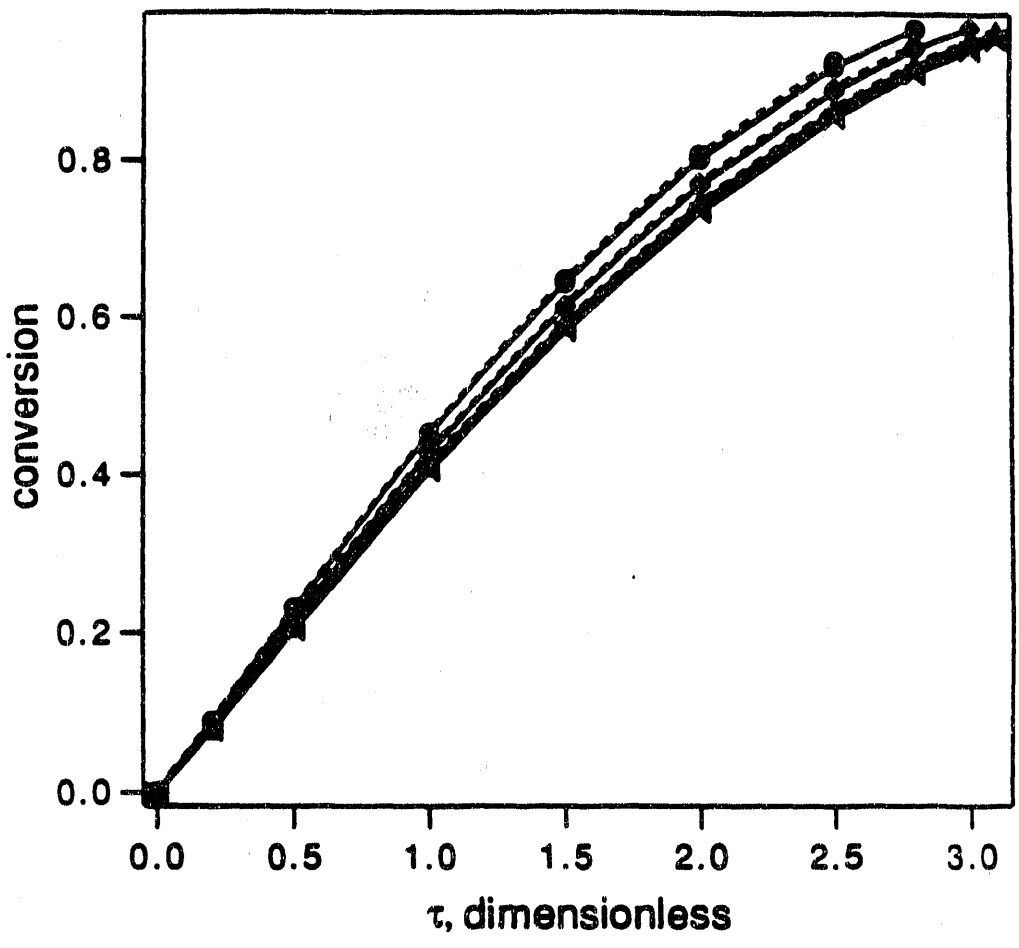

Figure 5. Conversion vs. dimensionless time for prolate and oblate spheroids($\bowtie$:$A_p(0) = 1$,Δ:$A_p(0) = 1.667$,$\circ$:$A_p(0) = 2.294$, $\bigcirc$:$A_p(0) = 3.2026$; solid lines : prolate spheroids, dashed lines : oblate spheroids).

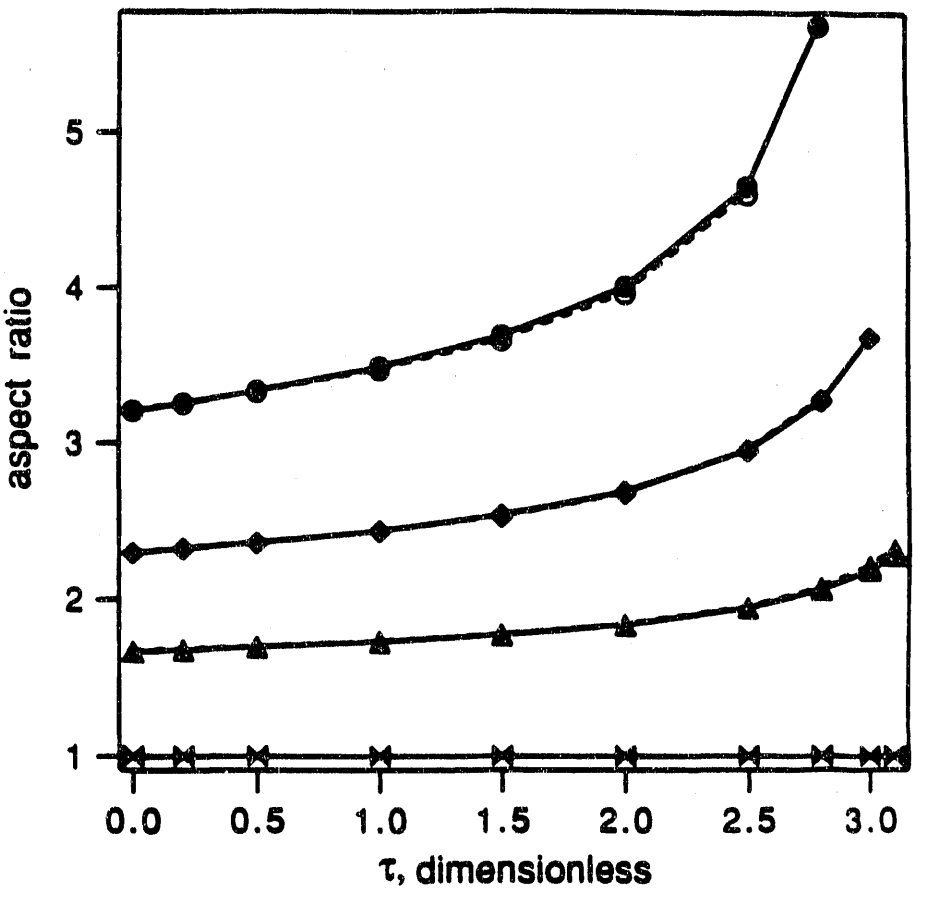

Figure 6. Aspect ratio vs. dimensionless time for prolate and oblate spheroids($\bowtie$:$A_p(0) = 1$,$\triangle$:$A_p(0) = 1.667$, $\circ$:$A_p(0) = 2.294$, $\bigcirc$:$A_p(0) = 3.2026$; solid lines : prolate spheroids, dashed lines : oblate spheroids).

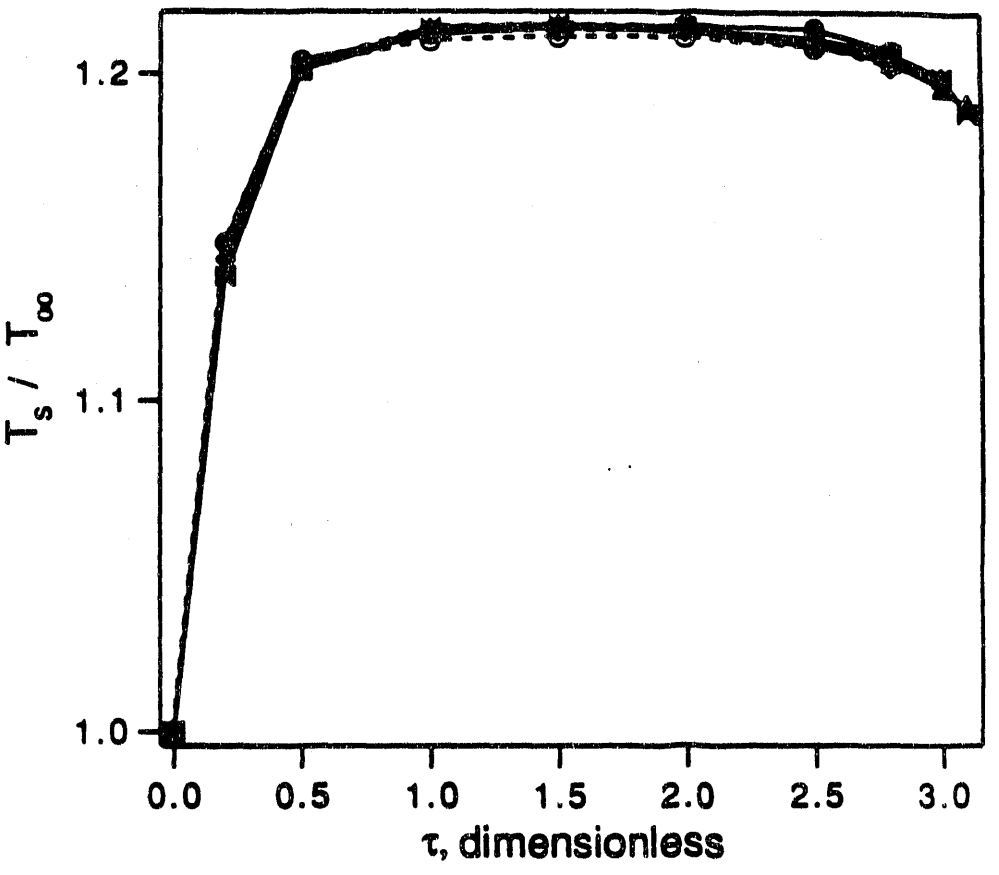

Figure 7. Transient particle temperature vs. dimensionless time for prolate and oblate spheroids($\bowtie$:$A_p(0) = 1$,$\triangle$:$A_p(0) = 1.667$, $\circ$:$A_p(0) = 2.294$, $\bigcirc$:$A_p(0) = 3.2026$; solid lines : prolate spheroids, dashed lines : oblate spheroids).

CHAPTER 5

CONCLUSIONS

A high volatile bituminous coal (Pittsburgh No. 8) was subjected to devolatilization and oxidation in an entrained laminar flow furnace. Devolatilization in pure nitrogen was carried out at 1200K and 1600K for residence times of 100 ms, 200 ms, 300 ms and 2 s. Devolatilization with simultaneous oxidation was carried out in 1% O_2-balance nitrogen and 5% O_2-balance nitrogen.

Scanning electron microscopy shows that the gross morphological features of the char continue changing during at least the first 300 ms of devolatilization at 1600K in pure N_2. These changes include loss of mass--which is largely completed by the first 100 ms--rounding of the particles and gradual enlargement of large openings, or blowholes, at the surface. The BET surface area and total pore volume also increase during the first 300 ms of devolatilization.

Devolatilization was accompanied by oxidation when the coal was treated in 1% O_2-N_2 or 5% O_2-N_2 at 1600K. Even at 100 ms residence time in 1% oxygen the mass loss was 25% beyond the loss engendered by devolatilization in pure nitrogen. In 5% O_2-N_2 the mass loss was significantly higher. These results suggest that in pulverized combustion, devolatilization and char burnout overlap significantly. The treatment of these two processes as consecutive, as done in combustion models, is clearly an approximation.

The variation of surface area with residence time in 1% O_2-N_2 and 5% O_2-N_2 was very different from that in pure N_2. In the presence of oxygen the surface area increased until about 100 ms and then decreased. The decrease observed for times larger than 100 ms is probably due to loss of micropores by a densification process catalyzed by oxygen. Oxidation experiments with the thermogravimetric analyzer revealed a complex dependence of low temperature reactivity (500°C) on the prior charring history. For chars that were prepared in pure nitrogen, the reactivity increased with the charring residence time at least up to 200 ms residence times. For chars prepared in O_2-N_2 mixtures, the reactivity decreased with the oxygen content in the charring atmosphere--at constant charring time. For fixed oxygen level in the charring atmosphere, the reactivity decreased with the

charring time. This decrease of the reactivity with the oxygen level and the charring time can be attributed to a combination of two factors. One is the densification with loss of micropore surface area. The other is the selective depletion of the more reactive part of the carbonaceous structure during char preparation.

Single particle experiments were conducted with an electrodynamic balance (EDB) using a CO_2 laser beam to heat the electrically levitated particle. The particle could only be heated to about 900°C beyond which charge loss occurred disrupting the levitation. Char particles that had been formed by devolatilization in pure nitrogen at 1200K and 1600K for two seconds were heated in pure nitrogen and in air. Heating in pure nitrogen at 900°C for up to 20 minutes did not induce any apparent changes in the size or shape of either the 1200K char or the 1600K char. In oxidation in air at temperatures below 900°C the 1600K char particles reacted at constant size up to 60% conversion. In contrast the 1200K char particles underwent significant size reduction under the same conditions. Since in both cases oxidation proceeded in regime I (strict reaction control) the shrinkage of the 1200K char particles can only be explained by densification--loss of micropore volume. Moreover, this densification which occurs only for the "greener" 1200K char requires the presence of oxygen.

The phenomena of densification and loss of surface area and reactivity observed in the TGA and EDB experiments have significant implications for particle combustion models. Existing models assume that oxidation enlarges the pores but does not affect the underlying structure or the intrinsic oxidation rate parameters. The results of the present experiments suggest that under certain conditions oxidation causes structural changes that affect the particle volume, micropore surface area, and intrinsic reactivity.

In connection with modeling particle combustion a theoretical study was carried out to evaluate the effect of particle shape on particle temperature, rate of combustion, and burnout time. For particles of equal volume, the pseudosteady temperature was found to be nearly independent of shape, but the combustion rate was found to increase with

increasing aspect ratio. To a high degree of accuracy, the total combustion rate depends on the particle surface area alone, i.e., particles of equal surface area but different volumes and shapes have the same rate. The effect of initial particle shape on the burnout transient was explored for a set of parameters typical of a bituminous coal char burning in the shrinking core regime. The calculations show the particle shape to become increasingly nonspherical with the progress of combustion and this change to be more pronounced for particles with larger initial aspect ratios. For particles of equal initial volume, the burnout time decreases slightly with the initial aspect ratio. For example a particle of initial aspect ratio 3.2 requires 12% less time to react 80% burnout compared to a spherical particle of the same initial volume.

END

DATE FILMED

8/25/92